Master Thesis

A Low-Cost, Highly-Maneuverable, Miniature Underwater Robot intended for Collective Behaviors

Florian Berlinger

Dr. Melvin Gauci (Harvard University)

Advisor

George Chatzipirpiridis (ETH Zürich)

Coordinator

Prof. Dr. Radhika Nagpal

Wyss Institute for Biologically Inspired Engineering

Harvard University

Prof. Dr. Bradley J. Nelson

Institute of Robotics and Intelligent Systems

Swiss Federal Institute of Technology (ETH Zürich)

April 2016

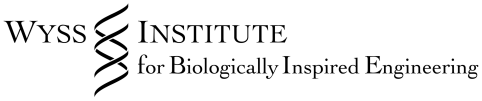

ETH

Eidgenössische Technische Hochschule Zürich
Swiss Federal Institute of Technology Zurich

Declaration of originality

The signed declaration of originality is a component of every semester paper, Bachelor's thesis, Master's thesis and any other degree paper undertaken during the course of studies, including the respective electronic versions.

Lecturers may also require a declaration of originality for other written papers compiled for their courses.

I hereby confirm that I am the sole author of the written work here enclosed and that I have compiled it in my own words. Parts excepted are corrections of form and content by the supervisor.

Title of work (in block letters):

A Low-Cost, Highly-Maneuverable, Miniature Underwater Robot intended for Collective Behaviors

Authored by (in block letters):

For papers written by groups the names of all authors are required.

Name(s):	**First name(s):**
Berlinger	Florian

With my signature I confirm that

- I have committed none of the forms of plagiarism described in the 'Citation etiquette' information sheet.
- I have documented all methods, data and processes truthfully.
- I have not manipulated any data.
- I have mentioned all persons who were significant facilitators of the work.

I am aware that the work may be screened electronically for plagiarism.

Place, date	**Signature(s)**
Cambridge, 28/04/2016	F. Berlinger

For papers written by groups the names of all authors are required. Their signatures collectively guarantee the entire content of the written paper.

Preface

This master thesis was written at the Wyss Institute for Biologically Inspired Engineering in Cambridge, Massachusetts. I spent the academic year 2015/2016 at the Self-organizing Systems Research Group, which is part of the John A. Paulson School of Engineering and Applied Sciences at Harvard University. The motivation to do so was my interest in the field of autonomous mobile robots in combination with my fascination for Prof. Radhika Nagpal's research on swarm robots. Furthermore, my desire to contribute to the advancement of the coordination of robotic multi-agent systems as well as the excitement to explore the American university culture.

First, I would like to express my gratitude to Prof. Radhika Nagpal, head of the Self-organizing Systems Research Group, for giving me the opportunity to write my master thesis there. I really enjoyed myself at your lab and I truly appreciate the time we spent together thinking about underwater swarm robotics.

Thanks as well to Dr. Melvin Gauci, my supervisor at Harvard University, for your support and advice during my research. We learnt a lot together. And I also believe we would be decent managers for Manchester United.

I would also like to thank Prof. Bradley J. Nelson, head of the Multi-Scale Robotics Lab at ETH, and George Chatzipirpiridis, for their endorsement of my master thesis in the USA.

Additionally, I would like to express my special thanks to the Swiss Study Foundation of which I have been a fellow since 2011. The Swiss Study Foundation supported my stay in Boston with an Annual Scholarship.

Moreover, I would like to mention Manuel Inauen and Bruno Koster from KUK Electronics. KUK provided coil samples for the propulsion system. Thanks.

Finally, I very much appreciate the love, enthusiasm and moral encouragement, which friends and family have shown to me.
Thank you Adina. Your smiling face made the time abroad easy for me.

Abstract

This thesis discusses the design of a low-cost, highly-maneuverable, and miniature underwater robot. The design addresses some key challenges towards the realization of a large-scale, underwater robot collective. Firstly, low-cost and ease of manufacture of individual units are paramount considerations for keeping the cost of the collective within reasonable bounds. Secondly, high maneuverability is desirable so that each individual can exhibit fast response to its neighbors' actions, thus making it possible to maintain a cohesive collective. Thirdly, miniaturization would make feasible the operation of a school of underwater robots within a laboratory environment, providing an affordable and convenient physical platform for the study of 3-dimensional collective behavior.

The current prototype is low-cost at a components value of $ 60, not considering sensing and communication. It has a body length of 10 cm, excluding the caudal fin. Four fins ensure 3-d maneuverability for up to 1 h of swimming time: a caudal fin provides forward thrust for velocities of up to 1 body length per second; a dorsal fin allows for vertical diving down to at least 3 m below the surface; a pectoral fin on either side of the body enables turn-on-the-spot.

The relatively high number of control surfaces is made possible by the low-cost nature of the propulsor. A permanent magnet is pivoted inside an electromagnetic coil, and aligns with an alternating magnetic field generated by the coil. A hinge transfers the oscillating motion to a flexible fin. The Magnet-in-Coil propulsor (MIC) has an extremely low component cost (under $ 1). Moreover, it avoids the necessity of sealing moving parts, such as rotary shafts; the MIC can be attached modularly to the outer hull of the robot, and only two wires are required to penetrate the hull. One major contribution of this thesis is to use multiple such propulsors on a single robot, hence achieving high maneuverability and miniaturization at a low cost.

The proposed robot shows the potential to become a scalable platform to study 3-dimensional swarming. In the next steps of the project, several robots will be coordinated into a collective by adding sensing and communication capabilities. Intended applications for a collective of underwater robots include search missions and the monitoring of harbors, oil platforms, or coral reefs.

Keywords:
Autonomous Underwater Vehicle (AUV), underwater robot, robot fish, underwater propulsion, electromagnetic propulsion, swarm robotics, swarm intelligence, collective behaviors

Zusammenfassung

Diese Arbeit beschreibt die Entwicklung eines günstigen, äusserst manövrierbaren, und sehr kleinen Unterwasserroboters. Einige Herausforderungen bei der Realisierung eines grossen Kollektivs aus Unterwasserrobotern wurden angepackt. Erstens ist die günstige und einfache Herstellung von einzelnen Robotern wichtig, um die Gesamtkosten fürs Kollektiv niedrig zu halten. Zweitens ist hohe Manövrierbarkeit notwendig, damit jeder Roboter schnell auf die Bewegungen seiner Nachbarn reagieren kann und somit das Kollektiv zusammenhält. Drittens ermöglicht die kleine Grösse mehrere Unterwasserroboter in einem Labor zu betreiben und damit auf einer physischen Platform kollektives Verhalten in 3-D zu studieren.

Der gegenwärtige Prototyp ist sehr günstig bei verbauten Komponenten im Wert von $ 60 ohne Berücksichtigung der Sensoren und Kommunikationsinstrumente. Er hat eine Länge von 10 cm ohne Flosse. Vier Flossen stellen 3-d Manövrierbarkeit für eine Schwimmzeit von bis zu einer Stunde sicher: Eine Schwanzflosse bietet Vortrieb für Geschwindigkeiten von bis zu einer Körperlänge pro Sekunde; eine Rückenflosse erlaubt vertikales Tauchen in Tiefen von mindestens 3 m; eine Brustflosse auf jeder Seite ermöglicht Drehen auf der Stelle.

Die vielen Steuerflächen werden durch einen günstigen Antrieb ermöglicht. Ein Permanentmagnet ist innerhalb einer elektromagnetischen Spule drehbar gelagert. Das Magnet richtet sich am alternierenden magnetischen Feld aus, welches von der Spule erzeugt wird. Ein Scharnier überträgt die oszillierende Bewegung an eine flexible Flosse. Der Magnet-in-Spule–Antrieb (MIS) hat extrem günstige Komponenten (unter $ 1). Ausserdem erübrigt sich das Abdichten von beweglichen Teilen wie rotierenden Wellen; der MIS kann modular an der Hülle des Roboters angebracht werden und nur zwei Stromkabel müssen die Hülle durchdringen. Ein wesentlicher Beitrag dieser Arbeit ist die Verwendung mehrerer solcher Antriebe auf einem Roboter, um hohe Manövrierbarkeit und Miniaturisierung bei geringen Kosten zu erreichen.

Der vorgeschlagene Roboter weist das Potential auf, eine skalierbare Platform zum Studium von 3-d Schwarmverhalten zu werden. Während den nächsten Schritten des Projektes werden mehrere Roboter zu einem Kollektiv koordiniert, indem Wahrnehmung und Kommunikation ermöglicht wird. Vorgesehene Anwendungen für ein Kollektiv aus Unterwasserrobotern umfassen Suchaktionen, und die Überwachung von Häfen, Ölplatformen und Korallenriffen.

Schlagworte:
Autonome Unterwasserfahrzeuge (AUV), Unterwasserroboter, Roboterfisch, Unterwasserantrieb, elektromagnetischer Antrieb, Schwarmrobotik, Schwarmintelligenz, kollektive Verhaltensweisen

Contents

List of Tables

List of Figures

Notation

The following notation applies where not otherwise specified.

Symbols

λ	Amplitude $[m]$
I	Current $[A]$
ρ	Density $[kg/m^3]$
d	Distance $[m]$
U	Energy $[J]$
F	Force $[N]$
f	Frequency $[Hz]$
l	Length $[m]$
B	Magnetic field $[T]$
P	Power $[W]$
p	Pressure $[Pa]$
r	Radius $[m]$
R	Resistance $[\Omega]$
ρ	Resistivity $[\Omega m]$
v	Velocity $[m/s]$
V	Voltage $[V]$
Q	Volumentric flow rate $[m^3/s]$
T	Torque $[Nm]$
C	Constant [-]
$g = 9.81$	Gravity $[m/s^2]$
N	Magnetic north pole
S	Magnetic south pole

Subscripts

x	x-direction
y	y-direction
z	z-direction
i	Inner (radius)
o	Outer (radius)
c	Coil
m	Magnet
w	Wire
Cu	Copper

Acronyms and Abbreviations

AC	Alternating Current
AUV	Autonomous Underwater Vehicle
BCF	Body and/or Caudal Fin
BL	Body Length
CAD	Computer-Aided Design
CMOS	Complementary Metal-Oxide-Semiconductor
CoB	Center of Buoyancy
CoG	Center of Gravity
EAP	Electro Active Polymer
EU	European Union
FPS	Frames per Second
IMU	Inertial Measurement Unit
IPMC	Ionic Polymer Metal Composite
LiPo	Lithium-ion Polymer

MC	Manufacturing Cost
MD	Maximum Depth
MIC	Magnet-in-Coil
MPF	Medium and/or Paired Fin
PCB	Printed Circuit Board
RC	Remote-controlled
RCAB	Recirculating Compressed Air Ballast System
ROV	Remotely Operated Vehicle
SMA	Shape Memory Alloy
SP	Sale Price
ToS	Turn-on-the-Spot
USA	United States of America
VDS	Vertical Displacement System

Universities

CSIRO	Commonwealth Scientific and Industrial Research Organisation
CUHK	Chinese University of Hong Kong
ETH	Eidgenössische Technische Hochschule
HIT	Harbin Institute of Technology
IIT	Israel Institute of Technology
MIT	Massachusetts Institute of Technology
MSU	Michigan State University
MTU	Michigan Technological University
NUS	National University of Singapore
NYU	New York University
OCU	Osaka City University
PKU	Peking University
SSS	Scuola Superiore Sant'Anna
TMU	Tokyo Metropolitan University

TTÜ	Tallinn University of Technology
UNIGE	University of Genova

1 Introduction

Striving for a simple, low-cost, underwater swarm robot is a desirable objective for several reasons. To begin with, the assessment of ideas coming from nature and their adoption to robotics together with the aspiration to reproduce natural behaviors on robotic systems (e.g. swarming) open the way towards a deeper understanding of fish and their underwater navigation while potentially leading to more capable robots. This process is often referred to as biologically inspired engineering.

Secondly, the development of an underwater collective will advance research in 3-d swarm robotics. 3-d swarming is yet almost completely unstudied on physical platforms, especially in large numbers. Models and simulations normally make simplifying assumptions. Insights gained from the coordination of underwater robots could pave the way for the design of more sophisticated aerial multi-agent systems as well.

Figure 1: Fish form schools and shoals to confuse predators, to swim more efficiently, or to find food more easily. The image shows a school of baracudas, photographed by the author.

Thirdly, having an underwater collective brings us closer to a better understanding of marine life. Design-wise inspired by nature, swarm robots may be deployed to study coral reefs, to monitor the growth of underwater plants, to observe the schooling behavior of fish (see Figure 1), and to collect scientific data from the oceans. As the source of life and as a future option for the cultivation of foods, it is well worth to explore the relatively unknown oceans.

Finally, applications involving underwater swarm robots like search and res-

cue missions, the surveillance of offshore oil platforms, harbor patrols, and ship hull inspections will contribute to a better society. An efficiently coordinated collective, for instance, would potentially provide faster and further reaching possibilities to find crashed aircrafts (illustrated in Figure 2).

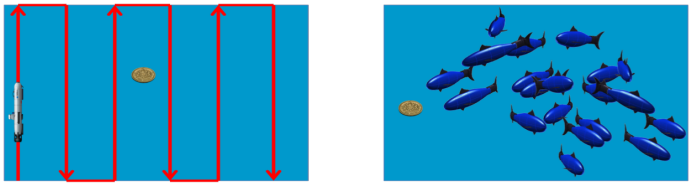

Figure 2: Left: Traditional search. Right: Collective search. A collective of robots can be spread like a grid across the search area to minimize search time.

The advantage of swarm robots in general is in the powerful solutions that evolve through the collaboration of simple individuals. Simple and low-cost robots working together in an efficiently organized swarm may outperform technologically superior individual robots regarding possible applications, scalability, flexibility, robustness, speed, reach, and functionality in various tasks. Such tasks span from collective construction through search and rescue missions to surveillance and monitoring applications (see Brambilla et al.[4]).

This thesis includes the design and the experimental validation of a miniature underwater vehicle, aimed at underwater monitoring in a collective on the order of 100 robots.

This chapter discusses the state of the art in miniature unmanned underwater vehicles and outlines the contributions of the proposed robot, Scuba Fish[1].

1.1 State of the art in miniature unmanned underwater vehicles

Different design approaches have evolved to tackle the three main locomotion challenges for underwater vehicles: propulsion, buoyancy, and attitude control. Small underwater vehicles are often biomimetic fish-like robots developed in

[1]Scuba Fish and Scuba Swarm are working names. SCUBA is an acronym for Self-Contained Underwater Breathing Apparatus, thus inappropriate for a final name of the robot.

academia whereas bigger vehicles mostly have a submarine-like appearance in order to travel long distances. A fish model, illustrated in Figure 3, introduces the necessary nomenclature for the description of propulsion, buoyancy and attitude control strategies.

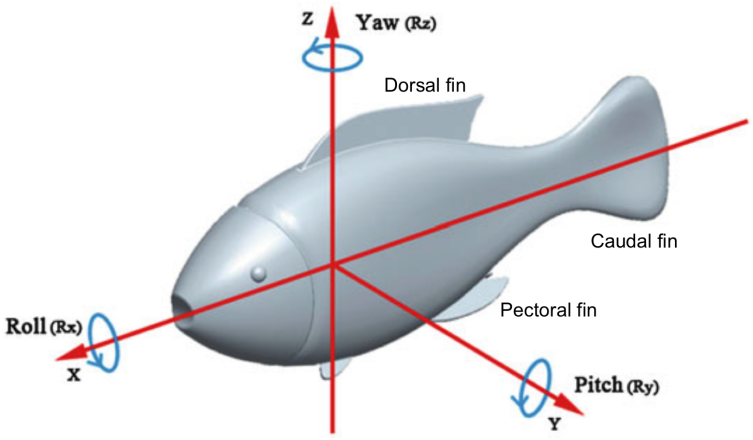

Figure 3: Nomenclature and orientations of robotic fish (adapted from [7]). The introduced definitions apply to all kind of underwater vehicles discussed in this thesis.

1.1.1 Propulsion, buoyancy, and attitude control in state-of-the-art underwater vehicles

Propulsion in x- or y-direction is usually generated through propellers, water jets, mechanical or pizeo-electrical oscillations of fins, or vortex ring thursters (see Watson et al.[32]). An advantage of propellers is their ability to provide thrust in both directions. Water jets have the benefit of a high power density thanks to the pressure built up in the jet's inlet. Oscillation-based systems have good maneuverability, high stability, and they are quieter than propellers.

Vertical displacements in the z-direction can be achieved dynamically or statically. Diving with a propulsion system, e.g. a propeller, is a dynamic displacement. Changing the vessel's density for an active buoyancy control is a static displacement. The latter may work with motor/syringe-, micro-pump-, or diaphragm-based systems as well as with electrolysis (cf. Watson et al.[32]).

A body is neutrally buoyant if its buoyancy exactly compensates for the pull

of gravity, i.e. if the body's density equals the density of the ambient medium. Forcing a body away from its neutral buoyancy requires extra thrust (dynamic diving). Alternatively, a change in its density (static diving) can effect a displacement in z-direction. Dynamic diving is favorable in small applications which only leave their neutrally buoyant level occasionally. Small applications cannot easily contain a complex and bulky system for a change in body density. Static diving has to be considered if frequent fluctuations in the z-direction occur. The required thrust for staying away from neutral buoyancy might justify the size of and the cost for a static displacement system.

Fish use their caudal fins (yaw angle) or pectoral fins (pitch and rarely roll angle) for attitude control. Submarines shift the center of gravity by using ballast tanks (roll angle), and they use foils or additional thrusters to change the pitch and yaw angle.

An overview on the discussed possibilities for propulsion, buoyancy, and attitude control is given in Figure 4.

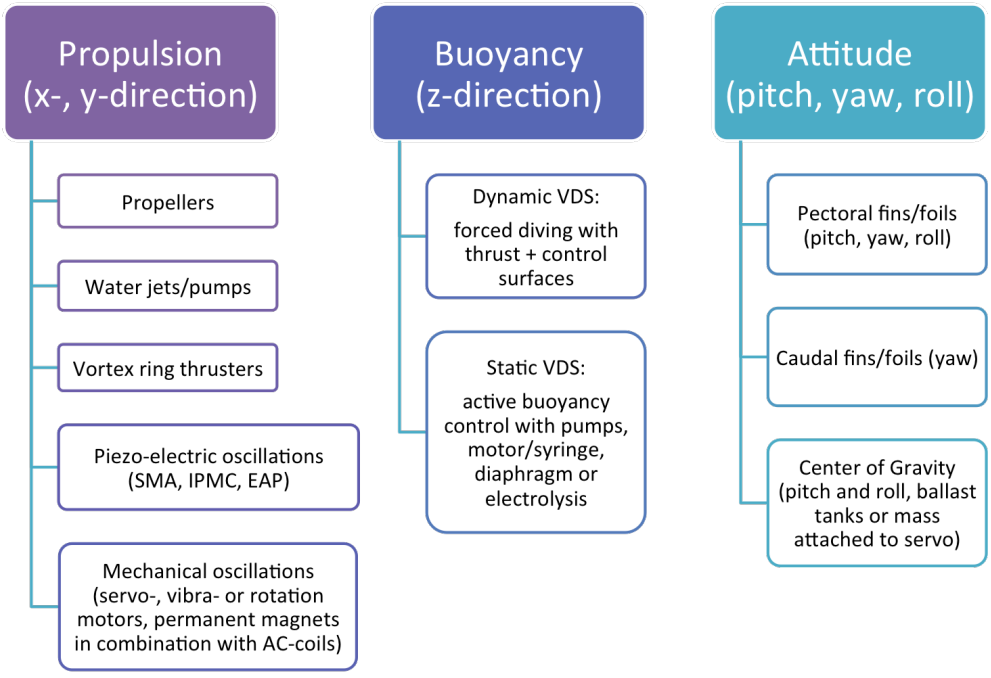

Figure 4: An overview on underwater propulsion systems, buoyancy handling, and attitude control.

Different combinations of propulsion, buoyancy, and attitude control systems have been incorporated in a vast number of underwater vehicles for various applications. Design approaches include single or multiple joint as well as soft-body fish, underwater gliders, or rather conventionally styled submarines. A selection of the latest publications in the field of miniature unmanned underwater vehicles is categorized and summarized in Table 1. Prototypical state-of-the-art underwater robots of each category are separately discussed in further detail thereafter. In addition, Du et al.[7] offer a comprehensive and up-to-date overview of the field of fish-like underwater robots.

Design	Propulsion	Actuators	Buoyancy	Dimensions	Applications	References
Single/multiple joint fish	Mechanical oscillation of fins (BCF, MPF)	Servomotors	Dynamic with fins	BL 117 mm, 100 $ (MC)	Research, education, no swarms, indoor	Kopman, NYU [10],[11]; Yu, PKU [34],[36],[35]
Soft-body fish	Piezo-electrical or mechanical oscillation of fins (BCF, MPF)	Smart materials (SMA, IPMC, EAP), wire-driven with servomotors	Dynamic with fins	BL 146 mm, 30 g	Research, no swarms, indoor	Salumäe, TTÜ [23]; Li, CUHK [14],[12],[13]; Wang, HIT [29],[31],[30]
Glider	Water jets	Jet-pumps	Static by inflation of a bladder	BL 500 mm, 4.15 kg, MD 3 m, $ 1000	Large range observations, swarms intended, outdoor	Mitchell, MTU [18]; Zhang, MSU [37]
Underwater toy, commercial	Propellers (submarine), oscillating fins (fish)	Motors, permanent magnets + AC-coil	Static (submarine), dynamic with fins (fish)	BL 50 mm, $ 20-40 (SP)	RC toys, research, exhibitions, no swarms, indoor	`www.youtube.com/watch?v=i3MFvGDXuSs`; `hexbug.com`; `robotswim.com`
Unconventional	Oscillating and momentum driven fins (BCF, MPF), thrusters	Fluidic elastomer channels + compressed gas, vibrating motors, servomotors, thrusters, permanent magnet + AC-coil	Dynamic with eccentric mass	BL 62 mm	Biomimetic robot fish, research, no swarms, indoor	Marchese, MIT [16]; Takesue, TMU [28]; Refael, IIT [21]; Rust, MIT [22]; Takada, OCU [27]
Swarm robot, control algorithms	Propellers	Motors	Static	BL 250 mm, 1.2 kg, € 1200	Leader-follower formation, harbor protection, collective navigation + docking, cooperative transportation	Mintchev, SSS [17]; Cui, NUS [6]; Simetti, UNIGE [26]; Dunbabin/Rus, CSIRO/MIT [8]; Shao, PKU [24]

Table 1: Classification of design approaches for miniature underwater vehicles and their respective literature references (predominant approaches and best proposed dimensions). Abbrievations are found in the notation at the beginning of the document.

1.1.2 Portraits of prototypical underwater robots

Portraits of prototypical designs for small underwater robots in the categories of Table 1 are presented in the following.

Single/multiple joint fish. Kopman et al.[10] proposed the usage of a servomotor (Traxxas 2065, waterproof) for the actuation of a caudal fin for price and simplicity reasons. The fish is 3-d-printed on a Dimension SST rapid prototyping machine (see Figure 5). The electronics include an Arduino Pro Mini microcontroller, a Nordic nRF2401A wireless transceiver, an LD33V voltage regulator, and a LiPo battery (3.7 V,180 mAh). The entire robot costs less than $ 100. Further manufacturing and design improvements could potentially reduce these costs to $ 25-30 per robot [11].

Furthermore, Kopman et al.[10] tested different attachable fins. A trapezoidal fin provided the highest thrust generation in comparison to a rectangular and a bioinspired fin.

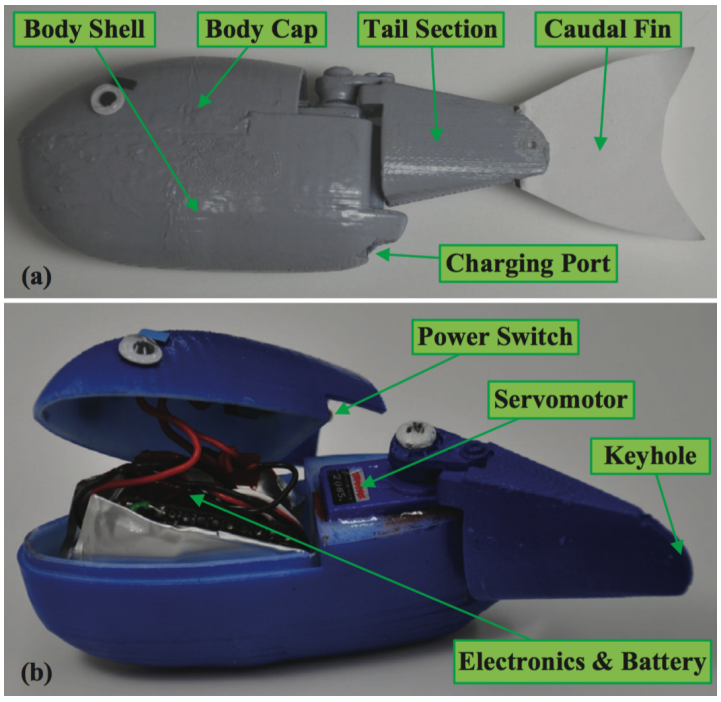

Figure 5: Fully assembled (a) and prior to sealing (b) Views of the biomimetic robotic fish. Length: 117 mm; height: 48 mm; width: 26 mm, without the caudal fin. (Image and caption from [10].)

Soft-body fish. FILOSE (Robotic FIsh LOcomotion and SEnsing) is a EU-funded research project[2]. The project aimed to build robots that sense the flow around them and react to changes in the flow pattern. Salumäe et al.[23] showed that flow-relative control reduces AUV's energy consumption. Their 50 cm long soft-tail fish is driven by a single servomotor. The servomotor generates thrust by creating tail vibrations through steel cables (see Figure 6).

A similar soft-body fish is described in Du et al.[7, p.173ff.]. The least complex design consists of eight individual components. The soft body can be cast inside a 3-d printed mold.

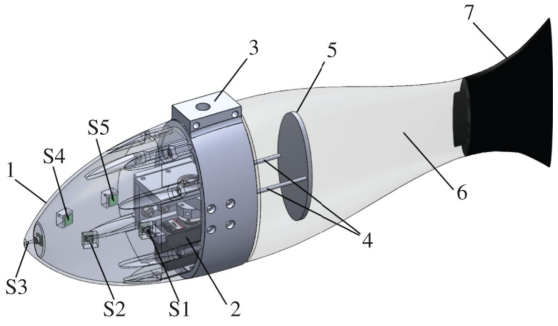

Figure 6: CAD view of the robot. 1, rigid head of the robot; 2, servo-motor; 3, middle part for holding the head and the tail; 4, steel cables; 5, actuation plate; 6, compliant tail; 7, rigid n; S1S5, pressure sensors. (Image and caption from [23].)

The usage of smart materials is another approach often encountered in soft-body fish designs. Wang et al.[30] proposed an "Embedded SMA wire actuated biomimetic fin: a module for biomimetic underwater propulsion". Their prototype is 146 mm in length and 30 g in mass. It uses SMA wires inside its biomimetic fin for swimming at almost 1 body length per second.

Glider. Gliders are usually big and carry a lot of sensors for large range underwater observations. Gliding allows to reduce actuation inputs to a minimum for prolonged underwater periods. Mitchell et al.[18] proposed GUPPIE, an inexpensive underwater glider for educational purposes (see Figure 7, left). GUPPIE is 502 mm long, 4.15 kg in mass, dives to a maximum depth of 3 m, and costs $ 1000. The glider "operates by drawing in and expelling water from three

[2] www.filose-project.eu

syringes attached to a rack" [18].

Zhang et al.[37] presented a "Miniature Underwater Glider: Design and Experimental Results". Their glider (see Figure 7, right) is 500 mm long and 4.2 kg heavy. They aimed to design a much smaller robot compared to traditional underwater gliders. Additionally, they point out the energy-efficient locomotion of gliders.

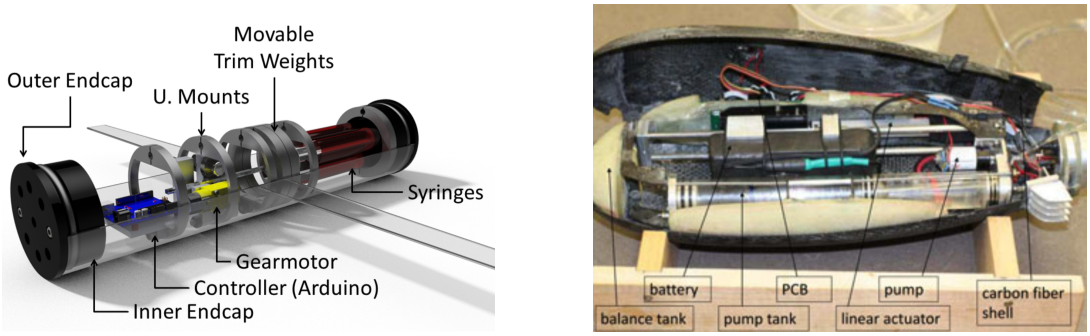

Figure 7: Left: GUPPIE 3D Model (image and caption from [18]). Right: Configuration of the internal components for the miniature underwater glider prototype (image and caption from [37]).

Underwater toy, commercial. JESSIKO is the 22 cm long robot fish of the French start-up Robotswim[3]. Robotswim's primary objective is to put artificial life in aquariums and pools. Furthermore, JESSIKO is sold as a research platform. The robot moves forward by flapping its caudal fin with a servomotor. It dives dynamically by changing the orientation of its front fin (see Figure 8). JESSIKO uses optical communication means. It is able to localize itself with respect to previously arranged beacons or cables. The robot is designed to function in a school of fish. Inductive charging is enabled. JESSIKO is potentially the most sophisticated, commercially available robotic fish at this scale. There are patents on JESSIKO.

Similar but simpler robotic fish are found in the toy sector[4]. These toy fish use two permanent magnets in combination with an oscillating electromagnetic coil in order to move the fins. A variation of this propulsion system was developed by Takada et al.[27] and will be discussed in Chapter 2.1.4.

Another interesting toy is the Air Hogs Divemaster RC submarine[5].

[3] www.robotswim.com
[4] www.hexbug.com/aquabot/
[5] www.youtube.com/watch?v=i3MFvGDXuSs

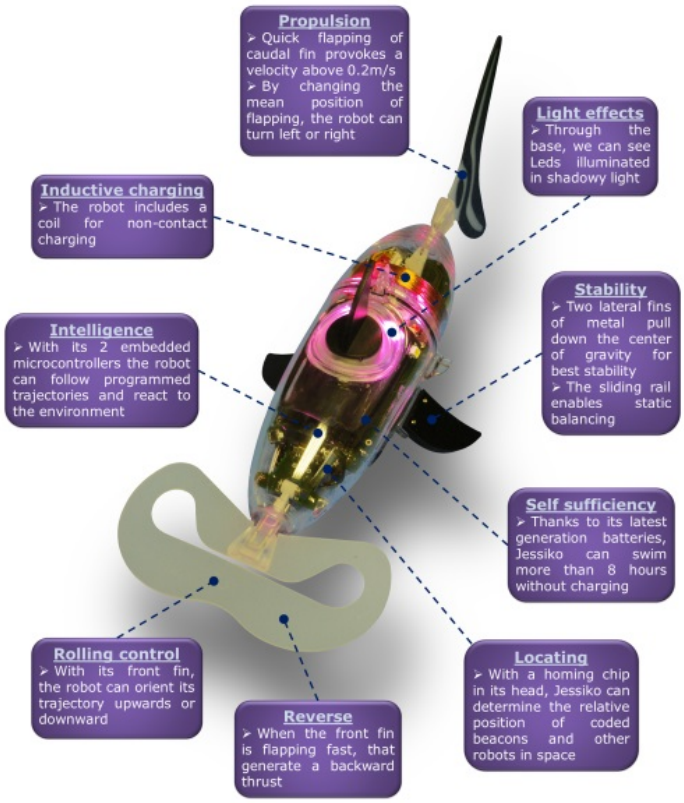

Figure 8: Features of JESSIKO. (Image accessed online on www.robotswim.com in April 2016.)

Unconventional. In the following, three unconventional designs will be introduced. Takesue et al.[28] published a "Proposal of [a] Miniature Aquatic Robot Utilizing Resonance of [an] Elastic Plate". Their most primitive prototype measures only 62 mm. Their robot is driven by a vibrating motor that oscillates elastic plates at the outer shell. Steering is achieved by attaching several plates of different thicknesses and different resonance frequencies respectively, as illustrated in Figure 9.

Asada's group proposed two roundish underwater robots shown in Figure 10. The spherical "Eyeball ROV" by Rust et al.[22] can change its orientation using a gimbal mechanism for moving an internal eccentric mass (Figure 10, left). It was designed to be fully holonomic yet poorly open-loop stable. The suggested design has an outer diameter of 12 cm. It is actuated by two thrusters.

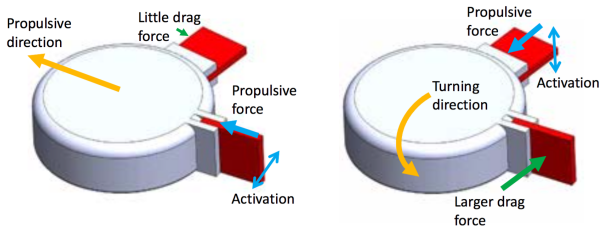

Figure 9: Miniature aquatic robot utilizing resonance of elastic plates. (Image from [28].)

Bhattacharyya et al.[3] designed EVIE (Ellipsoidal Vehicle for Inspection and Exploration), a football-like underwater robot (see Figure 10, right). EVIE uses four pump-jets for propulsion. It is intended to inspect underwater structures like pipes or ship hulls. The prototype is 203 mm long and 152 mm high. EVIE led to a start-up called Hydroswarm[6].

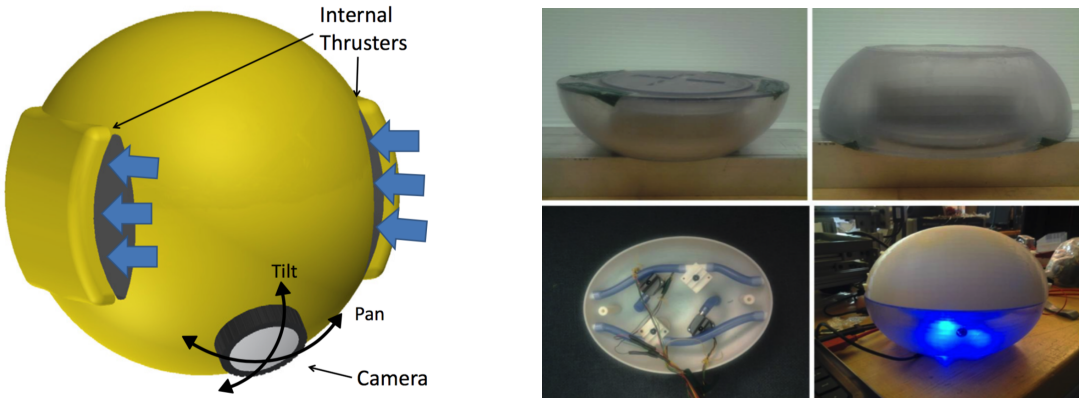

Figure 10: Left: Spherical ROV (image from [22]). Right: EVIE-1: 4 pumps in the submersible part. Straight jets. Water sealed part contains electronics including IMU and localization sensors (image and caption from [3]).

Swarm robot. CoCoRo (Collective Cognitive Robots) is another EU-funded project whose objective is an autonomous swarm of interacting, cognitive robots. Future tasks of CoCoRo-swarms include ecological monitoring, searching, maintaining, exploring, and harvesting resources in underwater habitats[7]. The project was executed by a consortium of five European universities, hosted by the University of Graz.

[6] `www.hydroswarm.com`
[7] `http://cocoro.uni-graz.at/drupal/home`

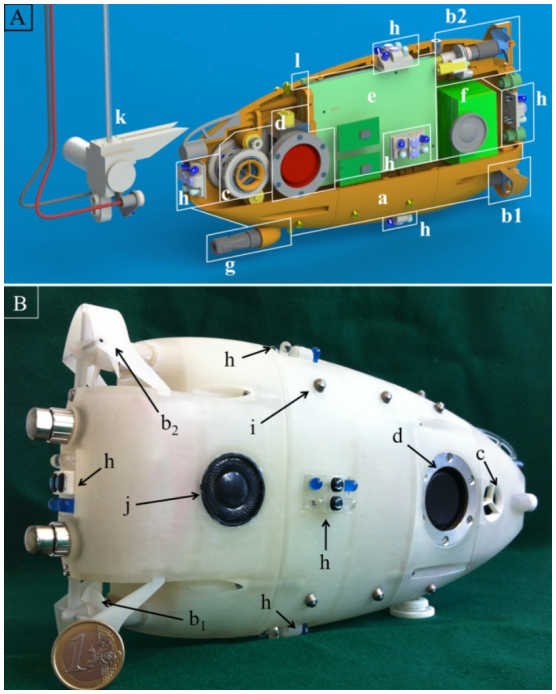

Figure 11: Overview of Jeff design. Fig. 2A shows a 3D model of Jeff's main mechatronics systems: a. shell, b. aft propulsion units, c. bow thruster unit, d. buoyancy system, e. control and power management PCBs, f. battery pack, g. expansion connector for sensors, h. blue lights, k. underwater docking station, l. microphone. Fig. 2B is a picture of Jeff in which can be seen: i. the electrodes for the potential field communication (only one is labelled) and j. the right loudspeaker. (Image and caption from [17].)

Mintchev et al.[17] explained the project's AUV "Jeff" (see Figure 11). Jeff uses two propellers (magnetic coupling) for propulsion plus a bow thruster for advanced maneuverability. The AUV features a buoyancy system which adjusts the overall volume of the robot for vertical displacements. Jeff is 250 mm long, has a mass of 1.2 kg, and is worth €1200. Communication is done via blue lights and electric fields (up to 1 m range). The sensor-set comes with a magnetometer, a gyro, an accelerometer, a pressure sensor, and a battery status monitor. Jeff can dive to a maximum depth of 3 m, driven by its eight-cell LiPo battery (880 mAh), for up to 120 min.

To sum up, a considerable research effort has been made in the field of underwater robots. Some researchers strive for the most authentic fish-like swimmers. Others look for tools for marine observations. Few try to coordinate a pur-

poseful swarm of underwater robots. None of the research findings have been implemented in commercial miniature underwater collectives for real-world applications in the sea so far. All of the discussed designs are tetherless. Available robots on the market are often expensive, big, and heavy, as well as not very maneuverable in spatially constrained environments.

1.2 Goals, contributions, and scope of Scuba Fish

The main goals of the Scuba Fish master thesis are the design and the experimental validation of a miniature underwater vehicle that will serve as a physical platform for studying 3-d swarming. The thesis focuses on the propulsion system, with the aim to achieve a simple low-cost actuation that can easily be scaled up. The target application of Scuba Fish is underwater monitoring in a collective in the order of 100 robots.

Scuba Fish is aimed to make three major contributions towards the state of the art. To begin with, Scuba Fish leads the scalability of underwater swarm robots to a new range. A low-cost and easy to manufacture design shall allow for the affordable and fast production of Scuba Fish in numbers that exceed existing platforms by an order of magnitude.

Secondly, the large number of robots in a Scuba Fish swarm will encourage the development of algorithms for new underwater applications. The development is aimed at eventually realizing meaningful scenarios like search and rescue missions, coral reef monitoring, ship inspections, or harbor patrols.

Ultimately, Scuba Fish is intended to close a gap in the state of the art. It aims for the right trade-off between the simplicity in the design and the autonomous sensing and actuating abilities of the robot needed for swarming. Scuba Fish follows a minimalistic design approach in order to keep the costs for an individual robot as low as possible. This way, a future collective of robots is made scalable. The size, the handling, and the coordinative abilities of Scuba Fish will be well-tuned with respect to future real-world swarm missions in the oceans.

The scope of this master thesis includes the design and the experimental validation of a single Scuba Fish. However, Scuba Fish project is intended to continue thereafter. Swimming control, underwater navigation, swarm behavior

and further intelligence will be implemented on the established Scuba Fish robotic platform.

1.3 Structure of this thesis

This thesis is split into four main parts. The structure of the thesis reflects the design process of Scuba Fish.

Chapter 2 explains the conception phase. Different concept studies for Scuba Fish were outlined and evaluated. The most promising locomotion approach with respect to the predefined project goals was finally chosen by the end of the conception phase.

Chapter 3 describes the validation of the chosen concept all the way to the realization of a first prototype. Applied physical principles, chosen actuators, sensors, and materials as well as the overall appearance of Scuba Fish are discussed and justified in detail.

Chapter 4 discusses a first closed-loop version of Scuba Fish with enhanced maneuverability.

Chapter 5 focuses on a set of closed-loop control experiments with a single Scuba Fish. It describes the experimental set-up, shows the control concepts, and discusses their validation with the experimental findings.

Finally, the conclusion in Chapter 6 summarizes the thesis. It shows the limits of the present Scuba Fish as well as recommendations for future developments. Furthermore, the conclusion reviews Scuba Fish's suitability for swarm robot applications and provides an outlook on the project's next steps.

For interested readers, the appendix offers additional and more detailed background insights into applied physical principles, hardware designs, control software, and the project's overall structure.

Symbols, indices, acronyms, and abbrievations used in mathematical equations, tables, and figures can be found in the previous notation section.

2 Locomotion concepts for Scuba Fish

The locomotion concepts for Scuba Fish are directly coupled to its overall design. The means of locomotion have to include at least the control of the forward thrust, the yaw angle, and the vertical thrust, combined with a body that can take these forces and transfer them to desired motions. The locomotion goal, which is the 3-d movement of the robot, is satisfied by such means.

This chapter aims to find an integrated locomotion concept that optimizes the following considerations:

- Maneuverability
- Velocity
- Efficiency
- Size
- Cost
- Number of actuators
- Complexity
- System integrability

The complete design requirements for Scuba Fish are found in the requirement list in Appendix D.2. In brief, the key consideration for the design is to think in terms of a swarm of about 100 robots rather than a single robot.

2.1 Assessment of propulsion systems

In a first step, four different propulsion systems for underwater robots were assessed. The assessment included propellers, pumps, servomotors, and oscillating coils. Propellers and pumps are encountered in submarine designs. Servomotors and oscillating coils power flapping fins in fish-like designs.

Further propulsion options like smart materials (piezoelectric, SMA and IPMC, discussed in [5],[10],[32]), vibrating motors, or fluidic elastomer channels in combination with compressed gas or liquids did not meet the basic requirements for a small, simple, low-cost, and autonomous underwater swarm robot. Piezoelectric actuators require high input voltages and the amplification of small deformations. Smart Memory Alloys (SMA) show low speed and slow response. Ionic Polymer Metal Composites (IPMC) struggle to provide strong output powers. Vibrating motors might lack the ability to provide sufficient thrust and maneuverability. Moreover, running several vibrating motors simultaneously to provide thrust and

directional control might cause interferences. There were no promising examples found of propulsion systems using vibrating motors. Fluidic elastomer channels require compressed gas or liquids coming from an onboard pressure cylinder or from pumps. This requirement makes them potentially bulky.

The main task of an underwater propulsion system is to overcome the robot's drag in water in order to maintain a forward movement. The estimated drag force F_D on a reasonable Scuba Fish design was derived in Equation 2.1.

$$F_{D,robot} = \frac{1}{2} \cdot \rho \cdot v_{robot}^2 \cdot C_{D,robot} \cdot A_{robot} \approx 1.5\,mN \tag{2.1}$$

A reasonable Scuba Fish design assumes the following parameters, which will be used again in upcoming equations:

Velocity of the robot relative to the fluid:	v_{robot}	$0.1\,\frac{m}{s}$
Velocity of the caudal fin relative to the fluid:	v_{fin}	$0.06\,\frac{m}{s}$
Drag coefficient of the robot (bullet shape):	$C_{D,robot}$	0.3
Drag coefficient of the caudal fin (rectangular shape):	$C_{D,fin}$	2
Cross-sectional area of the robot:	A_{robot}	$0.001\,m^2$
Cross-sectional area of the caudal fin:	A_{fin}	$0.002\,m^2$
Density of the fluid (water):	ρ	$1000\,\frac{kg}{m^3}$
Angle of the fish tail relative to the fish body:	θ	$12\,^\circ$
Angle of deflection of the caudal fin:	ϕ	$4\,^\circ$
Angle of attack of the caudal fin:	$\alpha = \theta + \phi$	$16\,^\circ$
Oscillation frequency of the caudal fin:	f	$1.5\,Hz$
Oscillation amplitude of the caudal fin:	λ	$16.5\,mm$
Voltage provided by the power supply:	V	$6\,V$
Current provided by the power supply:	I	$300\,mA$

Table 2: Parameter assumptions for a realistic design of Scuba Fish. These values are plugged into all equations that end up with a numerical result throughout this Chapter 2.

The small value of the drag force F_D indicates that most of the propulsion system's thrust force will be needed to accelerate Scuba Fish rather than maintaining a constant velocity. A thrust force F_T in the range of 20 mN can be expected to work well for Scuba Fish. This estimate is based on a comparison to the underwater robot of Kopman et al.[11].

Thrust force and power consumption estimates as well as size, cost and complexity are compared between the four considered propulsion systems in the following. The constant η of proportionality between thrust and power of a propulsion system is defined as follows:

$$\eta = \frac{\text{thrust force}}{\text{power consumption}} \qquad [\text{mN/W}] \quad (2.2)$$

All the comparable figures for locomotion systems were taken from robots and propulsion systems in the same dimension and power range. Therefore, a fair comparison is ensured and scaling effects of efficiencies are minimized.

2.1.1 Propellers

Propellers are the most common propulsion system encountered on ships and submarines. Big vessels are powered by combustion engines or even nuclear reactors whilst small underwater robots are equipped with DC motors. The key issue in mounting a DC motor to an underwater robot is the sealing of the rotating shaft. One or more couplings are usually required.

Sophisticated robots like the CoCoRo's Jeff use customized magnetic couplings [17]. Such couplings allow the contactless transmission of torques. Therefore, the robot's waterproof hull can be installed between the motor and the propeller shaft. Hardly any efficiency is lost during transmission. However, off-the-shelf and miniature magnetic couplings are not available on the market. Slightly oversized versions start at a price of $ 40.

A simpler solution found in hobbyist's RC boats are stuffing tubes like the one illustrated in Figure 12. A universal joint connects the motor shaft to the inclined propeller shaft. A stuffing tube is mounted around the propeller shaft with some radial clearance, which is filled with thick grease. The grease prevents water from entering the boat through the stuffing tube. However, it also increases the friction on the propeller shaft. Consequently, efficiency losses occur. Secondary efficiency losses appear due to the inclination of the propeller mounted at the far end of the propeller shaft. The thrust vector no longer points directly in the opposite direction of the desired motion. The inclination of the shaft is usually desirable to prevent damage on the motor from water leaks. The motor is mounted at a sufficient safety hight from the lower boat's hull. If the stuffing tube sealing was

perfectly waterproof, a straight connection from the motor to the propeller shaft with a simpler standard coupling could be used.

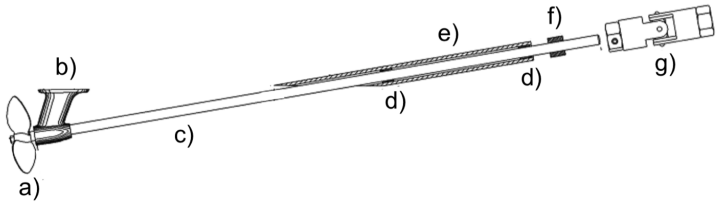

Figure 12: Stuffing tube: a) propeller; b) connection to the ship hull; c) propeller shaft; d) bronze bearings; e) stuffing tube running through the ship hull; f) collet with grubscrew; g) universial joint connecting the propeller to the motor shaft. (Illustration edited from `http://www.pt-boat.com/propshaft/propshaft.html`, accessed online in April 2016.)

Designers of low-cost toy submarines do not give high priority to the sealing of the motor shafts as their products are not expected to last very long and failure does not have critical consequences. They directly put the propeller on the motor shaft, applying enough grease to waterproof it for the usage in shallow waters. A smart design places the propulsion units outside of the submarine's main body, such that the electronics are safe in case the sealing breaks. Motors could theoretically be exchanged without affecting the whole submarine.

Waterproof DC motors which are directly mountable on the outside of an underwater robot were not found in the required size and quality range. Waterproofing a DC motor usually ends up in having a pump like the one explained later on in Figure 13.

The thrust force of a rotor is usually calculated using blade element theory (see Benini [2] for an example on marine propellers). Suppliers of motors and propellers often provide charts indicating thrust forces at different rotational speeds. An estimate of the propeller constant η_{prop} for a robot comparable to Scuba Fish is taken from CoCoRo's Jeff [17]:

$$\eta_{prop} \approx 100 \, \frac{mN}{W}$$

2.1.2 Pumps

The need to seal moving parts can be offloaded by using pumps for propulsion. The whole propulsion unit can be installed on the inside of the underwater robot.

Having no moving parts on the outer hull reduces the risk to get tangled up with other robots or in the underwater environment. However, pumps might get clogged by algae for instance. The maneuverability can be enhanced through thrust vectoring by adding a steering nozzle to the pump's outlet.

Miniature pumps are often used in medical applications. Centrifugal pumps would deliver sufficient flowrates for the propulsion of Scuba Fish. Smaller diaphragm pumps might be able to serve as steering thrusters.

High-quality pumps that are capable to deal with high pressures due to submersion start at a price of $\$\,60$. Having several of them for propulsion and maneuverability is size- and cost-wise not feasible; neither is the use of solenoid valves for thrust vectoring. Complete 3-d maneuverability would require at least four valves (up, down, left, right). There are other concepts for thrust vectoring like bending the outlet tube or installing a rudder. However, none of these are evidently simple.

Cost-efficient alternatives to high-quality pumps usually save on sealing the motor shaft properly. The disassembly of a $\$\,1$ low-cost pump is shown in Figure 13. A DC motor is covered by a waterproofing plastic hull. The motor shaft connects to an impeller. The impeller sucks the water from the axial inlet and ejectes it through the radial outlet.

The durability of low-cost pumps exposed to underwater pressure is doubtful.

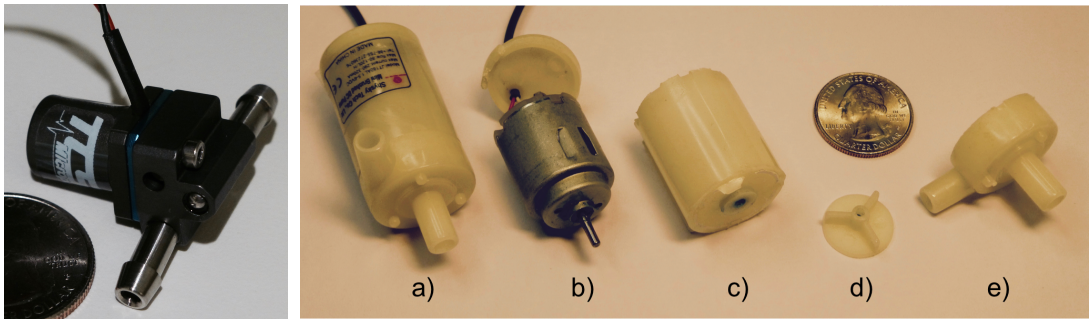

Figure 13: Left: High-quality pump. Right: Disassembly of a low-cost pump: a) complete pump; b) DC motor; c) plastic housing; d) impeller; e) inlet/outlet.

The constant η_{pump} of the low-cost pump depicted in Figure 13 was derived using the following values provided by the supplier:

1. Volumetric flow rate: $Q = 120\,\frac{L}{h} \approx 33.3\,\frac{cm^3}{s}$

2. Mass flow rate: $\dot{m} = Q \cdot \rho_{H_2O} \approx 33.3\,\frac{g}{s}$
3. Inlet/outlet radius: $r = 2.5\,mm$
4. Required voltage: $V = 6\,V$
5. Required current: $I = 320\,mA$

The thrust force F_{pump} is:

$$F_{pump} = \dot{m} \cdot v = \dot{m} \cdot \frac{Q}{r^2 \cdot \pi} \approx 56.6\,mN$$

The fluid's velocity v was derived with the help of the volumetric flow rate Q and the cross-section of the pump's outlet:

$$v = \frac{Q}{r^2 \cdot \pi}$$

Further, the power consumption P_{pump} is:

$$P_{pump} = V \cdot I = 1.92\,W$$

Finally, the pump constant η_{pump} is:

$$\eta_{pump} = \frac{F_{pump}}{P_{pump}} \approx 29.5\,\frac{mN}{W}$$

2.1.3 Servomotors

Traditionally, servomotors are installed for the precise position control in closed-loop systems. Using servomotors for propulsion is leading towards a flapping fin design. The integration of servomotors into underwater robots is straightforward as long as they are waterproof. Waterproof servomotors cost at least $\$\,20$. However, they are meant to be used on land, e.g. in RC cars that go through some puddles. The effects of prolonged exposure to underwater pressures are unknown. Buying cheaper standard servos and waterproofing the rotating shaft is considered to be too laborious and too unreliable, thinking of a large swarm of robots.

The thrust force of a flapping fin is most accurately assessed by running simulations or experiments. A simplification presented in [33] states the equations

for the thrust force F_T genereated by the fin, and the drag force F_D opposing the movement of the fin as follows:

$$F_{T,fin} = \frac{1}{2} \cdot \rho \cdot v_{fin}^2 \cdot C_{D,fin} \cdot A_{fin} \cdot \sin(\alpha) \tag{2.3}$$

$$F_{D,fin} = \frac{1}{2} \cdot \rho \cdot v_{fin}^2 \cdot C_{D,fin} \cdot A_{fin} \cdot \cos(\phi) \tag{2.4}$$

Running the Equations 2.3 and 2.4 with the parameter assumptions for Scuba Fish (cf. Table 2) delivers very small thrust and drag values $F_{T,fin}$ of around 5.5 mN and $F_{D,fin}$ of around 20 mN respectively. Averaging the thrust and the drag over one oscillation period by integration would probably enhance the results. The assumptions of static velocities v_{fin} and static angles α and ϕ might not be accurate.

Subsequently, measurement data from Kopman et al.[11] were analyzed in order to derive the constant η_{servo} of servomotors. Kopman et al. measured thrust forces F_{servo} of 20 mN while oscillating the caudal fin at a frequency f of 1.5 Hz and an angle θ of 12 ° relative to the body. Considering a moving tail length of 80 mm, the 12 ° angle θ corresponds to an amplitude λ of:

$$\lambda \approx \arctan(12\,^\circ) \cdot 80\,mm \approx 16.5\,mm \tag{2.5}$$

Plugging the parameters from the experiments in [11] into Equations 2.3 and 2.4 again delivers very small thrust and drag values.

The robot of Kopman et al. operates continuously for approximately 1 h on a 3.7 V / 180 mAh battery. Therefore, an average current draw I of 180 mA was assumed. The power consumption of the servomotor, neglecting the onboard microcontroller and transceiver, is:

$$P_{servo} = V \cdot I \approx 0.67\,W$$

Finally, the servomotor constant η_{servo} is:

$$\eta_{servo} = \frac{F_{servo}}{P_{servo}} \approx 29.9\,\frac{mN}{W}$$

The maximum thrust achievable with servomotors is constrained by the velocity of the servomotor. For instance, the Traxxas 2065 servomotor can move

at a maximum velocity of 0.2 s/60 °. This maximum velocity limits the oscillation's frequency and amplitude. The torques of servomotors are usually more than sufficient to deal with the drag force acting on the flapping fin.

A key advantage of flapping fins powered by either servomotors or oscillating coils is their ability to provide not only thrust but yaw control as well with a single actuator. A code sample on how to command a servomotor accordingly is given in Appendix C.4.3.

2.1.4 Oscillating coils

Oscillating coils used as a propulsion system were found in simple and cheap toy fish. Their working principle is explained by looking at the disassembly of such a $ 10 toy fish depicted in Figure 14. A pivoted lever transmits the oscillation from the coil to a caudal fin. The caudal fin generates thrust by flapping back and forth.

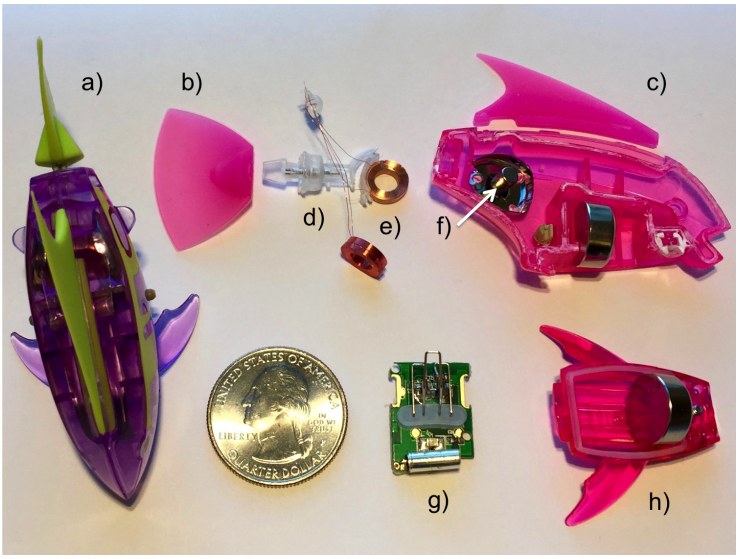

Figure 14: Toyfish disassembly: a) complete fish; b) actuated caudal fin; c) left part of the symmetrical body's hull; d) lever connecting the oscillating coils with the caudal fin, sealed with silicone rubber; e) air core coils with approx. 500 turns each; f) cylindrical permanent magnet; g) read switch mounted on a mini board; h) removeable belly holding two 1.5 V AG13 button batteries.

Running a DC current through a coil induces a magnetic field according to the Biot-Savart law. The direction of the current decides on the polarities of the coil's magnetic field according to Lenz's law. The polarities can be actively

switched with the help of an H-bridge. The toy fish in Figure 14 uses an even simpler passive read switch to change polarities. Having two concentric permanent magnets with opposed magnetic poles on either axial side of the air core coil completes the oscillating mechanism (see Figure 15).

During the first half of an oscillation cycle, the coil is pushed away from the initial magnet and pulled towards the magnet further apart. After switching the poles of the coil's magnetic field halfway through the oscillation cycle, the interaction repeats itself in opposite direction.

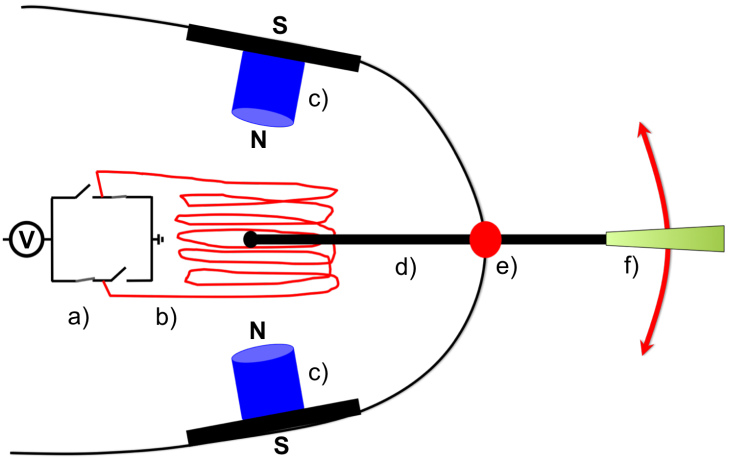

Figure 15: Top view on a coil propulsion system: a) H-bridge, changes current flow directions and polarities of the coil respectively; b) oscillating air core coil; c) cylindrical permanent magnets with opposing polarities, mounted on the sides of the fish's hull; d) Lever, connecting the oscillating coil with the caudal fin; e) pivot point, sealed with silicone rubber; f) caudal fin, providing thrust.

Controlling the coil's oscillation with an H-bridge is simple. A code sample for an Arduino interface is given in Appendix C.4.2.

Strong permanent magnets are available at various dimensions for as little as $0.3 per piece. Custom-made air core coils are sold in the same price range yet in high quantities. Finally, a $2 H-bridge elevates the total cost for the coil propulsion system to as little as $3.

Sealing is less of an issue than with continuously rotating shafts. A strong enough silicone rubber seal as shown in Figure 14 suffices. Alternatively, the whole tail of a fish-like underwater robot could be cast into a soft and flexible propulsion fin.

Unlike propellers, pumps, and servomotors, which are available in various

editions, a propulsion system consisting of a coil and magnets needs to be custom-made. The design of an optimized coil is estimated in Appendix A.1.

Shape-wise, the axial cross-section of a multilayered coil should be close to a square. Having a 1:1 ratio of the winding depth c to the length b minimizes the average distance between turns. Consequently, the magnetic field is concentrated as much as possible. The mean radius a of the turns should equal $3c/2$. Too large radii reduce the number of feasible turns N due to increased wire resistance. Too small radii fail to deliver sufficient inductance per turn. These optimal design guidelines were first published by Morgan Brooks in 1931. A coil following these guidlines is called a Brooks coil as shown in Figure 16. Fortunately, coils can deviate significantly form the Brooks coil until the induced magnetic field suffers substantially[8].

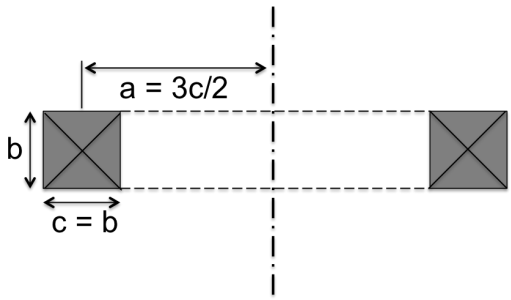

Figure 16: Parameters of a Brooks coil for a maximized magnetic field.

The coil itself is subject to a trade-off on the number of turns. On the one hand, increasing the number of turns is beneficial as they contribute to a stronger magnetic field. On the other hand, increasing the number of turns also leads to an increase in undesirable wire resistance. Assuming the power supply to be given with a fixed voltage V and maximum current I according to a desirable battery runtime, the minimum allowed resistance of the coil wire is $R_c = V/I$.

It remains to optimize the number of turns against the wire radius for a chosen coil size. Theoretically, the larger the wire radius the lower the resistance per unit length, and the more turns can be wound before the resistance budget is used up. However, there are physical limits to the coil size set by design constraints. Calculations shown in Appendix A.1 resulted in a small wire radius r_w in the range of 0.1 mm at a high number N of around 990 turns. Furthermore, by applying the

[8]R. Clarke: "An introduction to the air cored coil", `http://info.ee.surrey.ac.uk/Workshop/advice/coils/air_coils.html`

law of conservation of energy, the coil was shown to provide torques around the pivot point up to three times higher than the Traxxas 2065 servomotor used by Kopman et al.[10]. On the other hand, the coil's power consuption is estimated to be around three times higher as well. Consequently, the resulting constant η_{coil} of coils is comparable to the one of servomotors. The values, mathematically justified in Appendix A.1, have to be validated through experiments.

$$\eta_{coil} = \frac{F_{coil}}{P_{coil}} \approx 33.3 \, \frac{mN}{W}$$

The setup for early coil tests is shown in Figure 17. The two cylindrical neodymium magnets have a pull force of 33.8 N each. They are magnetized along the axis of their $\oslash 5 \cdot 10$ [mm] body. The air core coil was wound by hand using a continuous servomotor to spin a bobbin. The bobbin was simply a cylindrical magnet wrapped with a couple of tape layers to allow for the necessary clearance between the magnet's periphery and the coil's inner radius. An SN754410 H-bridge was mounted on a breadboard and commanded with an Arduino microcontroller. The H-bridge is used to switch the flow direction of the electrical current and the magnetic poles of the coil respectively.

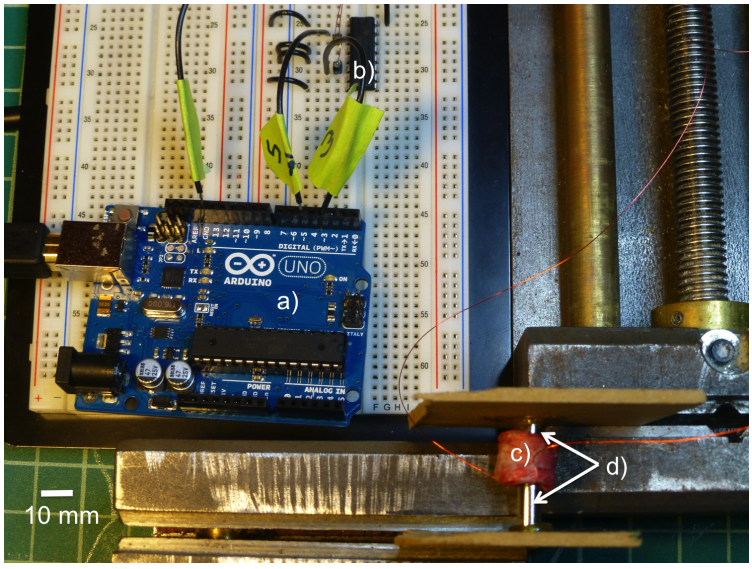

Figure 17: Test setup for oscillation experiments with coils and magnets: a) Arduino microcontroller; b) H-bridge on a breadboard; c) self-made coil; d) cylindrical permanent magnets.

Future coils for prototyping could be wound on a custom-made setup installed on a lathe. Alternatively, KUK[9] might offer further coil samples. Once the final coil design is fixed, manufacturing in bulk becomes cheaper.

An alternative coil propulsion system was demonstrated by Takada et al.[27]. Takada et al. oscillate a spherical magnet inside a fixed coil (see Figure 18) instead of oscillating a coil between two fixed cylindrical magnets (cf. Figure 15). The effect on the fish design is drastic: The pivot is now at the center of the magnetic sphere. A sealed lever entering the robot to a dry oscillation chamber is no longer required. The whole propulsion unit can be mounted on the outside of the robot's hull, saving space inside the robotic fish. The feasible amplitude of the oscillation is decoupled from the fish's width and the lever's length respectively.

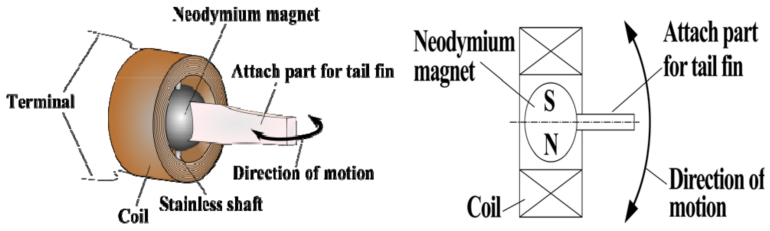

Figure 18: Coil propulsion system including an oscillating spherical permanent magnet inside a fixed air core coil. (Image from [27].)

Takada's robotic fish named FOCUS is 100 mm long, 13 mm wide, and 26 mm high. It includes a depth control system made up of a moveable weight attached to the lever of a servomotor. Two CMOS cameras are installed for navigation and for the tracking of fish. The propulsion system is not only scalable by increasing the coil and the sphere size but also by mounting several units in line, connected to the same hinge.

The actuation principle proposed by Takada was validated by rapid prototying (see Figure 19). The choice of a cylindrical magnet is on purpose: The pull force of a $\oslash 5 \cdot 10$ [mm] cylinder equals 33.8 N compared to 19.5 N for a $\oslash 10$ [mm] sphere as used by Takada. However, these values from the product descriptions from APEX[10] can only be a vague indicator for the strenghth of the magnetic fields. The pull forces might not consider the influence of different contact sur-

[9] www.kuk.ch
[10] www.apexmagnets.com

faces during experiments. More importantly, spheres are usually carved out of cylinders. Consequently, cylinders are up to four times cheaper than spheres. Moreover, the additional magnetic material a sphere shows in radial direction might not contribute too much to the magnetic field along its axis.

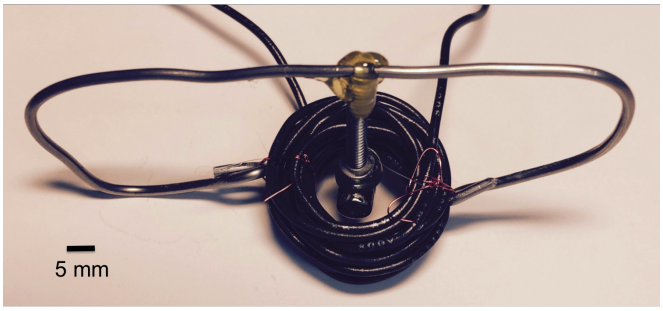

Figure 19: Prototype of a single magnet actuator: a) cylindrical permanent magnet; b) self-made coil; c) flapping shaft; d) passive hinge.

Shortly after Takada, Clark et al.[5] published on the optimization of speed and power usage by designing a highly effective flexible caudal fin. Their robotic fish for the experimental validation of simulations shows the same actuator with a magnet inside a single coil.

2.1.5 Concluding summary on propulsion systems

The most significant features of each propulsion system discussed previously together with a comparison of their η constants are shown in Figure 20. The performance constants of the four proposed systems are within the same order of magnitude. Therefore, none of the systems was excluded due to inferior performance. However, conflicts with basic design requirements and difficulties regarding system integration left propellers and pumps behind servomotors and oscillating coils. In addition, both servomotors and coils allow to control the yaw angle on top of generating forward thrust. While the servomotor is tempting for its proven functionality in fish-like robots, the coil is relatively new to science and possibly significantly cheaper. Most importantly, the coil is completely submergible and resistant to high pressures. Swimming tests with early prototypes shall provide further evidence for a well justified decision.

Flapping fins push the design towards a fish-like appearance, mainly because

of their torques acting on the main body. Takada et al.[27] praised a key advantage for surveying fish resources: “If a robot is sufficiently fishlike in appearance and does not use a screw propeller, real fish will not be easily surprised by it.”. Artificial robots can be introduced into natural fish swarms to study the interactions of swarming fish.

Propellers	**Pumps**
↗ Efficiency ↘ Sealings	↗ No sealings, no moving parts ↘ Size, cost
η 100mN/W	η 29.5mN/W
Servomotors	**Oscillating coils**
↗ Yaw incl., ready-to-use ↘ Lack of novelty, abuse of motion	↗ Yaw incl., cheapest ↘ Design uncertainties
η 29.9mN/W	η 33.3mN/W (?)

Figure 20: Decisive advantages and drawbacks of the discussed propulsion systems along with their respective energy efficiencies.

2.2 Swimming performances of three concept studies

Preliminary prototypes reviewed in the following served solely for the comparison of different propulsion systems for the generation of thrust and yaw maneuverability. Pitch control was not addressed. The robots were tared with block weights in order to match the density of water. The added block weights are usually seen on car wheels in order to counter rotational imbalances.

Two of the fish-like robots in Figure 21 feature streamlined bodies. They allow for a direct comparison of a servomotor and an oscillating coil in a standardized body shape. The third prototype shows a circular body. It was designed to weigh up additional maneuverability against velocity and power consumption respectively. Also, two different waterproof servomotors were tested. The leftmost robot is powered by a Traxxas 2065 servomotor while the middle robot uses a stronger HiTEC HS-646WP servomotor.

Preliminary tests were executed in a 84 cm by 51 cm plastic box filled with 5 cm of water. The ultimate goal of a flapping caudal fin is to generate an inverse

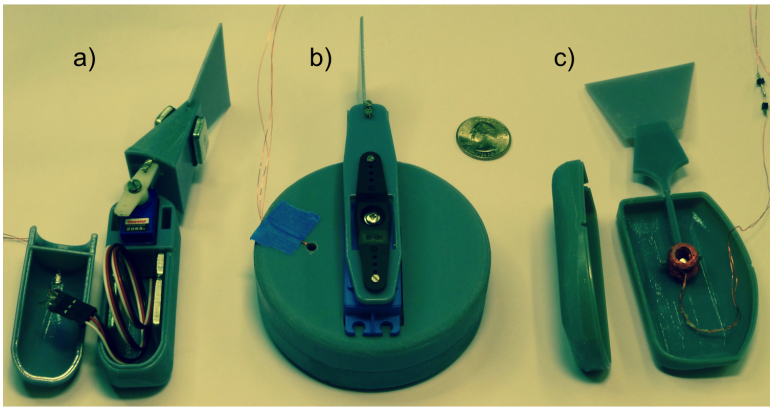

Figure 21: Concept fish: a) Kopman replication propelled by a Traxxas 2065 waterproof servo (see [10]); b) circular design for advanced maneuverability propelled by a HiTEC 646 waterproof servo; c) shape (a) fish propelled by an oscillating air core coil between two permanent magnets ($\oslash 5 \cdot 10$ [mm]).

Karman vortex street pointing backwards. The following knowledge was obtained through visual observations:

1. Symmetrical designs tend to oscillate in place rather than generating forward movement. Model b) in Figure 21 rotated its circular body around the motor shaft while keeping the tail stable. This behavior occured again after mounting the motor shaft with an offset from the symmetry axis of the circular body. It seems like the shape of the main body has to provide sufficient resistance to yaw and roll moments induced by the flapping fin. The following preliminary hypothesis is proposed: **Two bodies coupled on a shared axis of rotation oscillate inversely proportional to the ratio of their moments of inertia.** The moments of inertia are defined as the resistance to a rotation around the shared axis, caused by drag in water. Therefore, the more the body of a robotic fish is streamlined, the more undesired oscillations can be mitigated.

2. A fish can only move if the moments of the main body and the caudal fin do not cancel each other. Flapping fins may induce oscillations on the fish body. Ideally, the fish body would remain aligned stably with respect to the intended swimming motion, decoupled from the motion of the caudal fin. However, the flapping fins always shake the main body to some extent. The effect is obviously worst for symmetrical body designs as

they cannot oppose it (discussed in point 1). The effect also depends on the oscillation's frequency and amplitude. Finally, the effect presumably decreases with increasing forward velocities as additional inertia is gained and as the contribution to the total force vector diminishes.

With the servomotor fish, the main body actively oscillated around the motor shaft though to a smaller extent than the caudal fin. With the coil fish, it was the coil hitting the hulls of the fish body while flapping left and right that caused vibrations on the fish. The observed side effects on the servomotor fish were worse than the ones on the coil fish.

All caudal fins for these tests were made out of stiff 3-d printed material. A soft caudal fin, like seen in most small robotic fish, might mitigate the oscillation of the main body. The stiffer main body should provide more resistance than the flexible caudal fin.

3. A second iteration of tests was done with improvised flexible fins made out of duct tape. All of the three prototypes in Figure 21 showed improved swimming behaviors. There was evidence that a bending fin provides better thrust than a stiff fin. The flexibility of the fin has to be tailored to the predominant oscillation regime for swimming. The general tendency pointed towards stiffer fins for higher frequencies. In other words, higher drag froces acting on the fins go along with stiffer fins while small forces require more flexibility to induce the desired bending pattern. Several publications confirm the importance of the flexibility of the caudal fin (c.f. [9],[10],[15],[25],[27],[33]).

4. The oscillation of servomotors can be tuned regarding frequency and amplitude. The oscillation of coils can only be tuned regarding a pseudo-frequency. The time interval between switching the polarities of the coil can be set. This interval basically corresponds to the time the coil is waiting at either side of the fish hull before moving towards the opposite magnet. The movement itself is not controllable. It always happens at the same acceleration no matter how the time interval is set. The achievable velocity of coils surpasses the maximum velocity of servomotors.

5. The required thrust force for swimming is very low. The servomotors seem to be oversized regarding the torques they can provide.

6. Pressure acts badly on the sealings. There are certainly good reasons why comparable robots like Jessiko or Jeff swim in shallow waters and why underwater toys break if taken to the bottom of a pool.

7. Obtaining neutral buoyancy is not easy despite knowing the volume from the CAD model and beeing able to measure the mass on a balance. The final robot shall be well planned, experimentally calibrated, and exactly documented to allow for reproduction.

In conclusion, both locomotion concepts, servomotors and coils, proved to be feasible.

Two important insights were gained. Firstly, the fin design has to be in accordance with the intended oscillation. The stiffness of the fin directly influences the effectiveness of thrust generation.

Secondly, the importance of the shape of the underwater robot introduced by the chosen actuator was underlined. Symmetrical shapes are generally more vulnerable to undesired motions induced by the propulsion system. For example, large cargo vessels operate a single propeller while highly streamlined and symmetrical torpedos need a second propeller to cancel the induced torque. The same comparison holds for single engine propeller aircrafts and helicopters.

If symmetry were the ultimate goal, a propulsion system that does not move with respect to the surrounding fluid should be chosen (e.g. pumps), as well as higher control expenses due to instabilities and lower forward velocities due to a less streamlined body should be accepted.

2.3 Assessment of maneuverability systems

Different maneuverability systems were introduced in Section 1.1.1. The trade-offs regarding maneuverability involve turn-on-the-spot versus requiring a radius, and being able to change depth vertically versus having to move forward as well. Keeping in mind that the overall design goals are small size, low cost, and low complexity, the number of actuators should be kept as small as possible. Having a fish-like robot with a flapping caudal fin would already solve the yaw angle control. The control of pitch and roll angles in order to achieve desired attitudes and depths are discussed subsequently.

The forces acting on a swimming fish are illustrated in Figure 22. The body of the fish can be compared to the one of an airplane that has similar control surfaces. It quickly becomes evident that the appropriate placement of the center of gravity (CoG) and the control fins is crucial for satisfying swimming performances. The center of buoyancy (CoB) is equal to the center of gravity of the water displaced by the robot's body.

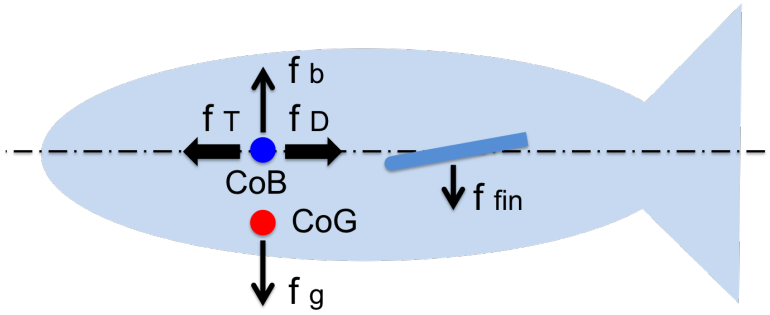

Figure 22: Front view on the forces acting on a swimming fish-like robot.

The fish is neutrally buoyant as long as the buoyant force f_b and the gravitational force f_g are levelled. It is important that these force vectors share the same axis in order to avoid undesirable pitching. **Placing the center of gravity (red) below the center of buoyancy (blue) gives the fish stability against unwanted roll. However, the pitch angle undergoes the same effect. Therefore if pitching is desired there is a difficult trade-off to be done here.** Furthermore, the thrust vector f_T and the drag vector f_D no longer necessarily run through the CoG. The fish remains moving at constant speed whenever thrust and drag cancel each other out. As soon as there is an imbalance, not only the velocity but also the pitch angle is affected due to the moment around the CoG. This pitch angle moment can be actively countered with pectoral fins. A shorttime change in pitch angle due to acceleration will induce additional drag opposing the pitching. Therefore, the fish is likely to return to its levelled swimming position.

Theoretically, a single actuator powering an oscillating caudal fin would be sufficient to move in 3-d space. Thrust and yaw are included by moving the caudal fin appropriately as shown before. Pitch could be controlled by using the amount of thrust force to change the lift generated by fixed pectoral fins. However, such a fish would have highly coupled and constrained maneuverability

parameters.

2.3.1 Dynamic diving by controlling the pitch angle

An investigation on static diving systems like piston tanks or Recirculating Air Ballast Systems (RCABS) led to the conclusion that no simple, small, low-cost, and ready-to-use options exist. The ability to hover without a vertical thruster is an advantage of static diving. An advantage of dynamic diving is the fact that a slightly positively buoyant robot floats back to the water surface if either the control signal is lost or the battery power is depleted.

The main cost for dynamic diving however is paid in terms of an increased power consumption. Forcing a body away from its neutral buoyancy obviously requires thrust force. The thrust force F_T is the difference between the buoyant force and the gravitational force acting on the robot (cf. Figure 22):

$$F_T = m_T \cdot g = (\rho_{fluid} - \rho_{robot}) \cdot V_{robot} \cdot g$$

Keeping the density of the robot close to the density of the surrounding fluid reduces the net force F_T to a minimum.

Ideas for dynamic diving most often involve the use of pectoral fins. Alternatively, shifting masses inside the robot's body could create the necessary momentum on the pitch angle. Takada et al. shifted the center of gravity successfully with both servomotors [27] and DC motors [38]. This solution avoids the need to seal moving parts.

2.3.2 Passive roll stability induced by the center of buoyancy

There are very limited benefits regarding maneuverability in having active roll angle control. Achieving passive roll stability is easily done by placing the robot's center of gravity below its center of buoyancy (cf. Appendix A.2).

2.4 Electronics, communication, and sensors

The concept studies discussed in this chapter were tethered to an external power supply and an Arduino Uno microcontroller. The next iteration shown in Chapter 3 was equipped with onboard power and processing. The latest version explained in Chapter 4 is completely autonomous, including sensors for closed-loop control.

The chosen onboard sensors used for underwater locomotion and navigation for the evaluation of a single robot are explained in the following.

An underwater local-sensing strategy to create coordinated behaviors that allow a collective of robots to function like a big sensing network and move the way natural swarms do remains a future challenge.

2.4.1 Underwater communication

A single robot reporting to a surface base station is developed within the scope of this thesis. Transmitting information from the robot to the surface or commands the other way round is feasible as long as diving depths are moderate. The use of a strong tranceiver is advised. The RFduino board for example hosts such a device by default.

The following collection of communication ideas for a swarm robot have to be evaluated outside the scope of this thesis:

- Magnets: The swarm is where the magnetic field is strongest. Swim along its gradient to stay with the collective of robots/magnets.
- Bluetooth: Bluetooth does not operate at a fixed frequency. It rather jumps between frequencies and picks the one offering the best connection. Superior to other radio waves including WiFi?
- Optics: Use vision and color filters in combination with blob detectors to detect the pattern on the bodies of your neighbours.
- Bluelights: Communicate at high frequencies using light waves.
- Sonar/lasers: Use sonars or lasers for local obstacle avoidance.
- Radio waves: Use radio waves and triangulation to localize your position relative to the collective.

2.4.2 Inertial measurement unit for attitude control

The inertial measurement unit allows to keep track of and to control the 3-d motion in water.

The used 9DOF MPU-9150 motion tracking device contains a 3-axis gyroscope, a 3-axis accelerometer and a 3-axis digital compass.

The I^2C communication software for the IMU is shown in Appendix C.1.1.

2.4.3 Pressure sensor for depth control

Pressure p in water adds up linearly with diving depth z to the atmospheric pressure C at the water surface:

$$p = -\rho_{fluid} \cdot g \cdot z + C \tag{2.6}$$

The diving depth z is obtained by solving Equation 2.6 that contains the pressure values p from the sensor data:

$$z = \frac{C - p}{\rho_{fluid} \cdot g}$$

Merging the z-value from the pressure sensor with the data from the IMU will result in more accurate estimates for the diving depth.

The MS5803-01BA miniature altimeter module was chosen to measure the diving depth of the robot. The sensor tip is covered by a silicone gel and ready to use in water. The sensor's operating range in air goes from 1 kPa up to 130 kPa at a resolution of 10 cm. Thinking in terms of water columns and assuming an atmospheric pressure of 100 kPa, the sensor will allow for diving depths of up to 3 m at an accuracy in the millimeter range. The fact that the pressure changes faster moving vertically in water than in air increases the resolution in water at the expense of a smaller range. There are alternative editions of the same sensor type, offering a wider diving range at lower resolution.

A 3-d printed enclosure was designed to test the MS5803-01BA in water, focusing on the validation of measured depth values, which was successful.

The I^2C communication software for the pressure sensor is shown in Appendix C.1.2.

2.4.4 H-bridge for controlling the oscillation of the coil

A SN754410 H-bridge is used to control the oscillation of the coil. The H-bridge can deal with continuous current outputs of 1 A at voltages of up to 36 V. Two coils can be connected and controlled independently with one H-bridge.

2.5 Vision of a swarming Scuba Fish

A smart design is envisioned, combining the requirements for Scuba Fish with the knowledge gained throughout the conception stage of the project.

A comprehensive design shall include onboard sensors for acceleration and depth, a transceiver for communication, and a camera for vision, optical flow and pictures, all powered by a LiPo battery and controlled by a microcontroller. For the sake of reliability regarding waterproofness as well as simplicity regarding the manufacturing, sealing of moving parts shall be avoided. Consequently, Scuba Fish shall be powered by one or more externally attachable propulsion systems consisting of coils and magnets. Further benefits of this propulsion strategy include minimal induction of oscillations to the main fish body and low-cost. Ideally, the coil could be used for wireless charging. Compactness, small size, and safety shall be achieved by diving a slightly positively buoyant Scuba Fish dynamically.

Altogether, Scuba Fish should be realizable for less than $ 100 a piece at a body length of around 140 mm including all fins. Maneuverability and velocity are estimated to fit the calm, clear, and shallow waters of coral reefs.

3 Validation of electromagnetic actuators

Electromagnetic actuators were identified as a low-cost and simple solution for propulsion. Similar propulsors are used by two more research groups to generate forward thrust. Clark et al.[5] study the thrust generation of different fin shapes and stiffnesses. Takada et al.[27] are interested into power efficient swimming.

A novel approach of combining several electromagnetic actuators to a highly-maneuverable yet miniature underwater robot was completed successfully for Scuba Fish.

This chapter follows the development process from the previous tethered and unconstrained swimming prototypes to an untethered fish enabled to conduct constrained maneuvers. An open-loop prototype based on Takada's [27] underwater robot was designed and evaluated. Furthermore, the prototype was equipped with two pectoral fins to test additional maneuvers.

3.1 Description of a first prototype with a Magnet-in-Coil propulsor

The first prototype using the same propulsion system as initially described by Takada et al.[27] is shown in Figure 23 (right). The fish-like robot has a length of 100 mm (without the caudal fin), a mass of 115 g, and it can swim at a maximum velocity of 8 cm/s for up to 40 min.

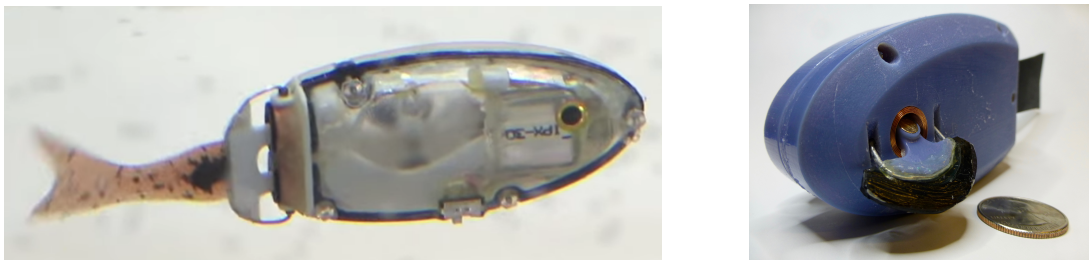

Figure 23: Left: Takada's fish in action. Right: Scuba Fish based on the same propulsion system with added pectoral fins.

The elliptical shape along the x-axis with a maximum hight of 60 mm was chosen in an attempt to minimize the drag in forward direction. The width of 26 mm was kept as low as possible for the same reason and for good dynamic stability.

3.1.1 Onboard electronics and further components of the prototype

The overall size of the prototype was largely constrained by the onboard electronics. The components of the robot fish are shown in Figure 24. In brief, the prototype contains a one cell LiPo battery, a microcontroller, two H-bridges mounted on stripboard, block weights for taring, a USB port for programming, external pins for charging and running, a servomotor to shift the center of gravity, two magnet-in-coil (MIC) propulsors as well as an exchangeable caudal fin.

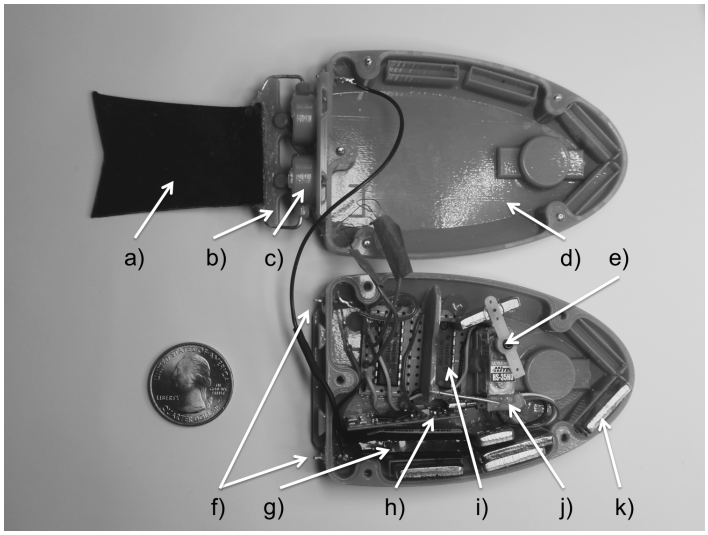

Figure 24: The configuration of a first MIC fish: a) exchangable caudal fin; b) flapping hinge hosting two magnets; c) propulsor block hosting two coils; d) two-sided hull, sealed with a rubber cord and tightened with bolts; e) servomotor with attached balancing mass, f) external pins for running and charging; g) 3.7V, 300mAh battery; h) Pro Micro 3.3V, 8MHz microcontroller; i) two H-bridges mounted on stripboard; j) USB port for programming; k) block weights for neutral buoyancy and taring of pitch and roll angles.

The 3-d printed hull was sealed with a silicone cord and tightened with five bolts. Having bolts allows to reopen the robot compared to the previously used adherent silicone rubber. However, opening is rarely necessary thanks to the external USB port. The lifetime of the silicone cord seal is limited to some 10 h of operation. Afterwards, it starts to become brittle and water enters the body. In order to eliminate the need for replacement of the silicone cord, the next iteration will have a 3-d printed gasket.

The electrical circuit of the prototype is depicted in Figure 25. For now, the electrical components were all soldered by hand. Once the circuit is final, a custom-made PCB will be designed.

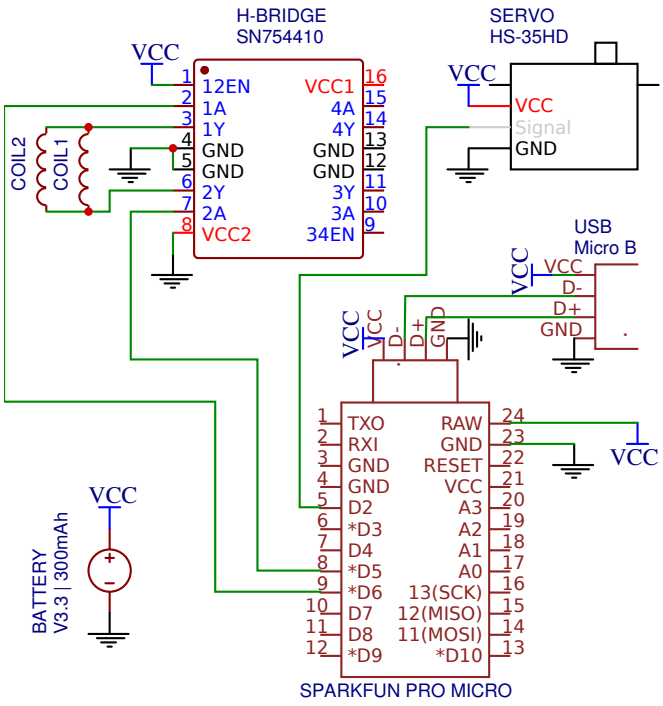

Figure 25: Schematic of the electrical circuit that includes two coils, two H-bridges, a servomotor, a battery, a microcontroller, and a USB port.

The electronics started to corrode after some 10 h of operation. Better sealing, silica gel, and an anti-corrosion coating shall mitigate this problem.

3.2 Evaluation of a first prototype with a Magnet-in-Coil propulsor

A first set of experiments included the measurement of swimming velocities and turning radii for different caudal fins. Figure 26 shows a set of different fins that was tested. The fins are easily exchangeable by connecting the ends of the hinge to the propulsion unit of the robot.

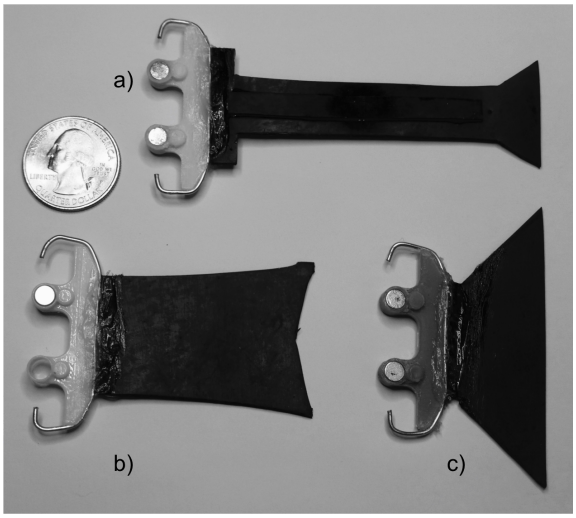

Figure 26: Caudal fins cut out of rubber sheets: a) tail fin; b) rectangular fin with a single magnet; c) trapezoidal fin.

The aim of the experiments was to gain insights into the impact of the shape of the caudal fin on the swimming performance. Three different fins were cut out of flexible rubber sheets with a thickness of 1.6 mm: A tail fin with a large length-to-width ratio as seen on Takada's fish (c.f. Figure 23), a rectangular fin, and a trapezoidal fin with a small length-to-width ratio.

Furthermore, a variation of the rectangular fin with a single magnet instead of two magnets was built. This fin allowed for a comparison of swimming velocities between one active MIC and two active MICs in line. Two active MICs should justify the doubled power consumption through superior swimming performances obtained in further experiments.

3.2.1 Theoretical thrust considerations for flapping fins

Several publications emphasize the importance of the flexibility of the caudal fin for effective thrust generation (see [9],[10],[15],[25],[27],[33]). A single instant of the fins repetitive flapping motion is shown in the left part of Figure 27. At the chosen instant, the blue fin rotates from the left to the right around a fixed dark blue pivot point. Each element of water (white) sees a force f by which it is displaced. The integration over the surface of the fin delivers the total instantaneous force F. According to Newton's third law, the robot sees the same force F it exerts on the water in opposite direction.

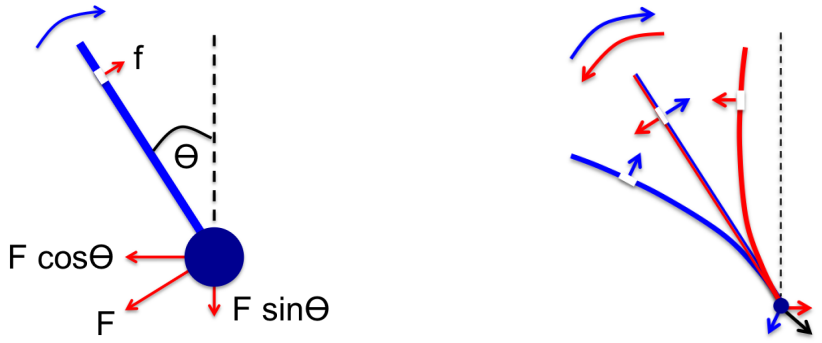

Figure 27: Left: The instantaneous thrust force generated by a flapping fin. The fin is depicted in blue, the pivot point, which is fixed to the body, is in dark blue, and all force vectors are in red. Right: A stiff fin (straight) compared to a flexible fin (bent) at the same point of the path back (red) and forth (blue).

Depending on the instantaneous angle θ, part of the force F, namely $F \cdot \sin\theta$, contributes to the desired motion in x-direction. The other part, $F \cdot \cos\theta$, tries to move the robot in y-direction. Therefore, it is important that the robot's shape has a low drag coefficient along the x-axis but a high drag coefficient along the y-axis. Such a shape allows the desired forward motion (surge) while offering resistance to the unwanted sidewards motion (sway).

The integration of all instantaneous forces F over the time of one flapping cycle finally leads to the net force driving the robot. A snapshot of one instant is shown in the right part of Figure 27. The fin on the way from the left to the right and its respective forces are drawn in blue. The fin on the way from the right to the left and its respective forces are shown in red. **In the case of a completely stiff fin, all instantaneous forces are symmetric. They cancel each other and provide zero net thrust force. In the case of a flexible fin, the bent axis of the fin changes the directions of the force vectors and allows for a positive net thrust force.** The net thrust force of the flexible fin is the sum of all blue and red vectors. For the depicted instant, it is shown in black at the pivot point.

The reason why a flexible fin bends with increasing distance from the pivot point lies again in Newton's law: The motor torque provided on the pivot point equals the sum of all forces along the fin times their respective distances from the pivot; the further away from the pivot the higher the force on a given fin

element. In other words, the further away a fin element is from the pivot the more distance it has to travel during the same time interval, resulting in higher drag forces on the element. Consequently, the fin bends towards its tip.

3.2.2 Introduction of indicators from fluid dynamics for the evaluation of swimming performances

Two indicators from fluid dynamics were chosen to assess the designs and the swimming performances of the developed prototypes:

1. The **Reynolds number** was used as one estimator on how big the potential impact of shape optimization on the swimming performance could be. Loosely speaking, the shape of an object moving in a fluid is of little importance at low Reynolds numbers ($Re < 3 \cdot 10^5$, laminar flows, e.g. mosquitos, c.f. [20]). However, it is of great importance at high Reynolds numbers ($Re > 3 \cdot 10^6$, turbulent flows, e.g. aircrafts). The Reynolds number calculated in Equation 3.1 with the parameters of the current Scuba Fish led to the conclusion that shape optimization is not crucial.

$$Re = \frac{\rho \cdot v \cdot L}{\mu} = 8000 \tag{3.1}$$

   Parameters: density of the fluid (water at 293 K) $\rho = 1000\,\frac{kg}{m^3}$; velocity of the robot relative to the fluid $v = 0.08\,\frac{m}{s}$; characteristic linear dimension of the robot (length) $L = 0.1\,m$; dynamic viscosity of the fluid (water at 293 K) $\mu = 0.001\,Pa \cdot s$.

2. The **Strouhal number** is used to describe oscillating flow mechanisms like the flapping fin of an underwater robot. Anderson et al.[1] estimated the optimal production of thrust and high efficiencies for oscillating foils at Strouhal numbers in the range of 0.3 to 0.4. Equation 3.2 was used to calculate the Strouhal numbers for Scuba Fish at different oscillation frequencies.

$$St_{TE} = \frac{f \cdot A_{TE}}{U} \qquad [\text{-}] \tag{3.2}$$

Parameters: fin frequency $f\,[Hz]$; total excursion of the trailing edge of the foil (fin amplitude) $A_{TE}\,[m]$; flow velocity (velocity of the robot relative to the fluid) $U\,[\frac{m}{s}]$.

Another indicator, a propulsive performance index S_w for robotic fish, was proposed by Nagai et al.[19]. S_w is the ratio of the distance swum during one oscillation period of the caudal fin to the length of the fish (see equation 3.3). The swimming velocity is denoted by v, the oscillation frequency by f, and the length of the fish by L. Larger values of S_w indicate more efficient swimming. The indicator allows for comparisons among different body lengths and includes the power consumption (which scales with frequency as explained later on).

$$S_w = \frac{v}{f \cdot L} \qquad [\text{-}] \quad (3.3)$$

3.2.3 Swimming velocities for four caudal fin designs at different oscillation frequencies

Four different caudal fins were run at the same maximum amplitude λ of 16 ° and for the same set of frequencies f between 1 Hz and 3 Hz. Three videos at each frequency for each fin were taken from above. The measured and averaged swimming velocities are illustrated in Figure 28. Standard deviations below 0.7 occured mainly because the open-loop fish never followed the exact same trajectory twice.

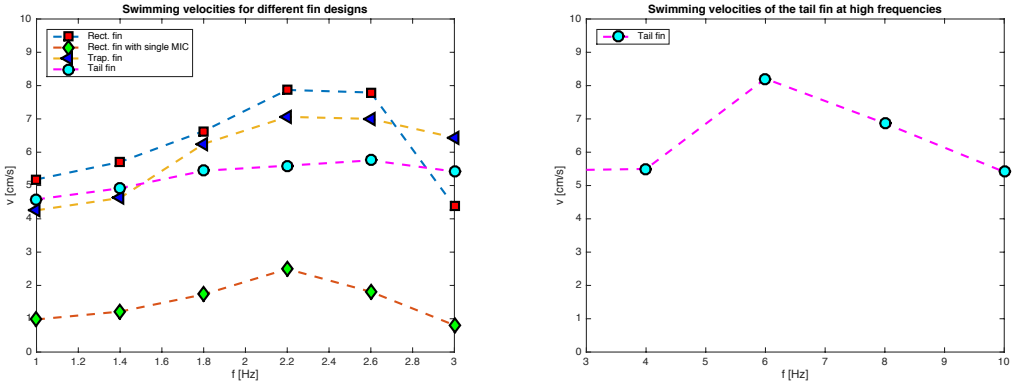

Figure 28: Left: Swimming velocities v for four different fin designs at frequencies f between 1 Hz and 3 Hz. Right: Swimming velocities v for the tail fin at high frequencies f between 3 Hz and 10 Hz.

The best result regarding swimming velocity in the frequency range of 1 Hz to 3 Hz was achieved with a rectangular fin at 2.2 Hz (c.f. Figure 28, left plot, Rect. fin). Generally, the swimming velocities of all shapes were close. The only slow performance resulted from an experiment with one active MIC instead of two (c.f. Figure 28, left plot, Rect. fin with single MIC).

While the rectangular and the trapezoidal fins showed decreasing velocities above frequencies of 2.2 Hz, the tail fin was running up until 10 Hz (cf. Figure 28, right plot). The tail fin set the velocity record of all tested fins at nearly 8.5 cm/s for a frequency of 6 Hz.

Prior to optimization, this current maximum swimming velocity v of around 8.5 cm/s is in between Takada's [27] 12 cm/s fish with two MICs and Clark's [5] 4 cm/s fish with a single MIC. The fishes featuring servomotors of Porfiri [10] and Takada [38] (two servomotors for propulsion) as well as Jessiko[11] reach velocities of 10 cm/s, 11 cm/s, and 20 cm/s respectively. Expressing swimming velocities in body lengths per second (BL/s), none of the mentioned fish goes above 1 BL/s whereas the current Scuba Fish design swimms at roughly 0.9 BL/s. It is noteworthy that the power consumptions to reach these velocities are unknown.

Considering power consumption, the actuation principle of the magnet-in-coil propulsor has to be explained in further detail. The coil can either be fully on, drawing a current and consuming power respectively, or fully off. This bang-bang control is executed by an H-bridge. During the on-state, a magnetic field is generated. The field strength is given by the coil specifications and cannot be controlled. In other words, the magnet inside the coil always sees the same acceleration during on-states. During the off-state, no magnetic field is generated. Thus, the controllable parameter is the interval during which the magnetic field is active. The interval of the magnetic field can be exploited for two purposes. First, to set a desired frequency at which the fin is flapping by alternating current directions for corresponding intervals. Second, to optimize power consumption by limiting the intervals at which current is drawn. As soon as the magnet reaches one end of its travel, the coil can be switched off. Power can be saved while the loaded fin continues to move. Once the fin reaches the end of its respective travel as well, the coil can be switched on again in reverse direction. Consequently, the **power consumption scales in direct proportion to the frequency of the**

[11] `www.robotswim.com`

oscillation. As a result, higher swimming velocities generally come at the price of higher power consumptions.

Turning with caudal fins works similarly. Swimming a curved trajectory requires a biased flapping motion of the fin. The fin oscillates around an angular offset from the x-y-plane. The interval of the on-state is set narrowly enough such that the fin does not have enough time to travel the full amplitude. At half way for example, the magnetic field is already inversed and the fin goes back the other direction. The occuring asymmetry causes the fish to turn. **The option to bias the oscillation offers two degrees of freedom (x and yaw) with a single propulsor.**

Another unintentional reason why a fin might not travel the full amplitude are excessive frequencies. If the frequency is chosen too high for a given fin geometry, the fin tip might not make it the full way before the magnetic field is inverted again. This effect, defined as overload within this thesis, results in drastic losses of thrust and velocity. Therefore, **the ideal fin geometry for a given propulsor is the one which almost makes the fin overload for a desired maximum frequency**. The propulsor does not waste excessive power and the fin generates the maximum possible impact on the water.

The overload frequency for a given propulsor and a given fin can be found empirically by analyzing the individual frames of swimming videos. In the following, the video frames of selected fins at selected frequencies were evaluated to gain further evidence on the swimming behavior shown in Figure 28. The evaluation explains why the rectangular and the trapezoidal fin overload at 2.6 Hz but the tail fin runs most efficiently at 6 Hz.

All videos were taken at 30 frames per second (FPS). The pictures in Figures 29 to 34 are arranged from the top left to the bottom right corner. The first frame is the top left one at 1/30 s, the second frame is the second picture in row one at 2/30 s and so on. The total number of pictures shows one flapping cycle. The number varies among the Figures and equals 30 FPS over the depicted frequency. The first picture of the subsequent cycle was always added to allow for the comparison with the initial state in the top left picture.

Figure 29 shows the single frames of the **rectangular fin at a frequency of 2.2 Hz**. The flapping cycle was in good resonance with the applied frequency. The fin had time to fully bend but was driven fast enough that each frame shows

it at a different point along its trajectory. A swimming performance of 8 cm/s resulted at a Strouhal number of 1.2 and a propulsive performance index S_w of 0.36.

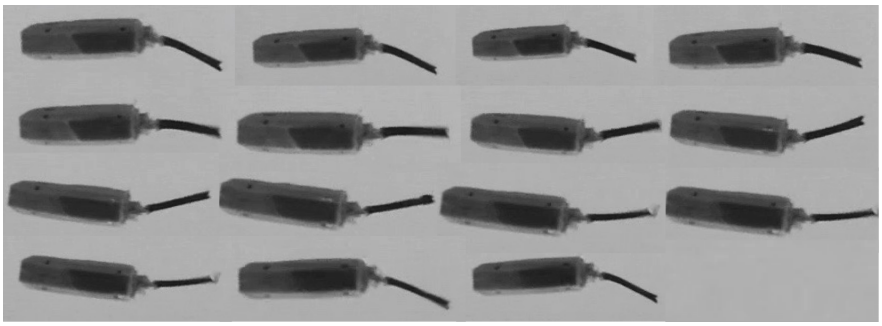

Figure 29: Rectangular fin at a frequency of 2.2 Hz. Single frames at intervals of 1/30 s, top left to bottom right.

The same **rectangular fin at the same frequency of 2.2 Hz** but **with a single active magnet-in-coil propulsor** is shown in Figure 30. Evidently, the amplitude of the fin tip was smaller compared to the double propulsor in Figure 29. The acceleration of a single MIC was too low to make the fin travel the full amplitude. A lower velocity of 2.5 cm/s at a Strouhal number of 2.2 and an S_w value of 0.11 occured. The doubled power consumption of the propulsor with two MICs is justified by the difference in velocities. It has to be said that neither the coil nor the magnet were optimized with respect to the achievable acceleration. Increasing the acceleration provided by a single MIC would be feasible by increasing the size of the coil and the magnet.

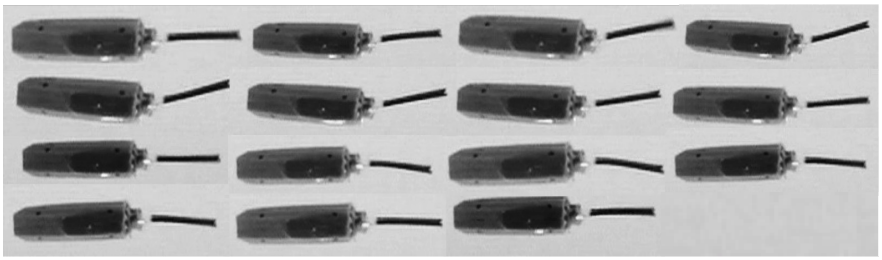

Figure 30: Rectangular fin with a single MIC at a frequency of 2.2 Hz. Single frames at intervals of 1/30 s, top left to bottom right.

Figure 31 shows the **rectangular fin at a frequency of 3.0 Hz**. Again, the amplitude of the fin tip was smaller compared to the frequency of 2.2 Hz depicted

in Figure 29. The fin overloaded because the acceleration from the propulsor was insufficient to make it travel the full amplitude in the given time interval.

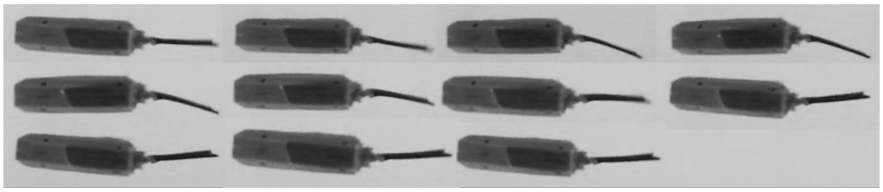

Figure 31: Rectangular fin at a frequency of 3.0 Hz. Single frames at intervals of 1/30 s, top left to bottom right.

Similar results leading to the same conclusions were observed with the trapezoidal fin. The maximum swimming velocity of 7.1 cm/s for a trapezoidal fin was reached at a frequency of 2.2 Hz. The Strouhal number was 0.93. An S_w value of 0.32 was derived.

Different observations were made on the tail fin. Unlike the other fins, the tail fin did not start to overload at some 2.6 Hz but added harmonics to its flapping motion. Figure 32 shows the **tail fin at a frequency of 1.0 Hz**. Clearly, the potential for maximum velocities was not used a such low frequencies. The fin stayed at very similar points of its trajectory for several frames along one cycle. The swimming velocity was 4.5 cm/s.

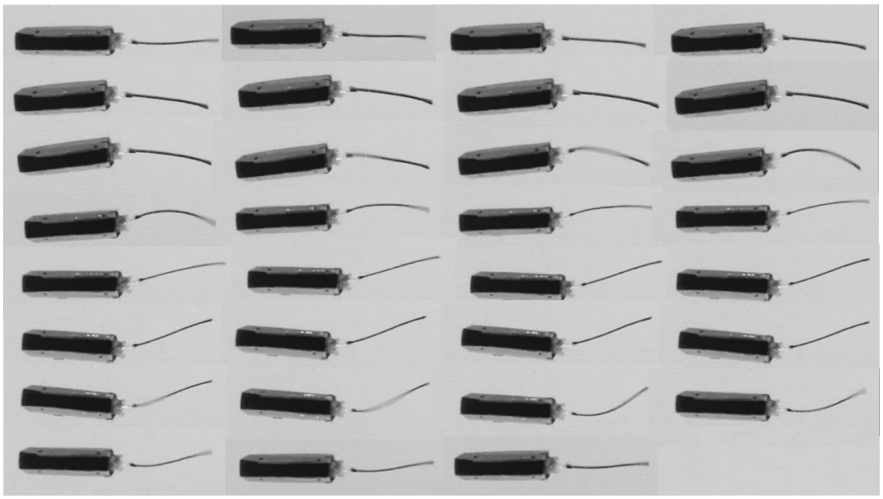

Figure 32: Tail fin at a frequency of 1.0 Hz. Single frames at intervals of 1/30 s, top left to bottom right.

Figure 33 shows the **tail fin at 6 Hz**. The fin reflects a first harmonic in resonance with the applied frequency. Comparing the way the fin bent to the rectangular fin at 2.2 Hz in Figure 29 it could be evaluated whether the the sum of all force vectors from each fin element was bigger. The swimming velocity of 8.5 cm/s is the highest which was reached with the current set of fins.

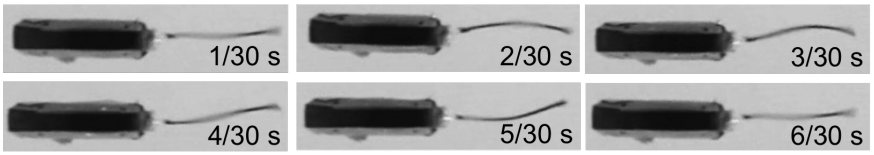

Figure 33: Tail fin at a frequency of 6 Hz. Single frames at intervals of 1/30 s, top left to bottom right.

The **tail fin at a frequency of 10 Hz** is shown in Figure 34. A second harmonic is identifiable. The deflection of the fin looks smaller compared to Figure 33. The motion observed in the video resembled more a vibrating tail than a flapping fin. The swimming velocity dropped to 5.5 cm/s. It might be that adding harmonics flattens the deflection of the fin and therefore decreases its thrust generation.

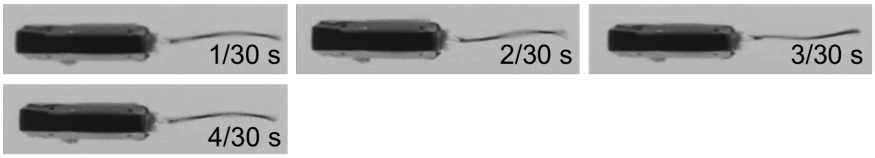

Figure 34: Tail fin at a frequency of 10 Hz. Single frames at intervals of 1/30 s, top left to bottom right.

3.2.4 Maneuverabilities for different fin configurations

The maneuverabilites of the tested set of fins are illustrated in Figure 35. The tail fin was too long and too flexible to provide any turning radius at all. The rectangular fin allowed to turn at a radius of 30 cm. The shorter trapezoidal fin brought that radius down to 10 cm or one body length respectively. Adding pectoral fins and turning without activating the caudal fin increased the maneuverability again. At a turning radius of 5 cm, which is below one BL, turn-on-the-spot (ToS) was well approached.

The observed range of pitching angles was between -12 ° and +12 °. The angles are shown on two prototypes in Figure 35. The prototypes and the circles were downscaled by the same factor to illustrate the turning radii compared to the size of the fish.

Pitching was achieved by shifting the CoG: A 10 g mass attached to a 9 mm lever was moved by a servomotor. At an angle of 12 °, gaining 1 m in depth would still require some 4.7 m of horizontal distance to be travelled. Increasing the pitching angle is feasible by increasing the lenght of the lever or the mass attached to it. Both measures require extra space inside the robot.

Pitching with the help of the pectoral fins showed to be ineffective. The effect of both pectoral fins running simultaneously on the pitch angle was intermittent only.

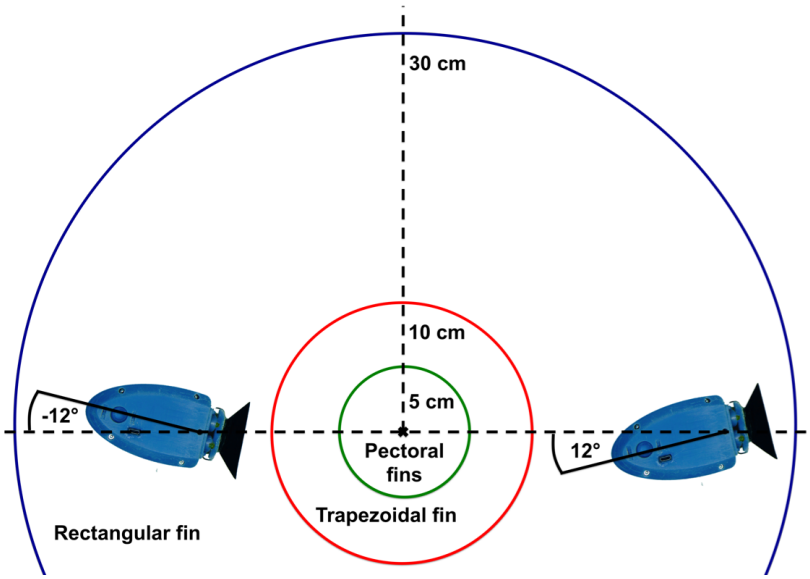

Figure 35: True-to-scale chart of turning radii for different fins, and of the pitch angle range for a servomotor. The outer blue circle shows the radius of the rectangular fin, the middle red circle the one of the trapezoidal fin, and the inner green circle shows the radius realized using the pectoral fins. The maximum pitch angles achieved by changing the CoG are shown on true-to-scale pictures of the robot.

3.2.5 Concluding summary on the swimming performances

The follwing conclusions were drawn from the experiments with a first open-loop prototype:

1. **Higher swimming velocities are reached with higher oscillation frequencies (up to an overload point) at proportionally higher power consumptions**. Consequently, the desired velocity has to be weighed up by its required power consumption. For example, the marginal velocity gain of 0.5 cm/s of the tail fin at 6 Hz compared to the rectangular fin at 2.2 Hz might not be worth the almost trippled power consumption.

2. The ideal geometry of the caudal fin for a given propulsion system and a desired range of frequencies can be found empirically by increasing the size until the fin reaches its overload point.

3. The turning radius achieved by biasing the movement of the caudal fin seems to be related to the length of the caudal fin. Shorter fins allow for narrower turning. At the same time, the shorter trapezoidal fin showed slightly inferior velocities compared to the rectangular fin. There is a trade-off between the maximum velocity and the minimum turning radius.

4. Diving with the help of a servomotor that changes the CoG and the pitch angle respectively requires long horizontal distances to gain depth. Diving with the help of the pectoral fins showed to be ineffective.

5. The double propulsor featuring two MICs in line was superior to a single MIC. It showed to be the right choice for the main propulsion system of the current prototype.

6. The Strouhal numbers were too high for an optimal generation of thrust according to Anderson et al.[1]. They can be reduced by increasing the swimming velocity, e.g. through shape-wise drag reduction, or by decreasing either the oscillation's amplitude, the frequency, or both. In our case, sacrificing velocity for lower frequencies would bring down the Stouhal number as well. Generally, Strouhal numbers are used for foils that are heaving and pitching, whereas our fin is only pitching. This might be an explanation for the lower efficiencies reflected by higher Strouhal numbers.

The next iteration incorporates all these findings to a closed-loop fish with enhanced maneuverability.

4 Development towards a swarming Scuba Fish

A swarm-enabled underwater robot has to be autonomous and intelligent regarding its swimming behavior as well as highly-maneuverable. To meet these goals, the swarming Scuba Fish was equipped with a microcontroller, an IMU, pressure sensors, a transceiver, batteriers, and several propulsors. It can operate autonomously or receive commands through its transceiver (see Appendix C.2.2). The transceiver sends sensor data to a mission control where they can be visualized in real time (see Appendix C.2.1).

This chapter shows a first closed-loop fish with enhanced maneuverability thanks to an added dorsal fin.

4.1 Design of a highly-maneuverable Scuba Fish

The shape of the latest Scuba Fish is based on the intersection of three ellipses. First, it is streamlined along the x-axis to provide minimal drag in forward direction. Second, it is slim along the z-axis to enable vertical diving. Third, it has the largest cross-sectional area along the y-axis for two main reasons: to withstand unwanted yaw-motions induced by the torques coming from the oscillation of the caudal fin while swimming forward, and to achieve good roll stability by placing the center of gravity as low as possible.

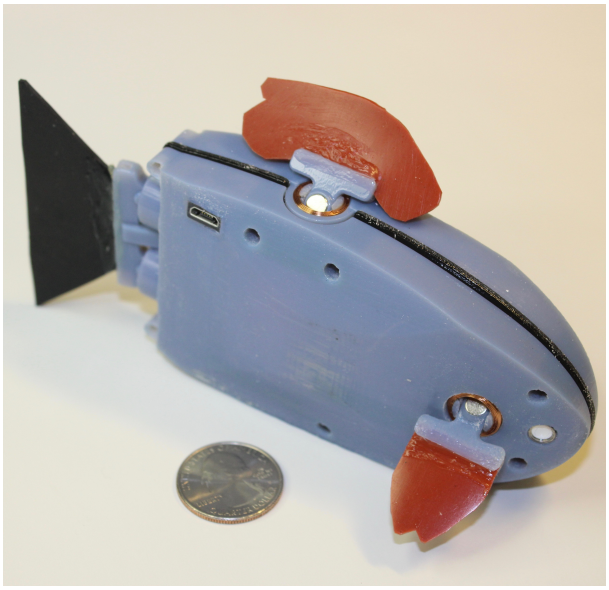

Figure 36: The latest prototype of Scuba Fish.

Two versions of the latest Scuba Fish were created. The smaller one has a volume of $100\,cm^3$. The larger one has a volume of $125\,cm^3$. The smaller version was right on the edge of miniaturization for the currently required carrying capabilities. The mass in g, which is equivalent to the volume in cm^3 [12], closely matched the accumulated mass of all components. Therefore, it left hardly any room for trimming towards good roll stability and a neutral pitch angle. Three rules of thumb were based on the previous design experience. First of all, the volume of the fish should be 1.5 times larger than the volume of all components together to allow for good placing and assembly of components. Secondly, the mass of the fish should surpass the mass of all components by 20 % to make the placement of additional trimming masses possible. Thirdly, heavy components like batteries should be spread along the lower belly of the fish to provide good roll stability.

Improved design features on the latest prototype include smaller pectoral and dorsal propulsors, a simplified caudal propulsor, an exchangeable 3-d printed gasket, and mounts for all electric components. The new pectoral and dorsal propulsors avoid a hinge mounted on the outside of the coil. Their mounting is installed inside the coil, allowing for smaller size. The gasket is made out of a printed stiff layer sandwiched between two Shore 40 flexible layers.

4.1.1 Dorsal fin for vertical diving

Previous iterations showed bad performances on diving by changing the pitch angle. Consequently, the servomotor used to shift the center of gravity was replaced by a dorsal fin used for the generation of thrust for vertical diving. The degree of freedom was changed from angular roll to linear z. Gaining depth while moving forward is still possible by activating the caudal and the dorsal fin simultaneously. Additional hoover capabilities were gained. Furthermore, the removal of the servomotor allowed for cost and size reductions. However, directional sensors at the nose of the fish (e.g. cameras) cannot be tilted easily anymore. Intermittent tilting can potentially be achieved with the help of the pectoral fins.

Scuba Fish is a slightly positively buoyant robot. It ascends to the surface whenever no actuation of the dorsal fin takes place, thus also in emergency situ-

[12] The volume of the submerged fish replaces water. $1\,cm^3$ of water has a mass of $1\,g$.

ations such as when the signal is lost or the batteries are used up. The actuation of the dorsal fin causes the robot to dive vertically at around 3.5 cm/s.

4.1.2 Closed-loop control with an IMU and two pressure sensors

Scuba Fish has a pressure sensor on each side of its nose (see Figure 37). They are mounted at an 18 ° angle from the x-z-plane. Their primary purpose is depth control. However, having two of them it is theoretically possible to identify pressure gradients caused by any kind of static or moving sources, to avoid obstacles by analyzing the pressure reflections from the flapping fins on nearby walls, and to fuse pressure values with the IMU data to obtain better closed-loop control and more accurate localization estimates.

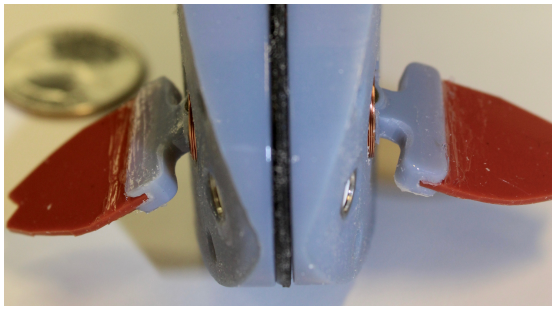

Figure 37: Pressure sensors for depth control and obstacle avoiding.

The IMU measures linear accelerations and angular velocities. A magnetometer on the same board captures the magnetic field around the fish. The IMU data is mainly used for closed-loop control. It can possibly be used for localization if corrected with external measurements in oder to cancel the additive errors from the integration over time. If used for localization, the IMU raw values have to be calibrated with measured distances from video data. The magnetometer is potentially unusable because it is mounted in the middle of five moving magnets.

4.1.3 Communication through a transceiver

For now, Scuba Fish uses its transceiver to communicate with an external mission control. Sensor data from the IMU and the pressure sensors can be sent to a second transceiver which is connected to a computer via another microcontroller. The data can be read from the COM port and visualized with MATLAB in real

time (see Appendix C.2.1). The transceiver is also the only possibility to log measurement data as the microcontroller on Scuba Fish does not have writing capabilities.

In the other direction, locomotion commands can be sent to Scuba Fish. MATLAB supports gamepads like the Xbox controller. Scuba Fish can be remote controlled for demonstration purposes. A first implementation of a keyboard controller is shown in Appendix C.2.2.

4.2 A decoupled propulsor for maximum modularity

A swarming Scuba Fish does not only have to be functional as a single robot, it has to offer high manufacturability and operability in a collective. A decoupled propulsor (see Figure 38) was designed in an approach to further simplifiy the design. The decoupled propulsor can be modularly attached to any location on the robots hull. Preferably, it is plugged into a socket to minimize drag. The propulsor is completely submersible. The modularity offers three advantages. First, broken propulsors can be replaced. Second, the modular propulsor can be used standalone to test fins without the need for Scuba Fish. Third, the manufacturing process is decoupled and simplified. High accuracy is only required for the functional propulsor. The hulls of Scuba Fish can be molded at lower costs.

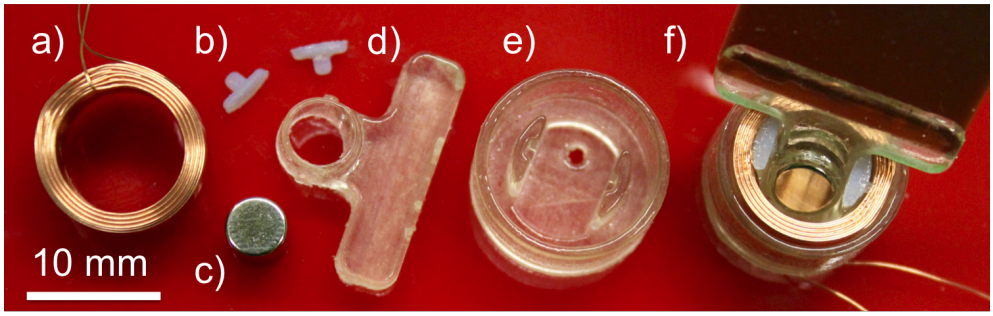

Figure 38: Modular propulsor: a) electromangetic coil; b) plugs that hold the hinge in place; c) permanent magnet; d) flapping hinge with mounts for the magnet and for a fin; e) propulsor hull with mounts for the coil, for the hinge, and with a hole for the power cables; f) the assembled propulsor.

4.3 Review of the design process

The evolution of Scuba Fish is shown in Figure 39. An iterative design process allowed to incorporate learnings from previous iterations to improve all the following designs.

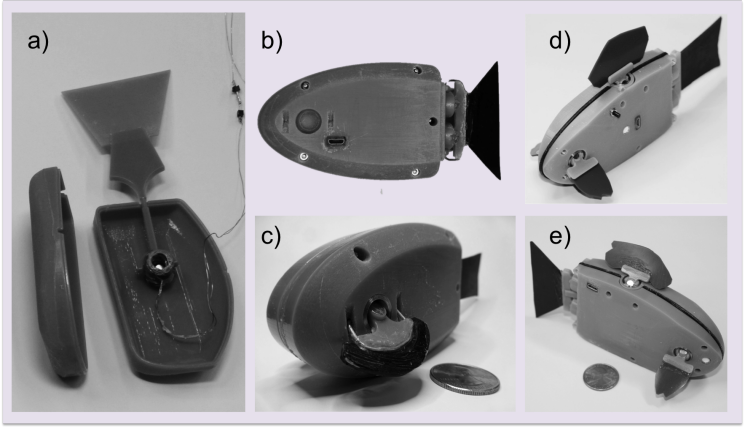

Figure 39: Evolution of Scuba Fish: a) concept study (CS), inspired by Hexbug's Aquabot; b) H1.0, inspired by Takada et al.[27]; c) H1.1, modified from H1.0; d) R1.0, the first vertical diver; e) F1.0, the latest version.

The features of the designs depicted in Figure 39 are specified in Table 3.

Design (c.f. Figure39)	CS (a)	H1.0 (b)	H1.1 (c)	R1.0 (d)	F1.0 (e)
Unthethered	✗	✓	✓	✓	✓
Closed-loop	✗	✗	✗	✗	✓
Forward swimming	✓	✓	✓	✓	✓
Forward turning	✗	✓	✓	✓	✓
Turn-on-the-spot	✗	✗	✓	✓	✓
Pitching	✗	✓	✓	✗	✗
Vertical diving	✗	✗	✗	✓	✓
Modular propulsor	✗	✗	✗	✓	✓
Streamlined shape	✗	✗	✗	✓	✓
Resealable hulls	✗	✓	✓	✓	✓

Table 3: Evolution of Scuba Fish. Design features at a glance.

Experiments with the latest version F1.0 of Scuba Fish are shown in Chapter 5.

5 Experiments with Scuba Fish

The following experiments are intended to outline preliminary underwater locomotion and navigation capabilities of Scuba Fish. All of the presented experimental data originate from test runs with the latest Scuba Fish as of April 2016.

This chapter explains the experimental setup and introduces a first selection of underwater maneuvers.

5.1 Experimental setup and test scenarios

The prototypes were tested in a 61 cm by 122 cm by 61 cm fish tank filled with fresh water (see Figure 40). One wall on each axis was covered with white corrugated plastic sheets in order to track the swimming robots more easily. The tank is placed on a cushioning foam mat on top of a wheeled cart. No filtering system is required. However, 20 % of the water has to be replaced once a month.

A high resolution camera installable on each axis of the tank allows to take videos of the swimming robots. Analyzing the video frames offers insights into the swimming behaviors. Video data can be evaluated and compared to onboard sensor data from the robot. This way, sensor data can be calibrated and validated. A blob detector in MATLAB tracks the movement of the fish. It is described in Appendix C.2.3.

Figure 40: Testing environment for Scuba Fish.

First experimental aspirations included constrained swimming along a line at constant depth and swimming towards a pressure source. Maintaining a constant

depth, swimming in a line, and aligning with a pressure source were shown to be feasible in air. Swimming in a line was also proven in water. The other two experiments had to be postponed due to problems with leaks and the communication via the transceiver.

5.2 Maintaining a constant diving depth

Maintaining a constant depth is a useful ability if it comes to swimming in a collective. It allows to reduce the complexity in coordinating a collective from a 3-d to a 2-d problem.

Designing Scuba Fish close to neutral buoyancy is important to minimize the control effort and the power consumption respectively. While diving, positive buoyancy has to be overcome by the thrust provided by the dorsal fin.

A bang-bang controller with hysteresis was implemented to maintain a constant depth using at least one pressure sensor. The desired pressure lies in between two thresholds. The dorsal fin is activated above a lower pressure threshold. The fish starts to dive due to the vertical thrust generated. The dorsal fin is deactivated below an upper pressure threshold. The fish starts to ascend because it is positively buoyant. The principle is illustrated in Figure 41.

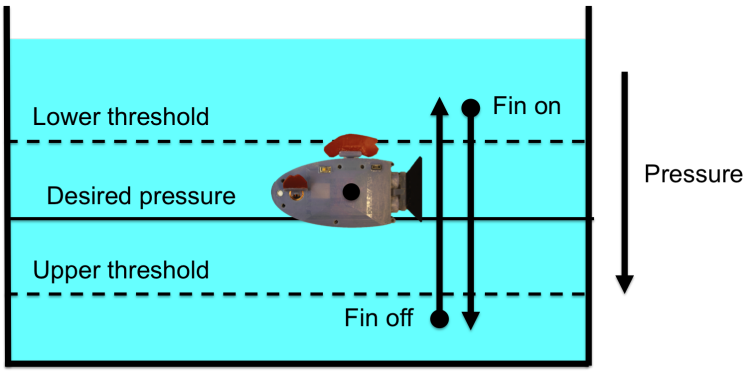

Figure 41: Diving at a constant depth.

The control software is shown in Appendix C.3.1. The maneuver was validated in air. An autonomous experiment in water failed due to leaks in the robot's hull. Water entering the robot constantly changed its buoyancy. An assisted test run where the vertical movement of the robot was simulated by hand showed the expected fin states for the dorsal fin (on/off). The parameters in water were:

lower threshold $thres_{low} = 102300\,\text{Pa}$; upper threshold $thres_{high} = 102500\,\text{Pa}$; desired pressure $p_{des} = \frac{thres_{high} - thres_{low}}{2} = 102400\,\text{Pa}$. The desired pressure is equivalent to a diving depth of around 10 cm below the water surface (depending on the time-dependent ambient pressure).

Both, the validation in air and the test run in water were captured on video. The videos can be seen on the project's data disk.

5.3 Swimming in a straight line

Swimming in a straight line is hardly possible open-loop. Assembly imperfections make Scuba Fish yaw. External disturbances may cause the same effect. The yaw angle velocity provided by the gyroscope was used to implement an I controller.

In a first step, the yaw angle velocity was integrated to get the yaw angle. Then, the yaw angle was further integrated for two reasons. Firstly, yaw angles occuring as a side-effect of the undulatroy forward motion should not provoke control action. They cancel each other if integrated (c.f. Figure 44). Secondly, the integration of the yaw angle defines an acceptable bandwidth from the nominal trajectory. A small yaw angle for a long time just as well triggers a control output like a large yaw angle for a short time. The integration of a constant velocity vector v at a constant and small yaw angle γ from the nominal trajectory delivers a relation for the magnitude h of the bandwith (c.f. polar coordinates):

$$h = \int_0^T v \cdot \sin(\gamma) dt \approx \int_0^T v \cdot \gamma dt = T \cdot v \cdot \gamma = d \cdot \gamma$$

The small-angle approximation for γ and the assumption of a constant velocity v are valid for small bandwiths and a small h respectively. The bandwidth is a tunable control parameter.

Considering any yaw angle but zero to be an error, this is an I controller. The concept is shown in Figure 42.

The control output is reinforced linearly with the exceedance of the acceptable bandwith. The control output is a flapping pectoral fin at increasing frequencies in order to generate more thrust.

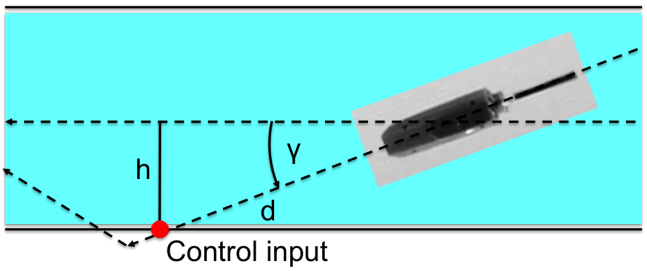

Figure 42: Swimming in a straight line.

The controller was evaluated with an experiment in water. The swimming trajectory of a test run in the tank is shown in Figure 43. The fish deviated some 7 cm from its initial course over a distance of 80 cm in forward direction. Neither the tank length nor the number of test runs were sufficient to draw tangible conclusions. Three explanations for the deviation are possible. Firstly, the occuring deviation reflected the best possible performance the fish can achieve at the chosen control parameters. Secondly, the initial condition of the fish was already misaligned to the straight line, i.e. the fish wanted to follow a different line than planned. Thirdly, the gyrometer inside the fish was not perfectly aligned with the coordinate system of the fish. In any case, deviations over long distances will occur as IMU errors are additive. The performance can be improved by using further information, e.g. the y-acceleration to compensate for drift.

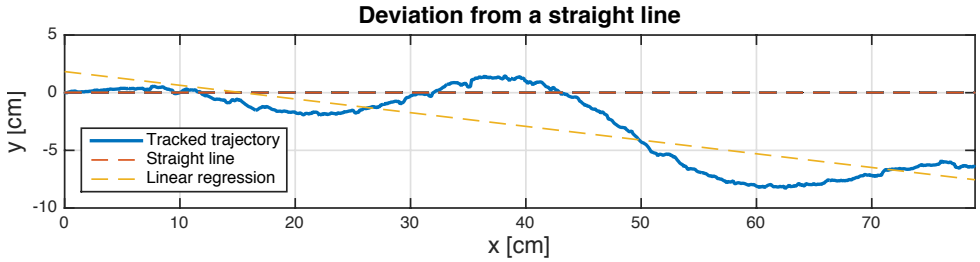

Figure 43: Scuba Fish trying to swim in a straight line using the pectoral fins for corrections.

To be more clear about the swimming performances of the robot, the IMU has to be calibrated in separately designed experiments. This can be done by comparing IMU values to external tracking values.

The comparison of onboard measurements with externally tracked values is shown in Figure 44 for the case of the yaw-angle. Both plots are unfiltered. The

upper one shows the raw values obtained by integration of the yaw-velocity from the gyroscope. The lower plot shows the yaw-angle read from the tracking video.

The plots qualitatively agree. A slight phase shift might have occured during the post-processing of the data due to different start times.

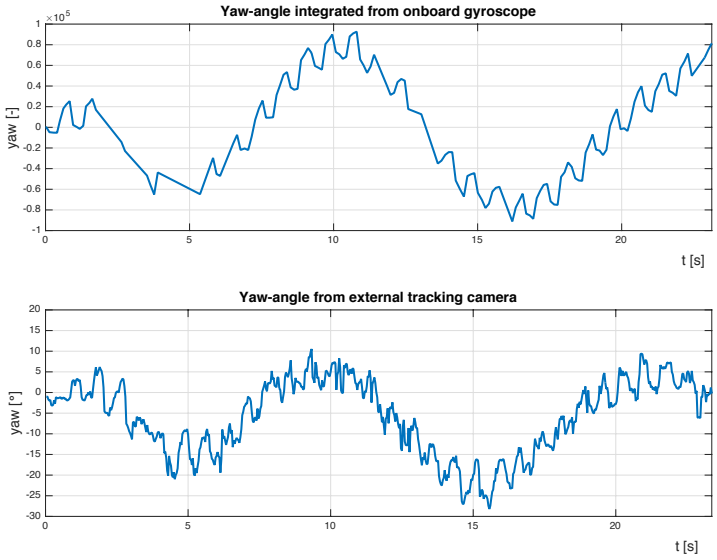

Figure 44: Comparison of the yaw-angles from the gyroscope and from the external camera observations.

Not to be confused with noise is the overlay of the yawing due to the oscillation of the caudal fin. The caudal fin was oscillated at a frequency of 1.25 Hz for this experiment. Evidence of the overlay is most easily observed in the section between $t = 15\,\mathrm{s}$ and $t = 20\,\mathrm{s}$ in the upper plot of Figure 44. The 5 s section shows 6 periods, corresponding to a frequency of $6/5\,s = 1.2\,\mathrm{Hz}$.

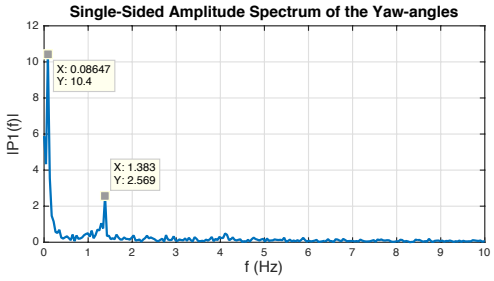

Figure 45: Frequency spectrum analysis of the observed yaw-angles.

A spectrum analysis of the yaw-angles confirms the observation of the yawing. The higher peak in Figure 45 belongs to the slower control periods. The lower peak represents the faster yawing periods.

The control input is compared to the control output in Figure 46. Conclusions for the tuning of control parameters can be drawn. The yaw integral causes control action whenever it leaves the dashed deadzone. The respective pectoral fin makes the fish start yawing in the opposite direction and drives the integral back towards the deadzone. The yaw integral largely overshoots. Consequently, the control output has to be reinforced by running the fins at higher frequencies.

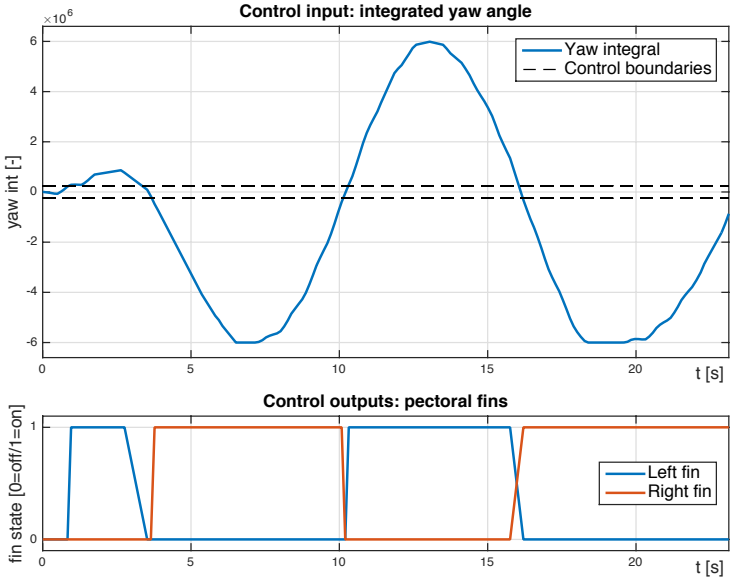

Figure 46: Control input versus control output.

A modified version of swimming in a straight line might mitigate the yawing occuring as a side-effect of the undulatroy forward motion. At a very narrow bandwidth h, the respective pectoral fin would be activated at every caudal fin kick in order to cancel the induced yaw moment. Such a reduction in yawing would potentially lead to an increase in forward velocity at the cost of additional power consumption.

Control using the values of IMUs is faced by additive errors. Significant drift may occur if the IMU cannot be corrected with external measurements from time to time.

The control algorithm for this experiment is shown in Appendix C.3.2.

5.4 Swimming towards a pressure source

Most importantly, swimming towards a static pressure source allows for homing after an expedition involving several robots. The robots swim towards a base station where they are collected all at once. Furthermore, swimming towards a static pressure source simulates the hunt for prey of living fish. Following a dynamic pressure source is an example for a fish following another fish.

The first subproblem is aligning with a pressure source. Scuba Fish has a pressure sensor on each side of its nose (c.f. Figure 37). The readings of the pressure sensors are compared and driven to a zero difference. The pressure value is assumed to be higher on the side of Scuba Fish facing the source. The opposite pectoral fin has to be activated to induce a rotation (see Figure 47). A P controller with sufficient settling time was implemented to solve this subproblem.

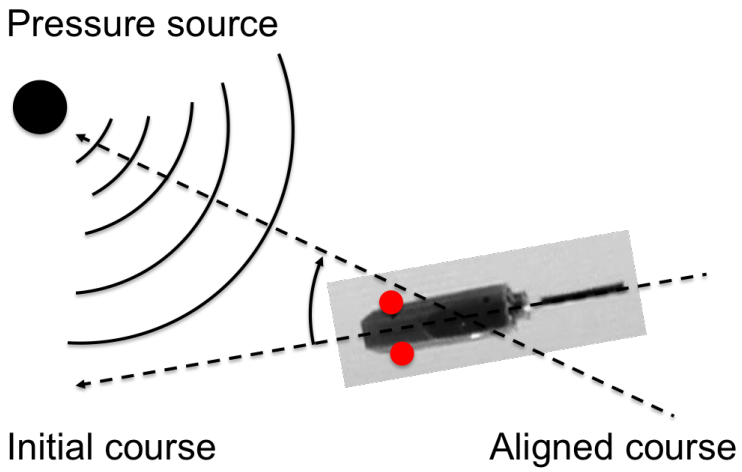

Figure 47: Swimming towards a pressure source.

The second subproblem is swimming towards a pressure source once aligned. The previously discussed algorithms for maintaining a constant depth and for swimming in a straight line can be used to address this subproblem. Furthermore, the aligning step may be repeated on the way towards the source.

The control software for the alignment subproblem is shown in Appendix C.3.3. It was validated in air. Experiments in water had to be postponed due to problems with leaks and the communication via the transceiver.

In a next step, the pressure sensors usability to do obstacle avoidance and wall following will be assessed. The pectoral fins are expected to cause observable pressure reflections from close static objects.

In the long term, a model of the robot might help to improve control. The prediction of control influence might be helpful once a large collective is concerned.

6 Conclusion

The following list summarizes the achievements of this thesis towards the development of a swarming underwater robot:

- Simple, miniature, and low-cost design.
- Modular and submersible propulsor that avoids the complex and potentially unreliable sealing of moving parts.
- High maneuverability provided by four independent propulsors.
- Exchangeable fins to study swimming performances with different fin shapes and stiffnesses.
- Untethered, autonomous robot that allows the implementation of closed-loop control, remote-controlled operations, and the visualization of measurement data in real-time.
- Testing environment with up to three installable cameras, which track the motion of the robot. Tracking software to convert the video data to travelled distances along each axis.

Subsequently, this chapter addresses limitations, optimizations, applications, and advantages of Scuba Fish.

6.1 Limitations of Scuba Fish

Scuba Fish at its present state faces four principal limitations.

First of all, Scuba Fish is currently operated as a single robot. It is able to sense its own movements with an IMU, to sense its environment with two pressure sensors, and to transmit these sensory data to an external mission control. However, it is not able to perceive other robots, to communicate to other robots, or to coordinate with other robots. In brief, Scuba Fish is not swarming yet.

Secondly, the design of Scuba Fish is not yet fully oriented towards a production in high numbers. The circuitry is manually soldered. The structural parts are 3-d printed. The assembly takes some 20 h. Each robot has to be trimmed to neutral buoyancy and pitch angle individually. The 3-d printed gasket has to be replaced whenever it starts leaking due to wear and tear.

Thirdly, Scuba Fish is neither optimized for power efficient swimming nor for reaching high velocities. A good enough fin was combined with a reasonably sized coil and magnet to a potentially suboptimal propulsion system.

Finally, Scuba Fish is handled as an individual robot. There is no strategy to collectively handle and maintain a swarm yet.

6.2 Outlook for future improvements

Future improvements shall mainly attack the present limitations of Scuba Fish.

First, sensing and communication strategies for swarming have to be prototyped and tested in water. Then, several robots have to be manufactured and tested together. Lastly, algorithms for collective behaviors have to be implemented.

Second, the manufacturing and assembling processes of Scuba Fish have to be simplified. A reproducible PCB has to be developed to avoid the time intensive soldering of electronic components. A mold for the manufacture of the hulls has to be designed. A fabrication method for the high-accuracy propulsors has to be identified. Alternatively, the propulsors have to be simplified. Ideas include 3-d printing the propulsors as single parts with support material wherever free movement is required, or self-aligning magnetic hinges hold in place by additional permanent magnets.

At the same time, the design of Scuba Fish may be further miniturized to increase propulsion efficiency and to decrease the necessary tank size to study 3-d swarming with a meaningful collective.

Once the final design and all components are known, Scuba Fish has to be tuned to be perfectly buoyant and neutral in pitch to avoid manual trimming. For this to be possible, variability in the manufacturing process has to be minimized. A final design may be glued instead of bolted at the cost of sacrificing the ability to reopen the robot.

Third, further material and shapes for efficient fins have to be assessed. An optimal coil design has to be set that generates the highest thrust while fitting into the electric circuit of Scuba Fish.

Last, the handling of Scuba Fish has to optimized for high numbers. Wireless programming has to be enabled. An interface for mass charging has to be designed. Ideas include a magnetic rail on which robots self-align to charging

docks. Finally, an easy way to deploy, collect, and store Scuba Fish has to be found.

In the next steps of the project, several robots will be coordinated into a collective by adding sensing and communication capabilities.

6.3 Potential applications of Scuba Fish

Scuba Fish shows the potential to become a scalable platform to study 3-d swarming in an affordable manner and reasonably-sized laboratory environment.

Intended applications for a collective of underwater robots include search and rescue missions, harbor patrols, the surveillance of offshore oil platforms, the exploration of coral reefs, and the monitoring of underwater food plantations.

6.4 Advantages of Scuba Fish

Scuba Fish is low-cost at a total components value of $ 60 (it is intended that the final robot will cost under $ 100). High-maneuverability is achieved by using four fins - one caudal, two pectoral, and one dorsal - which provide the robot with forward motion, turn-on-the-spot, and vertical diving capabilities. This relatively high number of control surfaces is made possible by the low-cost nature of the propulsor. The latest prototype has a body length of 10 cm, excluding the caudal fin.

Scuba Fish offers a potential alternative where monolithic, individual underwater robots are not the most suitable choice. In addition, the highly-maneuverable and miniature nature of the robots would also allow for operation in complex environments like coral reefs.

Finally, Scuba Fish offers the possibility to exchange fins and to oscillate them at different frequencies. This possibility makes Scuba Fish an interesting unthethered system to study the fluid dynamics of undulatory motions caused by different fins.

References

[1] J. M. Anderson, K. Streitlien, D. S. Barrett, and M. S. Triantafyllou. Oscillating foils of high propulsive efficiency. *Journal of Fluid Mechanics*, 360:41–72, 1998.

[2] E. Benini. Significance of blade element theory in performance prediction of marine propellers. *Ocean Engineering*, 31:957–974, 2004.

[3] S. Bhattacharyya and H. Asada. Control of a compact, tetherless ROV for in-contact inspection of complex underwater structures. *2014 IEEE/RSJ International Conference on Intelligent Robots and Systems*, (Iros):2265–2272, 2014.

[4] M. Brambilla, E. Ferrante, M. Birattari, and M. Dorigo. Swarm robotics: A review from the swarm engineering perspective. *Swarm Intelligence*, 7(1):1–41, 2013.

[5] A. J. Clark, X. Tan, and P. K. McKinley. Evolutionary multiobjective design of a flexible caudal fin for robotic fish. *Bioinspiration & biomimetics*, 10(6):065006, 2015.

[6] R. Cui, S. Sam, B. Voon, E. How, and Y. Sang. Leader follower formation control of underactuated autonomous underwater vehicles. *Ocean Engineering*, 37(17-18):1491–1502, 2010.

[7] R. Du, Z. Li, K. Youcef-toumi, and B.-i. F. U. Robots. *Robot Fish*. Springer, 2015.

[8] M. Dunbabin, P. Corke, I. Vasilescu, and D. Rus. Experiments with Cooperative Control of Underwater Robots. *The International Journal of Robotics Research*, 28(6):815–833, 2009.

[9] K. L. Feilich and G. V. Lauder. Passive mechanical models of fi sh caudal fi ns : effects of shape and stiffness on self-propulsion. *Bioinspiration & Biomimetics*, 10(3):36002, 2015.

[10] V. Kopman and M. Porfiri. A Miniature and Low-Cost Robotic Fish for Ethorobotics Research and Engineering Education I: Bioinspired Design. *ASME Dynamic Systems and Control Conf.*, pages 209–216, 2011.

[11] V. Kopman and M. Porfiri. Design, modeling, and characterization of a miniature robotic-fish for research and education in biomimetics and bioinspiration. *IEEE/ASME Transactions on Mechatronics*, 18(2):471–483, 2012.

[12] Z. Li, R. Du, and F. Sme. A Novel Double - Hull Boat with Biomimetic Wire - Driven Flapping Propulsors. pages 14–16, 2014.

[13] Z. Li, R. X. Du, Y. Zhang, and H. Li. Robot Fish with Novel Wire-Driven Continuum Flapping Propulsor. *Applied Mechanics and Materials*, 300-301:510–514, 2013.

[14] Z. Li, W. Gao, R. Du, and B. Liao. Design and analysis of a wire-driven robot tadpole. pages 1–7, 2015.

[15] K. N. Lucas, P. J. M. Thornycroft, B. J. Gemmell, S. P. Colin, and J. H. Costello. Effects of non-uniform stiffness on the swimming performance of a passively- fl exing , fi sh-like foil model. *Bioinspiration & Biomimetics*, 10(5):56019, 2015.

[16] A. D. Marchese, C. D. Onal, and D. Rus. Autonomous Soft Robotic Fish Capable of Escape Maneuvers Using Fluidic Elastomer Actuators. *Soft Robotics*, 1(1):75–87, 2014.

[17] S. Mintchev, E. Donati, S. Marrazza, and C. Stefanini. Mechatronic design of a miniature underwater robot for swarm operations. *2014 IEEE International Conference on Robotics and Automation (ICRA)*, pages 2938–2943, 2014.

[18] B. Mitchell, E. Wilkening, and N. Mahmoudian. Developing an underwater glider for educational purposes. *Proceedings - IEEE International Conference on Robotics and Automation*, pages 3423–3428, 2013.

[19] M. Nagai, G. Maeda, and K. Irabu. Study on Swimming of Fish. *Bulletin of Science and Engineering 17: University of the Ryukyus, Naha, Japan*, (15-21), 1979.

[20] E. M. Purcell. Life at low Reynolds number. *American Journal of Physics*, 1977.

[21] G. Refael and A. Degani. Momentum-Driven Single-Actuated Swimming Robot. 2015.

[22] I. C. Rust and H. H. Asada. The eyeball ROV: Design and control of a spherical underwater vehicle steered by an internal eccentric mass. *2011 IEEE International Conference on Robotics and Automation*, pages 5855–5862, 2011.

[23] T. Salumäe and M. Kruusmaa. Flow-relative control of an underwater robot. *Proceedings of the Royal Society A*, 469(20120671):1–19, 2013.

[24] J. Shao, L. Wang, and J. Yu. Development of an artificial fish-like robot and its application in cooperative transportation. *Control Engineering Practice*, 16(5):569–584, 2008.

[25] R. M. Shelton, P. J. M. Thornycroft, and G. V. Lauder. Undulatory locomotion of flexible foils as biomimetic models for understanding fish propulsion. pages 2110–2120, 2014.

[26] E. Simetti, G. Casalino, a. Turetta, E. Storti, and M. Cresta. Towards the use of a team of USVs for civilian harbour protection: USV interception of detected menaces. *IFAC Proceedings Volumes (IFAC-PapersOnline)*, 7:145–150, 2010.

[27] Y. Takada, K. Koyama, and T. Usami. Position Estimation of Small Robotic Fish Based on Camera Information and Gyro Sensors. *Robotics*, 3(2):149–162, 2014.

[28] N. Takesue, T. Mitsuzumi, and M. Nagasawa. Proposal of Miniature Aquatic Robot Utilizing Resonance of Elastic Plate. 2015.

[29] Z. Wang, G. Hang, J. Li, Y. Wang, and K. Xiao. A micro-robot fish with embedded SMA wire actuated flexible biomimetic fin. *Sensors and Actuators, A: Physical*, 144(2):354–360, 2008.

[30] Z. Wang, G. Hang, Y. Wang, J. Li, and W. Du. Embedded SMA wire actuated biomimetic fin: a module for biomimetic underwater propulsion. *Smart Materials and Structures*, 17:025039, 2008.

[31] Z. Wang, Y. Wang, J. Li, and G. Hang. A micro biomimetic manta ray robot fish actuated by SMA. *Robotics and Biomimetics (ROBIO), 2009 IEEE International Conference on*, pages 1809–1813, 2009.

[32] S. A. Watson and P. N. Green. Propulsion Systems for Micro-Autonomous Underwater Vehicles (AUVs). *Robotics Automation and Mechatronics ...*, pages 435–440, 2010.

[33] Y. Xu, D. Qin, K. Road, C. Liu, and H. Zhang. THRUST ANALYSIS ON A SINGLE-DRIVE ROBOTIC FISH whit an elastic joint. *Proccedings 27th European Conference on Modelling and Simulation*, 4(Cd), 2000.

[34] J. Yu and L. Wang. Parameter Optimization of Simplified Propulsive Model for Biomimetic Robot Fish. *Proceedings of the 2005 IEEE International Conference on Robotics and Automation*, 2005(April):3306–3311, 2005.

[35] J. Yu, L. Wang, and M. Tan. A framework for biomimetic robot fish's design and its realization. *Proceedings of the 2005, American Control Conference, 2005.*, pages 1593–1598, 2005.

[36] J. Yu, S. Wang, and M. Tan. A simplified propulsive model of bio-mimetic robot fish and its realization. *Robotica*, 23(1):101–107, 2005.

[37] F. Zhang, J. Thon, C. Thon, and X. Tan. Miniature Underwater Glider: Design and Experimental Results. 19(1):394–399, 2014.

[38] Y. Zhao, M. Fukuhara, T. Usami, and Y. Takada. Performance of Very Small Robotic Fish Equipped with CMOS Camera. *Robotics*, 4(4):421–434, 2015.

A Physical principles

Hand calculations on physical principles can serve as a first estimate for an expected robot behavior, thus be useful during the design process. Time permitting, they have to be confirmed through computer simulations. Simulations are also a great tool for parameter optimization. Only experiments with the real robot can finally provide reliable evidence about its behavior.

A.1 Coil design

The design of an optimized coil seeks values for the number of turns N and the wire radius r_w. Furthermore, estimates on the coil's ability to provide thrust force will be elaborated. The following calculations were done for the electromagnetic propulsor design found in the Aquabot from Hexbug.

These parameters are given due to restrictions on power and dimensions:

1. Supplied voltage: $V = 6\,V$
2. Maximal current: $I = 300\,mA$
3. Inner coil radius: $r_i = 3\,mm$
4. Outer coil radius: $r_o = 6\,mm$
5. Coil length: $l_c = 10\,mm$

The resistance of the coil R_c is the the length of the N-times wound wire multiplied by the copper wire's resistivity ρ_{cu} over its cross-sectional area:

$$R_c = \frac{\rho_{cu} \cdot N \cdot (r_i + r_o) \cdot \pi}{r_w^2 \cdot \pi} = \frac{V}{I}$$

In addition, the resistance of the coil equals voltage V over current I as all drawn current at a given voltage has to run through the coil. The ratio between the number of turns N and the wire radius r_w can be expressed by known and constant parameters:

$$\frac{N}{r_w^2} = \frac{V}{I} \cdot \frac{1}{\rho_{Cu} \cdot (r_i + r_o)} = C, const \tag{A.1}$$

Further, the number of turns N can be written as a function of the wire radius r_w and the coil dimensions, namely coil length l_c, inner coil radius r_i, and outer coil radius r_o:

$$N = \underbrace{\frac{l_c}{2 \cdot r_w}}_{\text{turns per layer}} \cdot \underbrace{\frac{r_o - r_i}{2 \cdot r_w}}_{\text{no. of layers}} \tag{A.2}$$

Now, plugging expression A.2 into equation A.1 leads to:

$$\frac{l_c \cdot (r_o - r_i)}{4 \cdot r_w^4} = C \tag{A.3}$$

Solving equation A.3 for the wire radius r_w delivers the first desired parameter:

$$r_w = \left(\frac{l_c \cdot (r_o - r_i)}{4 \cdot C} \right)^{1/4} = \left(\frac{l_c \cdot (r_o - r_i)}{4 \cdot \frac{V}{I} \cdot \frac{1}{\rho_{co} \cdot (r_i + r_o)}} \right)^{1/4}$$

Finally, plugging the expression A.1 for the wire radius r_w back into equation A.2 provides the corresponding number of turns N.

The whole math was done for the coil dimensions enumerated before and led to a small wire radius r_w in the range of 0.1 mm at a high number of around 990 turns N.

It has to be pointed out that these design considerations lead towards an optimized coil regarding the strength of the induced magnetic field for a given power supply. Basically, the number of turns N is maximized within the allowed resistance of the coil wire given by V/I. The resulting magnetic field is:

$$B_c = \mu_0 \cdot I \cdot \frac{N}{l_c} \tag{A.4}$$

Measurements or calculations regarding the thrust force generated by a coil propulsor were not found in literature. Reliable results should be achieved with simulations. A rough estimate is based on the law of conservation of energy, where energy is volume times magnetic energy density. The states of energy are compared for the permanent magnet beeing entirely inside and outside the hollow coil:

$$\triangle U = \frac{L \cdot r^2 \cdot \pi}{2 \cdot \mu_0} \cdot \left(\underbrace{\frac{\mu_m}{\mu_0} \cdot (B_c + B_m)^2}_{\text{magnet inside}} - \underbrace{B_c^2}_{\text{magnet outside}} \right) \tag{A.5}$$

A realistic value for the magnetic field strength B_c generated by the coil is 37 mT according to equation A.4. The magnetic field of the employed neodymium permanent magnets is approximately 1470 mT each. Neodymium has a μ_m/μ_0 ratio of 1.05. L is the travel between the hollow coil and the magnet while r is the average of the coil's inner radius and the magnet's outer radius.

Now looking at equation A.5, the value of B_c seems only marginally relevant. This suggests that a week magnetic field induced by the coil would still provide a large enough $\triangle U$. Consequently, power could be saved by reducing the electric current according to equation A.4. However, it is likely that the voltage had to be stepped up in order to achieve the same power output. Experiments with a coil and various currents could provide evidence. It has to be mentioned that equation A.5 is usually applied to air core coils hosting iron kernels instead of permanent magnets.

The resulting force F is the change in energy $\triangle U$ divided by the travel L:

$$F = \frac{\triangle U}{L}$$

The force F is as high as 20.4 N for the chosen coil and magnets. Plugging this force value into equation A.6 together with reasonable oscillation parameters being a 1.5 Hz frequency f and a 10 mm amplitude λ results in a power generation of around 1.23 W:

$$P = F \cdot v = F \cdot f \cdot 4 \cdot \lambda \tag{A.6}$$

This power value is roughly the double of Kopman's 0.67 W described in [11]. Assuming a lever length d of 20 mm, the coil would generate a torque T of approximately 40.9 Ncm at the pivot point:

$$T = F \cdot d$$

In comparison, the Traxxas 2065 servomotor used in Kopman's design can bring up a maximum torque of 23 Ncm. The force and torque provided by the

coil seem too large.

A.2 Roll stability of submerged bodies

Submerged bodies are roll stable whenever their center of gravity (CoG) is placed below their center of buoyancy. The center of buoyancy (CoB) is equal to the center of volume. The center of gravity can be influenced by having sections of different densities within the volume of the body.

Stable bodies (CoG below CoB) experience a counteracting roll torque whenever deflected from their equilibrium. Unstable bodies (CoG above CoB) keep rolling when deflected and eventually become stable but upside-down. The attacking forces and moments on a submerged rolling body are illustrated in Figure 48. The same considerations apply for pitch stability.

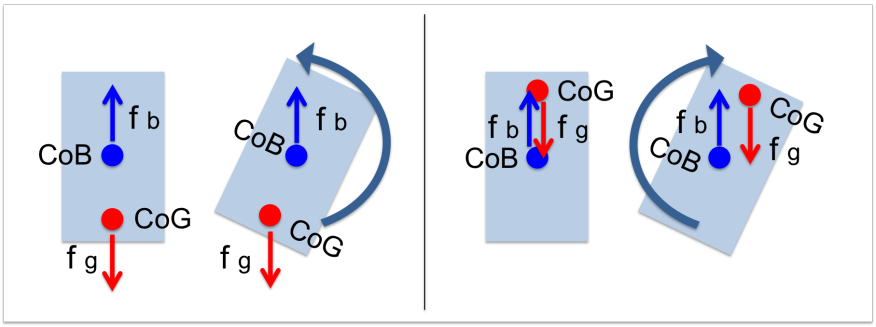

Figure 48: Roll stability depending on the position of the center of gravity (CoG) relative to the center of buoyancy (CoB). LEFT: Stable. RIGHT: Instable.

Scuba Fish achieves good roll stability by carrying heavy parts such as batteries and added block weights in its lower belly.

B Hardware

This section addresses design considerations for Scuba Fish. It provides detailed information on all parts used for Scuba Fish, it explaines the CAD model and the circuitry, and it includes an assembly guide.

B.1 Parts list of the latest Scuba Fish prototype

An overview on the different components of Scuba Fish and their respective properties is given in Table 4. Suppliers are linked to their respective websites.

All listed components add up to a total cost of $ 171.26. Further consumables include "Loctite Super Glue", "Loctite Silicone Waterproof Sealant", "3M Foam Tape", "Corrosion-X Anti-Corrosion Spray", and standard soldering equipment (solder, flux, shrink tubes, stripboard). Altogether, the current Scuba Fish values an estimated $ 175.

The cost of the **circuitry** can be drastically reduced by avoiding the expensive breakout boards. If bought without the boards, the ATMEGA328P chip as used on the Arduino costs $ 1.90[13], the MPU-6050 IMU chip costs $ 12.95[14], and the nRF24L01+ transceiver chip costs $ 3.50[15]. On the other hand, a custom-made PCB might add some $ 20 while saving the $ 7.50 wire costs and some 8 h of assembly time. The optimized circuitry would cost an estimated **$ 90.95**.

The cost of the **chassis** can be reduced by changing the manufacturing process from 3-d printing to molding. A relatively expensive mold has to be manufactured once. The final chassis cost should not be more than ten times the material price for the molded plastic. Plastic pellets are available at around $ 1/kg[16]. The total mass of the 3-d printed parts is about 0.040 kg. Therefore, the chassis should be producible at a cost of some **$ 0.40**.

The cost of the **propulsors** can be reduced by sourcing low-cost coils. Hartai Technology Industry Co.[17] offered comparable coils at $ 0.18 per piece. The propulsors using this coil would be available at **$ 5.47**.

[13] http://www.atmel.com/devices/atmega328p.aspx
[14] https://www.sparkfun.com/products/10937
[15] https://www.sparkfun.com/products/690
[16] http://www.alibaba.com/showroom/plastic-pellets-price.html
[17] http://www.hartai.com/en/html/main.asp

Name	Description	Supplier	Cost	Qty	Remarks
Circuitry at a total value of $ 124.95					
μC	Arduino Pro Mini	Sparkfun	9.95	1	3.3V,8MHz
Transceiver	nRF24L01+	Sparkfun	19.95	1	Breakout
IMU	MPU-9150, 9DOF	Sparkfun	34.95	1	Breakout
H-bridge	SN754410	Sparkfun	2.35	2	Quad Half
USB	Micro-B, IP67	Digi-Key	2.47	2	5 lines
Altimeter	Pressure sensor	Digi-Key	18.98	2	3m depth
On-Off	IP67	Digi-Key	2.28	1	Slide switch
Battery	Turnigy nanotech	HobbyKing	1.36	2	3.7V,160mAh
Wire	9564T1	McMaster	0.15	50	Ultra Flex
Chassis at a total value of $ 21.74					
Left hull	Printed housing	J. Weaver	8.00	1	Objet500
Right hull	Printed housing	J. Weaver	6.00	1	Objet500
Seal	Printed gasket	J. Weaver	0.60	1	Objet500
Bolt/nut	M1.6x12mm	Amazon	0.90	7	Slotted
Block weight	5g trimmer	Amazon	0.21	4	Buoyancy
Propulsors at a total value of $ 24.57					
Caudal hinge	Printed propulsor	J. Weaver	0.60	1	Objet500
Hinge clamp	Printed propulsor	J. Weaver	0.10	1	Objet500
Dorsal hinge	Printed propulsor	J. Weaver	0.40	1	Objet500
Pectoral hinge	Printed propulsor	J. Weaver	0.40	2	Objet500
Hinge plug	Printed propulsor	J. Weaver	0.04	6	Objet500
Magnet	M5x5mmCYL	Apex	0.30	5	NdFeB
Coil	ZAU, 5Ohm	Kuk	4.00	5	9.2x12.3x5.5
Fin	Rubber sheet	Amazon	0.12	4	Flexible
Shield	Mu-metal	Amazon	0.45	1	Block B-field

Table 4: The components of Scuba Fish at a glance.

Generally, switching from single prototypes to a small series production would potentially further reduce the total cost by up to 20 %. A **final components cost** of $0.8 \cdot (90.95 + 0.40 + 5.47) =$ **77.46** [USD] should be feasible.

B.2 Computer-aided design of the latest Scuba Fish prototype

The chassis of Scuba Fish was designed in SolidWorks. This section shall help to simplify the understanding of the current model F1.0. Anyone who intends to modify or develop the current model might want to read this section beforehand.

The model includes single parts, subassemblies, and the main assembly. Bought parts were either modeled or downloaded from GrabCAD[18]. All sketches were drawn in the x-y-plane (front plane) and extruded along the z-axis. The single steps in the design tree were labeled according to their respective purpose. Parts to be 3-d printed have to be saved as .stl-files. Assemblies to be 3-d printed (several parts with different Shore hardnesses) have to be saved as .stl-files and the box saying "Save as individual parts" has to be ticked.

Scuba Fish consists of two hull parts, a gasket, and four hinges. The design starts with a part called "Body". "Body" defines the shape of Scuba Fish, which is a shell created by the intersection of three ellipses. "Body" develops the shell up to the point where features are necessary which are not identical on both hull parts.

At the end of "Body", the model was mirrored at the x-z-plane. The resulting body was cut along the x-z-plane running through the origin of the coordinate system. The left side was saved in "Left_Hull" whereas the right side was saved in "Right_Hull". Both, "Left_Hull" and "Right_Hull" share the geometries of their parent part "Body". Any changes in "Body" will show up in "Left_Hull" and "Right_Hull".

Subsequently, both hulls were elaborated to their final geometries. The hinges are simple single parts. The gasket called "Seal" was derived from "Body" as well. The "Seal_Sandwich" is the final gasket consisting of a stiff "Seal"layer enclosed between two flexible Shore 40 layers.

[18] `https://grabcad.com/`

The assembly combines all the single parts and subassemblies to the final robot (see Figure 49). It allows to check for mountability, to check whether all parts fit together, and to optimize the arrangement of the electronics inside the robot.

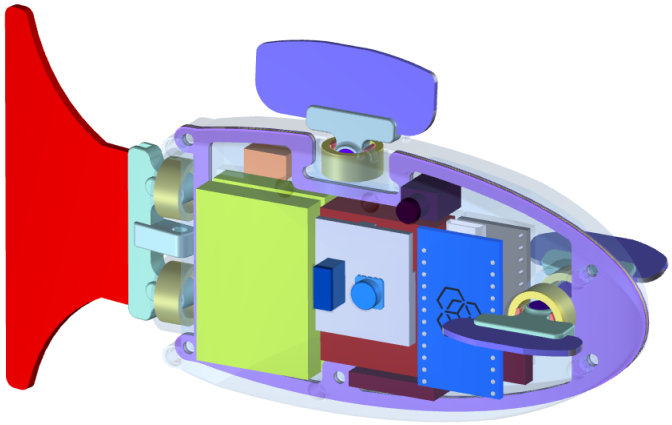

Figure 49: A computer model of Scuba Fish.

In addition to the actual model, there were two extensions created. A decoupled caudal propulsor named "PropDec" can be extended or attached to any body. It allows the study of caudal fins without needing the actual Scuba Fish.

A version F1.1 of Scuba Fish was created with decoupled pectoral and dorsal propulsors. It allows to print and to assemble the fragile propulsors separately. The version F1.2 is a copy of F1.1 designed for the usage with new coils.

B.3 Electronics and circuitry of the latest Scuba Fish prototype

The electronics of Scuba Fish (see Figure 50) include two batteries, an Arduino microcontroller, two waterproof USB ports for programming and charging, an OnOff-switch, an SPI transceiver, an IMU and two pressure sensors on an I^2C bus, and two quad half H-bridges commanding five coils for three single and one double propulsor. Further information on individual components is found in Table 4.

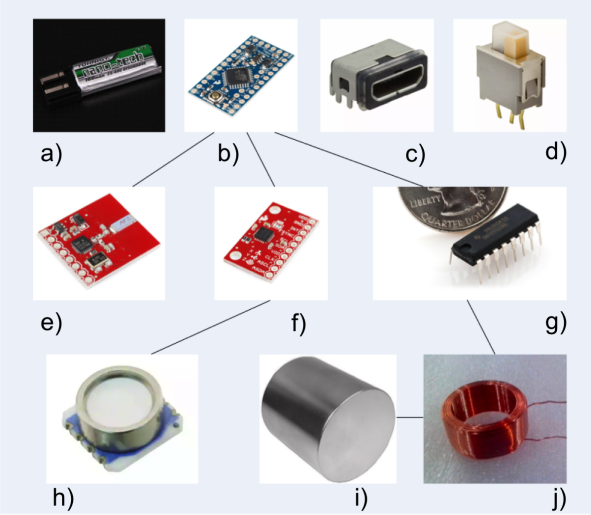

Figure 50: Overview on the electronic components: a) battery; b) microcontroller; c) USB port; d) OnOff-switch; e) transceiver; f) IMU; g) H-bridge; h) pressure sensor; i) magnet; j) coil.

The schematic in Figure 51 shows the wiring of the above components. It serves for assembly work and for the development of a PCB.

A detailed Arudino pinout for reference purposes follows in Figure 52.

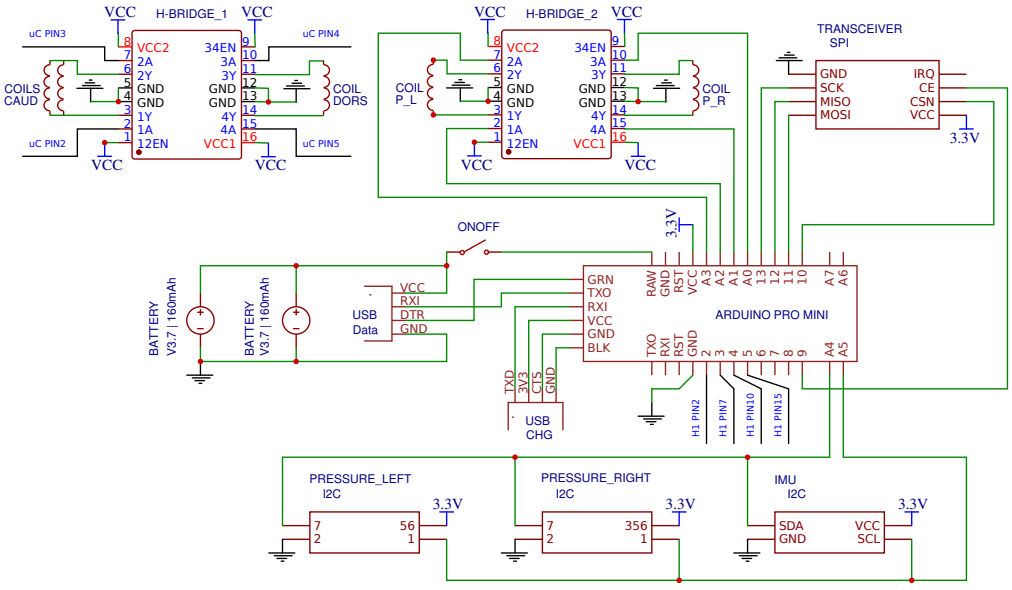

Figure 51: Schematic of the complete electrical circuit.

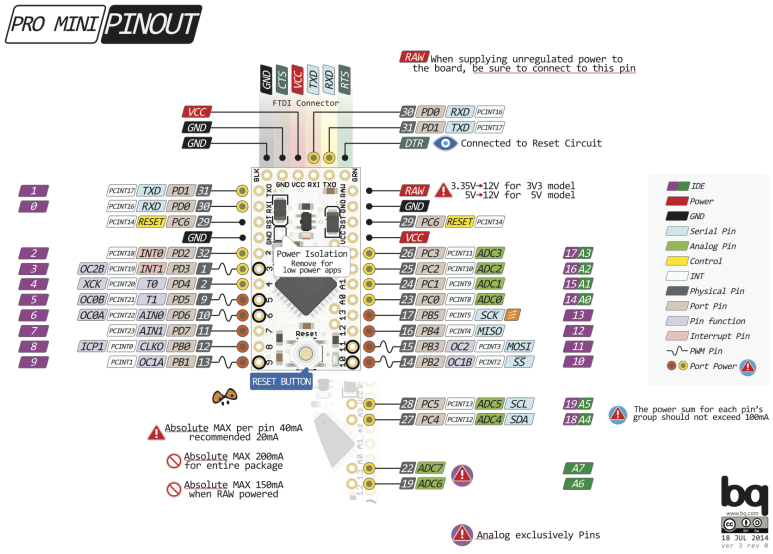

Figure 52: Arduino Pro Mini pinout. (Image accessed online on http://forum.arduino.cc/index.php?topic=152386.0 in April 2016.)

The two waterproof USB - Micro B ports serve for charging and programming. Each of them has four out of five lines in use.

Charging is done via the GND and VCC lines of the left USB (looking from behind along the x-axis of the robot). A modified cable was prepared. A programmable charger has to be set to LiPo, 3.7 V, 300 mAh. Charging at a recommended rate of 1 C takes 1 h.

Programming requires both USB ports for six FTDI-lines. A modified cable combining two USB - Micro B males to an FTDI male was prepared. The blue end of the cable goes to the right USB, the unmarked end goes to the left USB (same as charging). The far end of the cable connects to an FTDI breakout board[19]. Finally, a USB mini cable connects the FTDI board to any computer for programming via the Arduino environment.

The standard assignments for the USB - Micro B lines are shown in Figure 53 for reference purposes.

[19] `https://www.sparkfun.com/products/9873?gclid=COu-pMaLh8wCFVZahgodS-0J2Q`

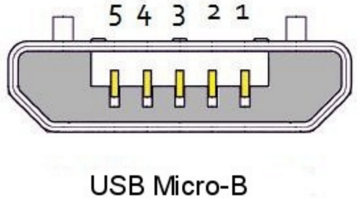

Pin	Name	Cable color	Description
1	VCC	Red	+5 VDC
2	D-	White	Data -
3	D+	Green	Data +
4	ID	n/a	USB OTG ID
5	GND	Black	Ground

Figure 53: USB - Micro B pinout. (Image accessed online on http://www.hobbytronics.co.uk/usb-connector-pinout in April 2016.)

The two pressure sensors have to be set up on different I^2C modes to work simultaneously. Both need pin 1 for SCLK, pin 2 for GND, and pin 7 for SDA. The left one combines pins 5 and 6 to a single VCC cable. CSB is on low and the adress is set to 0x77. The right one combines pins 3, 5, and 6 to a single cable. CSB is on high and the adress is set to 0x76. The pinout of the pressure sensors is shown in Figure 54.

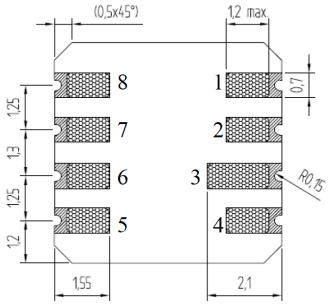

Pin	Name	Type	Function
1	SCLK	I	Serial data clock
2	GND	G	Ground
3	CSB	I	Chip Select (active low)
4	NC	NC	-
5	VDD	P	Positive supply voltage
6	PS	I	Communication protocol select SPI / I2C
7	SDI/SDA	I	Serial data input
8	SDO	O	Serial data output

Figure 54: Pressure sensor pinout. (Image from the datasheet: Measurement Specialities: “MS5803-01BA Miniature Variometer Module”.)

B.4 Assembly of the latest Scuba Fish prototype

The assembly of Scuba Fish includes three main steps. They are explained in this section. A total assembly time of about 20 h per robot should be considered.

B.4.1 Cleaning the 3-d prints

Starting with the 3-d prints allows for enough time to reprint parts in case they do not fit or breake during the cleaning procedure. Water jets should be avoided

for cleaning as they could damage the fragile propulsors. A knife, tweezers, and pins were used to scratch off the support material from the parts. Safety gloves should be weared.

The sockets for the coils on the two hulls shall be cleaned first. They include the fragile propulsor mountings and require extra care.

The parts shall be rinsed below a water tap after cleaning most of the support material. A second iteration of scratching and rinsing shall provide a clean finish.

The five coils shall be inserted to their respective sockets right after cleaning. This measure reduces the risk of breaking a propulsor mounting.

The cleaned hulls are shown in Figure 55. The cleaning process for all parts takes around 3 h.

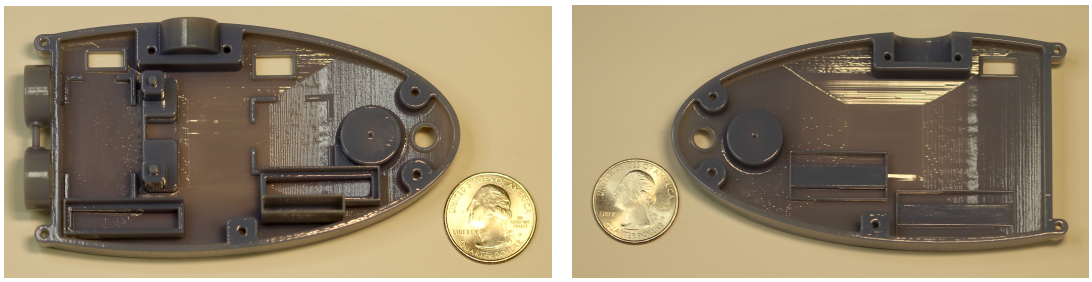

Figure 55: 3-d printed hulls of Scuba Fish.

B.4.2 Soldering the electronic components

Soldering the electronic components takes most of the time and effort to build a Scuba Fish. Special attention has to be paid to cable lengths and routing. Tweezers and a mini vise are helpful tools. Ultraflexible wire (see Table 4) and the corresponding wire stripper shall be used. The schematic in Figure 51 shows how to connect the electric components.

The pressure sensors have to be prepared as explained in Section B.3.

The two coils powering the caudal fin have to be soldered in parallel. Powering both individually with the subassembled fin in place provides evidence on the respective magnetic fields. The field directions have to match.

The H-bridges can be pre-soldered to a piece of veroboard (12 by 10 holes) as shown in Figure 56. The outgoing cables are soldered directly to the legs of the H-bridges in order to minimize the total size.

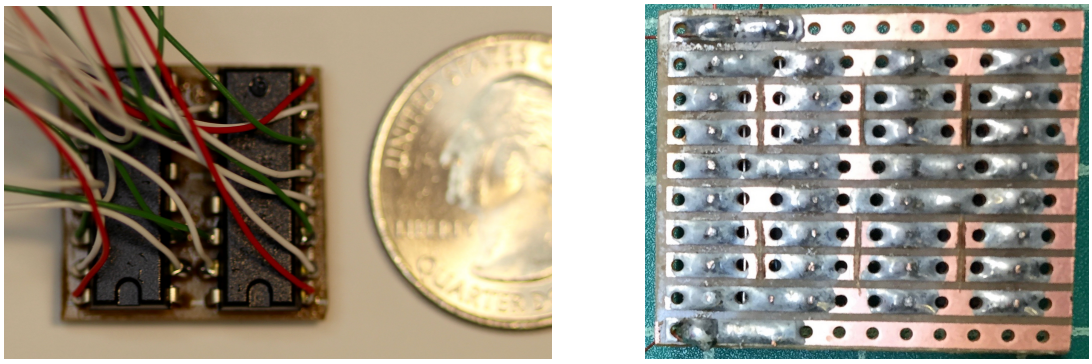

Figure 56: H-bridges on veroboard.

After some 8 h, the soldered circuitry may look similar as in Figure 57. Before assembling, all uninsulated solder joints and the chips on each board shall be coated with Corrosion X.

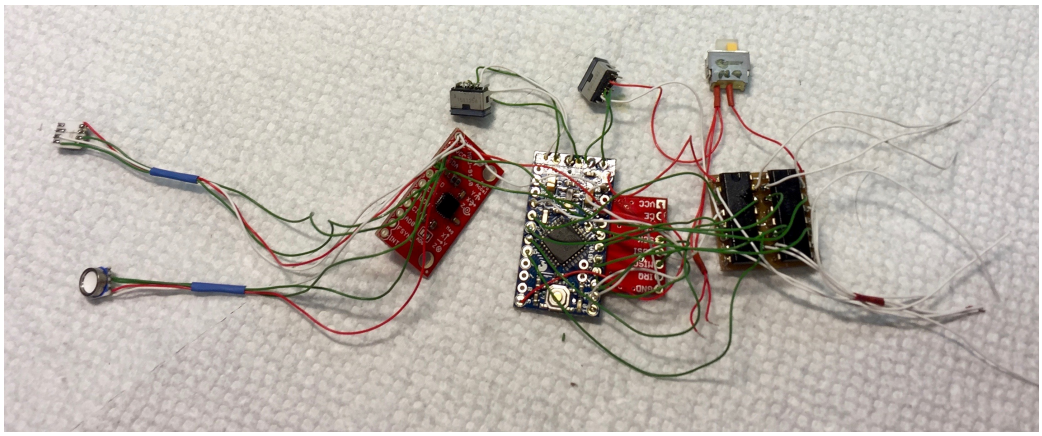

Figure 57: The soldered circuitry before assembly.

B.4.3 Assembling the fish

In a first step, the electronic components shall be put in place. They stick well on foam tape if previously cleaned with alcohol (Corrosion X does not stick). Then, all coils shall be connected to the respective cables coming from the H-bridges. Once they are proven to work, the wire connections shall be insulated with shrinking tube. This part of the assembly should not take more than 1 h.

Waterproofing the fish takes some 2 h. Safety gloves should be weared. Tweezers and pins are useful tools.

The USB ports, the OnOff-switch, and the two pressure sensors have to be covered with silicone rubber from the inside. Applying some silicone on the housings of these parts before pushing them through the hull improves the seal. Silicone insulates the cables and solder joints at the same time. It takes around 2 h to dry.

The USB ports and the OnOff-switch have to be glued to the hull from the outside to withstand pushing forces from plugging the cables or operating the switch.

A small piece of Mu-metal was placed on top of socket for the pectoral propulsor of the left hull. It mitigates magnetic coupling between the two pectoral fins.

The propulsors shall be installed at the end of the assembly. Building the four propulsors takes some 2 h. The fins are cut from rubber sheets. There is a 3-d printed template for the standardized rectangular caudal fin. The magnets are glued with superglue. The caudal fin is mounted on the shaft of the left hull. A part named "HingeClamp" has to be glued to it. The other fins are mounted inside the sockets. Each of them is fixed with two plugs named "HingePlug". Good flapping mobility around the pivot axis has to be ensured.

Finally, the gasket is put in place and the fish is gently tightenend with seven bolts. The assembled robot ideally looks like in Figure 58.

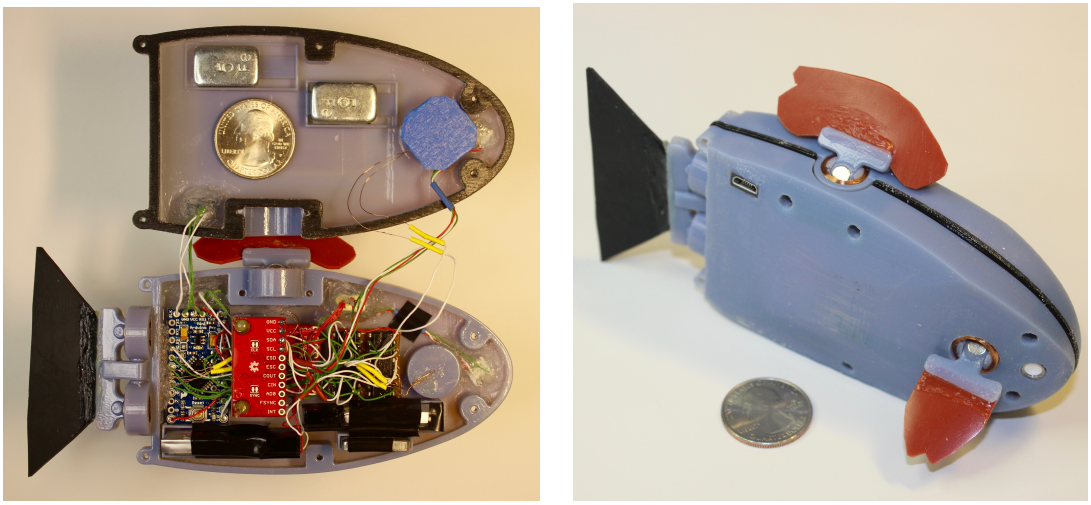

Figure 58: The fully assembled Scuba Fish. Left: Open. Right: Closed.

The remaining 2 h were spent for checking connections and testing subgroups of the circuitry.

Balancing the fish to achieve neutral buoyancy and pitch has to be done experimentally once the assembly is complete. The volume (out of the CAD or measured in a measuring cylinder) as well as experience from previous iterations provides an educated guess to start with.

C Software

Any code running on Scuba Fish may deviate from the code samples shown in the following. The examples shall illustrate the basic navigation, communication, and control concepts from a software perspective.

The open-source electronics platform Arduino was used for Scuba Fish. It allows to compile and upload C-style code to any Arduino-compatible board. It is well documented and comes with loads of libraries and examples.

Creating a project starts with opening a new file. Additional files may be included by adding tabs. Only one file within a project may contain the setup "void setup() {}" and the main loop "void loop() {}". Functions in other tabs can be called from the main loop.

C.1 The software structure on Scuba Fish

The robot runs a main file "ScubaFish" that calls functions from three more files named "IMU", "PressureSensor", and "Transceiver" (discussed seperately in the following sections). A simplified main file is shown in Figure 59.

```
// Assign global variables for readings from the psensor and the IMU
int32_t temp_left, pres_left, temp_right, pres_right;
int16_t ax, ay, az, gx, gy, gz, mx, my, mz;

// Initialize IMU, psensor, and transceiver
void setup()
{
  initialize_IMU();
  initialize_pressure_sensors();
  initialize_transceiver();
}

// Call functions to read IMU and psensor, and to send data via transceiver
void loop()
{
  read_IMU(ax, ay, az, gx, gy, gz, mx, my, mz);
  read_pressure_sensors(pres_left, temp_left, pres_right, temp_right);
  transceiver_loop();
}
```

Figure 59: Main file running on Scuba Fish.

C.1.1 Reading the IMU

The 9DOF MPU-9150 IMU combines two chips: the MPU-6050, which contains a 3-axis gyroscope and a 3-axis accelerometer, as well as the AK8975, a 3-axis digital compass. The communication to the Arduino microcontroller is done via I^2C. There are two libraries (I2Cdev.h and MPU6050.h) that have to be installed (downloaded and added to the /Arduino/libraries folder). They are found on github[20]. A simplified IMU file is shown in Figure 60.

```
// Include libraries
#include "Wire.h"
#include "I2Cdev.h"
#include "MPU6050.h"

// Define accelgyro struct
MPU6050 accelgyro;

// Initialize IMU (called from ScubaFish)
void initialize_IMU() {
    accelgyro.initialize();
}

// Read IMU (called from ScubaFish)
void read_IMU(int16_t& ax, int16_t& ay, int16_t& az, int16_t& gx, int16_t& gy, int16_t& gz, int16_t& mx, int16_t& my, int16_t& mz)
{
    accelgyro.getMotion9(&ax, &ay, &az, &gx, &gy, &gz, &mx, &my, &mz);
}
```

Figure 60: Code sample for reading the IMU.

The sensor values may be written to the serial monitor in the following order: temperature [$°C$]; compass x,y,z [magnetic field strength]; gyroscope x,y,z [rotation distance over time]; acceleration x,y,z [distance over time squared]. The compass has a fixed full scale range of $\pm 1200\,\mu T$ corresponding to [-4096, +4095] or 13 bits respectively. Consequently, the compass readings have to be divided by 4096 and multiplied by $1200\,\mu T$ to get values in μT.

The chosen sensitivity settings define the scale of each of the six IMU axes. Default scales are set to $\pm 2\,g$ for the accelerometer and to $\pm 250\,°/s$ for the gyroscope. The output scale for any setting is [-32768, +32767], corresponding to 16 bits. Therefore, the MPU-6050 values have to be divided by 32768 and multiplied by $2\,g$ for the accelerometer and by $250\,°/s$ for the gyroscope in order to end up with meaningful units being m/s^2 and $°/s$ respectively.

The gravity vector is already subtracted from the acceleration readings. The values represent the net acceleration. The compass values might be biased if used for an oscillating coil fish that features several strong permanent magnets.

[20] https://github.com/jrowberg/i2cdevlib/tree/master/Jennic

C.1.2 Reading the pressure sensors

The MS5803-01BA pressure sensor is communicating to the Arduino microcontroller via I^2C. An example of the function to read the raw sensor values is shown in Figure 61. The raw values are mathematically converted to meaningful pressure readings as specified on the data sheet of the pressure sensor.

```
bool readRawValue(uint32_t* D, uint8_t index)
{
  uint8_t convert_command;

  // 2 values to be read: pressure and temp.
  if (index == 1)
  {
    convert_command = CMD_CONVERT_D1;
  }
  else
  {
    convert_command = CMD_CONVERT_D2;
  }

  // tell ADC to start conversion
  Wire.beginTransmission(I2C_ADDRESS);
  Wire.write(convert_command);
  Wire.endTransmission();

  delay(10);

  // tell chip to send ADC value
  Wire.beginTransmission(I2C_ADDRESS);
  Wire.write(0x00);
  Wire.endTransmission();

  // read the values received from the chip
  Wire.beginTransmission(I2C_ADDRESS);
  Wire.requestFrom(I2C_ADDRESS, (uint8_t) 3);

  if(Wire.available() < 3)
  {
    // TODO: error handling
  }
  else
  {
    uint8_t byte2 = Wire.read();
    uint8_t byte1 = Wire.read();
    uint8_t byte0 = Wire.read();

    *D = (((uint32_t) byte2) << 16) | (((uint32_
  }
  Wire.endTransmission();
}
```

Figure 61: Code sample for reading the pressure sensor.

C.1.3 Communication through transceivers

The supplier's hookup guide[21] provides all necessary information on how to operate two transceivers in SPI mode. The RF24 library from the hookup guide was installed by placing its folder in /Arduino/libraries. It contains a working example named "GettingStarted" (open Arduino, then follow File/Examples/RF24/GettingStarted). The code was modified to send data from the IMU and the pressure sensors from the robot to an external mission control (see Figure 62). The other way round, commands can be sent from the mission control to the robot. The robot can be reomote controlled (see Section C.2.2).

Important: Both transceivers have to be connected to an Arduino Pro Mini board. The pinout is shown in Figure 51. A hookup with the Arduino UNO

[21] https://learn.sparkfun.com/tutorials/nrf24l01-transceiver-hookup-guide?_ga=1.164138815.1823697433.1460077619

```
// Include libraries
#include <SPI.h>
#include "RF24.h"

// Define MessageStruct
struct MessageStruct
{
  unsigned long timestamp;
  int32_t pres_left;
  int32_t pres_right;
};
MessageStruct msg_out;

// Set up nRF24L01 radio on SPI bus plus pins 9 & 10
RF24 radio(9,10);

byte addresses[][6] = {"1Node","2Node"};

// Initialize transceiver (called from ScubaFish)
void initialize_transceiver()
{
  radio.begin();
  radio.setPALevel(RF24_PA_MAX);
  radio.openWritingPipe(addresses[1]);
  radio.openReadingPipe(1, addresses[0]);
  radio.startListening();
}
```

```
// Send message (called from ScubaFish)
void transceiver_loop()
{
    unsigned long got_time;
    if( radio.available()){
      while (radio.available()){
        radio.read( &got_time, sizeof(unsigned long) );
      }

      update_msg();

      radio.stopListening();
      radio.write( &msg_out, sizeof(MessageStruct));
      radio.startListening();
    }
}

// Update message with new readings
void update_msg()
{
  msg_out.timestamp = millis();
  msg_out.pres_left = pres_left;
  msg_out.pres_right = pres_right;
}
```

Figure 62: Code sample for transmitting sensor values from Scuba Fish to Mission Control.

failed presumably due to power issues[22].

The receiving transceiver is connected to a computer. The sensor data can be copied from the serial monitor and logged in a .txt file. A code sample for the receiving transceiver at Mission Control is shown in Figure 63.

```
// Include libraries
#include <SPI.h>
#include "RF24.h"

// Define MessageStruct
struct MessageStruct
{
  unsigned long timestamp;
  int32_t pres_left;
  int32_t pres_right;
};
MessageStruct msg_in;

// Set up nRF24L01 radio on SPI bus plus pins 9 & 10
RF24 radio(9,10);

byte addresses[][6] = {"1Node","2Node"};

// Set up transceiver
void setup() {
  Serial.begin(9600);

  radio.begin();
  radio.setPALevel(RF24_PA_MAX);
  radio.openWritingPipe(addresses[0]);
  radio.openReadingPipe(1,addresses[1]);
  radio.startListening();
}
```

```
// Receive messages from Scuba Fish
void loop() {
    radio.stopListening();

    unsigned long start_time = micros();
     if (!radio.write( &start_time, sizeof(unsigned long) )){
     }

    radio.startListening();

    unsigned long started_waiting_at = micros();
    boolean timeout = false;

    while ( ! radio.available() ){
      if (micros() - started_waiting_at > 200000 ){
          timeout = true;
          break;
      }
    }

    if ( timeout ){
    }else{
        radio.read( &msg_in, sizeof(MessageStruct) );
        unsigned long end_time = micros();

        Serial.print(msg_in.timestamp);
        Serial.print("   ");
        Serial.print(msg_in.pres_left);
        Serial.print("   ");
        Serial.println(msg_in.pres_right);
    }
}
```

Figure 63: Code sample for receiving sensor values at Mission Control from Scuba Fish.

[22] https://arduino-info.wikispaces.com/Nrf24L01-2.4GHz-HowTo#PP

C.2 Add-ons to the basic functionality

The transceiver was used to implement two add-ons with MATLAB for demo purposes: a real-time visualization of data and a remote control. Furthermore, this section explains the MATLAB script for tracking the robot with a camera.

C.2.1 Real-time visualization of sensor data in MATLAB

Transceiver data from the IMU and the pressure sensors can be visualized in a MATLAB figure in real time. The data is read from the serial port through which the Arduino is connected to the computer. A well documented online example[23] was modified for the purposes of Scuba Fish. Further information and function names are found in the MathWorks documentation[24].

The code running on Scuba Fish is unchanged. A "Serial" file was added to Mission Control in order to print the data received from the fish to the serial port of the computer.

The MATLAB code is split in three sections. First, a new serial connection is established. Second, data is read from the serial port. Third, data is plotted in a figure. A simplified version is shown in Figure 64.

```
%% GENERATE SERIAL CONNECTION
comPort = 'COM53';
obj = serial(comPort);
set(obj,'DataBits',8);
set(obj,'StopBits',1);
set(obj,'BaudRate',9600);
set(obj,'Parity','none');
fopen(obj);

%% CREATE PLOT WINDOW
if (~exist('h','var') || ~ishandle(h))
    h = figure(1);
    set(h,'UserData',1);
end

if (~exist('button','var'))
    button = uicontrol('Style','togglebutton','String',...
        'Stop','Position',[0 0 50 25], 'parent',h);
end
```

```
%% DRAW DATA IN PLOT WINDOW
if(~exist('myAxes','var'))

    buf_len = 50;
    index = 1:buf_len;
    zeroIndex = zeros(size(index));
    tcdata = zeroIndex;
    limits = [102000 103000];

    myAxes = axes('Xlim',[0 buf_len],'Ylim',limits);
    grid on;

    l = line(index,[tcdata;zeroIndex]);

    drawnow;
end
```

```
%% MAIN FILE
mode = 'R';

while (get(button,'Value') == 0 )
    tc = readTemp(arduino,mode);
    tcdata = [tcdata(2:end),tc];
    set(l,'Ydata',tcdata);
    drawnow;
    pause(0.2);
end

%% READ FUNCTION
function [output] = readTemp(s,command)
fprintf(s,command);
output = fscanf(s,'%f');
end
```

Figure 64: Code sample for the real-time visualization of sensor data in MATLAB.

[23] http://www.instructables.com/id/Arduino-and-Matlab-let-them-talk-using-serial-comm/?ALLSTEPS

[24] http://www.mathworks.com/help/matlab/matlab_external/writing-and-reading-data.html

C.2.2 Remote controlling Scuba Fish

Remote controlling Scuba Fish uses the transceivers in the other direction. A key is read from the computer keyboard, using the getkey file[25] in MATLAB. The key is passed to the robot via the serial port and the transceivers. On the robot, the key triggers the respective function that causes the desired motion.

C.2.3 Tracking Scuba Fish with an overhead camera

The evaluation of Scuba Fish motions is done in MATLAB. The single frames of a tracking video are read ("readFrame()") and saved ("imwrite()") in .tif images. One image is opened and two known points are assigned with the cursor. This step is necessary to find the conversion between pixels and the distance in cm. Finally, a loop runs through all the .tif images and applies a blob detector to each single one. The blob detection includes blurring ("imgaussfilt()"), conversion to HSV ("rgb2hsv()"), saving the HUE values, setting some thresholds for a b/w colormask ("im2bw()"), and finally finding the blob properties such as centroids ("regionprops()").

The required camera information is its resolution in pixels and its frame rate in FPS.

C.3 Closed-loop control experiments

This section shows code samples used in the experiments described in Chapter 5.

C.3.1 Maintaining a constant diving depth

The bang-bang controller for maintaining a constant diving depth is run in the "void loop()" of the main file named "ScubaFish". The pressure values are filtered (see Appendix C.4.1) and compared to preset thresholds on the desired diving depth. Depending on the comparison, the "dorsal_fin_state" is changed. If the pressure is higher than the high threshold, the dorsal fin is switched off and the robot starts to ascend. If the pressure is lower than the low threshold, the dorsal fin is switched on and the robot starts to dive. The dorsal fin is activated with a function call and run similarly like in the example of Appendix C.4.2. The controller is shown in Figure 65.

[25] `http://www.mathworks.com/matlabcentral/fileexchange/7465-getkey`

```
if (dorsal_fin_state == 0)
{
  if (pres_filtered < THRESH_LO)
  {
    dorsal_fin_state = 1;
  }
}
else
{
  if (pres_filtered > THRESH_HI)
  {
    dorsal_fin_state = 0;
    digitalWrite(dorsal_pin_1, LOW);
    digitalWrite(dorsal_pin_2, LOW);
  }
}

if (dorsal_fin_state == 1)
{
  dorsal_fin_function();
}
```

Figure 65: Code sample for depth control.

C.3.2 Swimming in a straight line

Swimming in a straight line is achieved with an I controller. A simplified void loop shown in Figure 66 illustrates the concept. A deadzone is chosen where no control action takes place (x_0). Whenever the integral of the error (yaw_pos) reaches either boarder of the deadzone, control kicks in. The control output (y, scales with the frequency of the flapping pectoral fin and with the generated thrust respectively) increases proportionally to the exceedance of the deadzone (y_0 to y_1). The control input (yaw_pos_int) is capped at an upper value (x_1) in an attempt to prevent the system from going unstable.

```
void loop()
{
  const double x_0 = DEAD_THRESH;
  const double y_0 = PERIOD_MAX;
  const double x_1 = POS_INT_MAX;
  const double y_1 = PERIOD_MIN;

  const double m = (y_0 - y_1)/(x_0 - x_1);
  const double y_min = y_1;

  transceiver_loop();

  read_IMU(ax, ay, az, gx, gy, gz, mx, my, mz);
  yaw_vel = (-gy) - YAW_OFFSET;
  yaw_pos += yaw_vel;
  yaw_pos_int += yaw_pos;

  if (yaw_pos_int > POS_INT_MAX)
  {
    yaw_pos_int = POS_INT_MAX;
  }
  if (yaw_pos_int < -POS_INT_MAX)
  {
    yaw_pos_int = - POS_INT_MAX;
  }

  if (yaw_pos_int > DEAD_THRESH)
  {
    double x = fabs(yaw_pos_int);
    double y = y_0 + m*(x - x_0);
    if (y < y_min)
    {
      y = y_min;
    }
    pectoral_left_fin_off();
    pectoral_right_fin_function(y);
  }
  else if (yaw_pos_int < -DEAD_THRESH)
  {
    double x = fabs(yaw_pos_int);
    double y = y_0 + m*(x - x_0);
    if (y < y_min)
    {
      y = y_min;
    }
    pectoral_right_fin_off();
    pectoral_left_fin_function(y);
  }
  else
  {
    pectoral_left_fin_off();
    pectoral_right_fin_off();
  }
}
```

Figure 66: Code sample for swimming in a line.

C.3.3 Swimming towards a pressure source

A P controller drives the pressure difference measured by the two sensors at the nose of Scuba Fish to zero. Consequently, the robot aligns with the pressure source. Whenever the pressure difference is outside an acceptable range (x_0), the corresponding pectoral fin is activated proportionally to the exceedance of that range (y). The concept is shown in Figure 67.

```
void loop()
{
  int32_t PRES_LT, TEMP_LT, PRES_RT, TEMP_RT;
  read_pressure_sensors(PRES_LT, TEMP_LT, PRES_RT, TEMP_RT);
  read_IMU(ax, ay, az, gx, gy, gz, mx, my, mz);

  error = (PRES_LT - PRES_LT_OFFSET) - (PRES_RT - PRES_RT_OFFSET);
  error_filtered = EMA_filter(error);

  double x_0 = 25.0;
  double y_0 = 2000.0;
  double x_1 = 75.0;
  double y_1 = 500.0;

  double m = (y_0 - y_1)/(x_0 - x_1);

  if (error_filtered > x_0)
  {
    double y = y_0 + m*(fabs(error_filtered) - x_0);
    if (y < y_1)
    {
      y = y_1;
    }
    pectoral_left_fin_function(y);
    pectoral_right_fin_off();
  }
  else if (error_filtered < -x_0)
  {
    double y = y_0 + m*(fabs(error_filtered) - x_0);
    if (y < y_1)
    {
      y = y_1;
    }
    pectoral_left_fin_off();
    pectoral_right_fin_function(y);
  }
  else
  {
    pectoral_left_fin_off();
    pectoral_right_fin_off();
  }
}
```

Figure 67: Code sample for aligning with a pressure source.

C.4 Development code

This section shows code that was either developed on the way to the present source code for Scuba Fish, or code that is used in helper functions of the current software.

C.4.1 Alpha filter

An alpha filter was used to filter data from the pressure sensors and the IMU. An alpha filter takes into account the history of measurements and weighs it up against the current measurment. The function is shown in Figure 68.

```
double EMA_filter(double raw_in)
{
  const double alpha = 0.1;
  static double filtered_out;
  static bool initialized = 0;

  if (!initialized)
  {
    filtered_out = raw_in;
    initialized = 1;
  }
  else
  {
    filtered_out = (1.0 - alpha)*filtered_out + alpha*raw_in;
  }

  return filtered_out;
}
```

Figure 68: The alpha filter function used to filter sensor data.

C.4.2 Control of oscillating coils

The oscillation of the coil is caused by changing the direction of the current flow and the polarities of the induced magnetic field respectively. The current flow is dictated by an H-bridge. The switching time interval defines the frequency of the oscillation. The full amplitude is fixed by design. Playing with the delay time parameter allows to send the coil only halfway of the full amplitude before already switching back polarities. Thus, control over the yaw angle is possbile. An example is shown in Figure 69.

```
int cwPin = 5;
int ccwPin = 6;

void setup() {
  pinMode(cwPin, OUTPUT);
  pinMode(ccwPin, OUTPUT);
}

// Very important: note that with this chip (SN754410)
// 0 => motor on while 1 => motor off. So PWM of 255
// is motor off, PWM of 0 is full speed.
```

```
void loop() {

  // Activating the H-bridge after a desired delay
  analogWrite(ccwPin, 255); // make ccwPin permanently closed
  analogWrite(cwPin, 0); // make cwPin permanently open

  delay(200); // keep doing for 200ms

  analogWrite(cwPin, 255); // make cwPin permanently closed
  analogWrite(ccwPin, 0); // make ccwPin permanently open

  delay(200); // keep doing for 200ms
}
```

Figure 69: Code sample for the control of an oscillating coil fish.

C.4.3 Control of servomotors

Servomotors can easily be controlled with the Arduino microcontroller. Several servomotors can be connected to the Arduino board at the same time. An example of how to command a servomotor is given in Figure 70.

```
#include <Servo.h>

Servo caudal; // create servo object to control the caudal servo

void setup() {
  caudal.attach(9); // attaches the servo on pin 9 to the caudal object
}

// (consider max. servo speed: 0.2sec/60deg)

// OSCILLATION
int ampl = 20;  // amplitude [deg]
float freq = 1; // frequency [Hz]

int incr = 1; // increment [deg]
float del = 1000/(2*ampl*freq)*incr; // delay [ms]

int offset[] = {ampl/2, ampl/2};  // offset in dep. of amplitude, defines steering angle

// MANEUVERS
int rep = 0;

int straight[] = {90-ampl/2, 90+ampl/2};  // swimm straight
int left[] = {straight[0]+offset[0], straight[1]+offset[1]};  // turn left
int right[] = {straight[0]-offset[0], straight[1]-offset[1]}; // turn right

// MOTION COMMANDS
void loop() {

// e.g. swim a square
oscillate(straight, incr, del, 10); // oscillate(direction, ..., ..., repetitions)
oscillate(left, incr, del, 3);
oscillate(straight, incr, del, 10);
oscillate(left, incr, del, 3);
oscillate(straight, incr, del, 10);
oscillate(left, incr, del, 3);
oscillate(straight, incr, del, 10);
oscillate(left, incr, del, 3);
}


void oscillate(int move[], int incr, float del, int rep){

int pos = 0;  // variable to store the servo position

  for(int i = 1; i <= rep; i++){  // repeat maneuver 'rep' times
    for (pos = move[0]; pos <= move[1]; pos += incr) {  // amplitude: goes from 'move[0]' degrees to 'move[1]'
                                                        // degrees in steps of 'incr' degrees
      caudal.write(pos);  // tell servo to go to position in variable 'pos'
      delay(del); // frequency: waits 'del' ms for the servo to reach the position (consider max. servo speed!)
    }/
    for (pos = move[1]; pos >= move[0]; pos -= incr) {
      caudal.write(pos);
      delay(del);
    }
  }
}
```

Figure 70: Code sample for swimming a square with a servomotor fish.

D Project management

This section of the Appendix shows documents related to the organization of the project, such as the project plan and a requirement list.

D.1 Project plan for Scuba Fish

The project plan for Scuba Fish is split in five stages as shown in Figure 71. First, the scope and the goals of the project were defined and the corresponding literature was reviewed. Second, conceptions for possible designs were created and assessed. Third, the most promising design was chosen and developed. Fourth, the resulting prototype was tested and evaluated. Fith, the project was documented and transfered to the next design cycle.

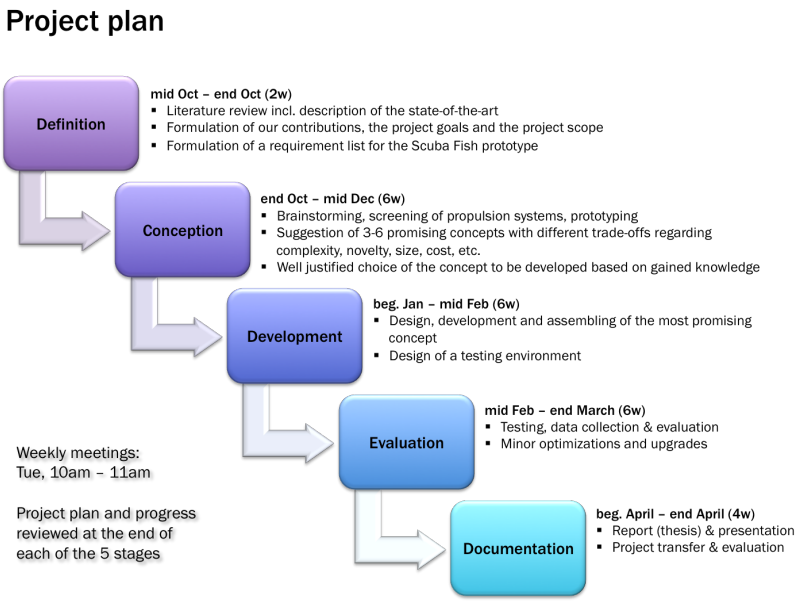

Figure 71: Scuba Fish project split in five stages.

D.2 Initial requirement list for Scuba Fish

The requirement list as shown in Figure 72 lists all the requirements that an ideal Scuba Fish should fulfill. Their importance was weighted from 1 (least important) to 5 (most important). The requirement list served as a guideline during the design process of Scuba Fish.

Requirement list

#	Description	Quantification	Reason	Validation	Imprt (1-5)
1	Diving depth	20' (≈6m)	Reasonable reef depth	Test & measure	3
2	Battery runtime	2h	Stable sea cond., suff. obs. time	Run & measure @ std. cond.	3
3	Waterproofness	Fully dry	Shield sensors from water	Test & inspect	5
4	Body length (BL)	4" (≈10cm)	Swarm, maneuverability, uniqueness, impact on others	Measure	4
5	Fish cost (if 100 ordered at a time)	USD 50	Swarm scalability, applications	Calculate	3
6	Assembling time per fish	15min	Swarm of 100 built in 3 man-days	Measure	3
7	Swarm scalability	100 members	Replicate fish school behavior	Test & observe	3
8	Swimming speed	4"/s (=1BL/s)	Reasonalbe range (≈0.5mi/cycle)	Test & measure	2
9	Precision of motion	σ of 1' (=3BL)	Position of individual swarm member not crucial	Test & measure	2
10	Stability against ext. stimuli	1N pull force	Avoid drift by currents or other fish	Test & measure	1
11	Carrying capabilities	Communication, obst. avoidance	Carry sensors for swarm functionalities	Design	4
12	Collision resistance	Bump with full speed	Keeps working after collision with reef due to imprecise motion	Test & observe	2
13	Thethering	Ok for prototype	Full autonomy has to be possible	Design	5
14	Buoyancy control	Dynamic, stable	For size and simplicity	Test & measure	4
15	Holonomy/turning radius	Partly	Turn on spot ideal for constrained navigation	Test & inspect	3

Figure 72: Requirement list.

Data disc on the Scuba Fish project

All project data such as reports and presentations, pictures and videos, or Arduino and Matlab files are recorded on a data disc, handed in during the project transfer together with this thesis.

E Abstract for Oceans'16

This section of the Appendix contains an abstract about the design of Scuba Fish. The abstract was submitted to the Ocean's 16 conference in Monterey[26]. Besides, it may serve as a self-contained summary on the design of Scuba Fish.

[26] http://www.oceans16mtsieeemonterey.org/

A Low-Cost, Highly-Maneuverable, Miniature Robot intended for Collective Behaviors

F. Berlinger, M. Gauci, J. Dusek and R. Nagpal

Self-organizing Systems Research Group, Harvard University

This abstract discusses the design of a low-cost, highly-maneuverable, and miniature underwater robot. The design addresses some key challenges towards the realization of a large-scale, underwater robot collective. Firstly, low-cost and ease of manufacture of individual units are paramount considerations for keeping the cost of the collective within reasonable bounds. Secondly, high maneuverability is desirable so that each individual can exhibit fast response to its neighbors' actions, thus making it possible to maintain a cohesive collective. Thirdly, miniaturization would make feasible the operation of a school of underwater robots within a laboratory environment, providing an affordable and convenient physical platform for the study of 3-dimensional collective behaviors. Nature offers ample evidence that collectives have the potential to outperform individuals in certain aspects; for instance, it has been shown that fish school to improve their locomotion efficiency, avoid predators or capture prey. As such, a school of underwater robots would open up applications for which current, monolithic robots are not the most suitable choice [1]. Such applications may include search missions and environmental monitoring over large areas (see Fig. 1). In addition, the highly-maneuverable and miniature nature of the robots would also allow for operation in complex environments like coral reefs. In the next stages of the project, other necessary features for collective behaviors, such as sensing and communication, will be addressed.

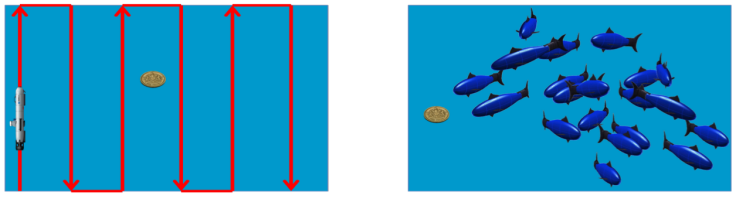

Figure 1: *Traditional search (left) versus collective search (right). A collective of robots can be spread like a grid across the search area to minimize search time.*

I. Introduction

The current prototype is shown in Fig. 2. It is low-cost at a total components value of $60 (it is intended that the final robot will cost under $100). High-maneuverability is achieved by using four fins—one caudal, two pectoral, and one dorsal—which provide the robot with forward motion, turn-on-the-spot, and vertical diving capabilities. This relatively high number of control surfaces is made possible by the low-cost nature of the propulsor, discussed in the next section. This prototype has a body length of 10 cm, excluding the caudal fin.

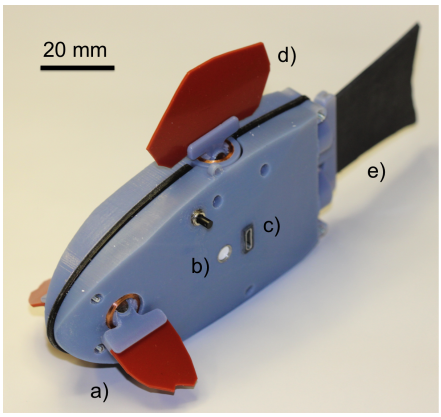

Figure 2: *The robot and its features: a) pectoral fin, b) pressure sensor, c) USB port, d) dorsal fin, e) caudal fin.*

II. Propulsion system

Takada et al. [2] introduced a Magnet-in-Coil propulsor (MIC), as illustrated in Fig. 3. A permanent magnet is pivoted inside an electromagnetic coil, and aligns with an alternating magnetic field generated by the coil. A hinge transfers the oscillating motion to a flexible fin. This propulsor has two main advantages that make it suitable for our design. Firstly, it has an extremely low component cost (under $1). Secondly, it avoids the necessity of sealing moving parts, such as rotary shafts; the MIC propulsor can be attached modularly to the outer hull of the robot, and only two wires are required to penetrate the hull. This increases the robot's reliability and reduces its manufacturing difficulty. Our contribution is to use multiple such propulsors on a single robot, hence achieving high-maneuverability and miniaturization at a low cost.

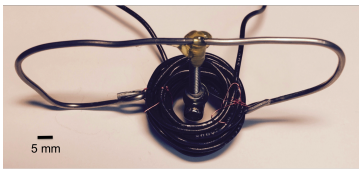

Figure 3: *A simplified model of a Magnet-in-Coil propulsor that powers the oscillating fins of the robot.*

III. Swimming performances

Four independent MICs on the robot (c.f. Fig. 2) ensure 3-dimensional maneuverability for up to 1 h of swimming time: a caudal fin (e) provides forward thrust for velocities of up to 1 body length per second; a dorsal fin (d) allows for vertical diving down to at least 3 m below the surface; a pectoral fin (a) on either side of the body enables turn-on-the-spot.

IV. Onboard intelligence

A microcontroller, a transceiver, an IMU, two pressure sensors and two batteries allow for untethered, closed-loop swimming behaviors. The robot can operate autonomously or receive commands through its transceiver. The transceiver sends sensor data to a base station where they can be visualized in real time. Two waterproof USB ports enable charging and programming the robot without the necessity of opening it.

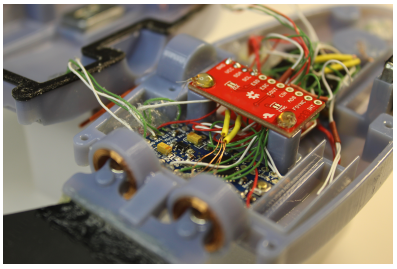

Figure 4: *The inside of the robot.*

Preliminary experiments suggest that a number of intelligent maneuvers are possible, including: (1) depth control and (2) aligning with a pressure source using pressure sensors; (3) swimming in a straight line using the IMU; (4) swimming towards a pressure source combining (1), (2) and (3).

V. Potential applications

The proposed underwater robot shows the potential to become a scalable platform to study 3-dimensional swarming in an affordable manner and reasonably-sized laboratory environment. In the next steps of the project, several robots will be coordinated into a collective by adding sensing and communication capabilities. Intended applications for a collective of underwater robots include search and rescue missions, harbor patrols, the surveillance of offshore oil platforms and the monitoring of coral reefs or underwater food plantations.

References

[1] M. Brambilla, E. Ferrante, M. Birattari and M. Dorigo. Swarm Robotics: A review from the swarm engineering perspective. *Swarm Intelligence*, 7(1):1-41, 2013.

[2] Y. Takada, K. Koyama and T. Usami. Position Estimation of Small Robotic Fish Based on Camera Information and Gyro Sensors. *Robotics*, 3(2):149-162, 2014.